AN ABSTRACT OF THE THESIS OF

Carl J. Talsma for the degree of Master of Science in Water Resources Engineering presented on June 6, 2018.

Title: Sensitivity and Partitioning in Remote Sensing Based Evapotranspiration Models.

Abstract approved:

_____

Stephen P. Good

Satellite Based evapotranspiration (ET) models have become a dominant means to estimate large-scale surface fluxes of water. Global and regional ET estimates are important parameters in many climate forecasts and hydrologic models. However, large scale partitioning of ET into soil evaporation, transpiration, and canopy interceptions remains largely unknown and modeled estimates have been shown to diverge strongly. This study examines three such remote sensing-based models: the Penman-Monteith model from the Moderate Resolution Imaging Spectroradiometer (PM-MOD), the Priestley-Taylor Jet Propulsion Laboratory model (PT-JPL), and the Global Land Evaporation Amsterdam Model (GLEAM). Modeled ET and component estimates are compared against a compiled dataset of field estimates using stable isotopes, sap flux, and other methods. Results are analyzed across land cover type, precipitation regime, and field methods. Overall, we find large deviations between field and modeled estimates of soil evaporation (RMSD = 90-114%, r^2 = 0.14-0.25, N = 35), interception (RMSD = 62-181%, r^2 = 0.39-0.85, N = 13), and transpiration (RMSD = 54–114%, r^2 = 0.33-0.55, N = 35) compared to the deviations found in the total ET estimate (RMSD = 35-49%, r^2 = 0.61-0.75, N = 35). We then conduct a Monte Carlo sensitivity analysis using varying degrees of parameter uncertainty to determine how forcing data error influences model estimates and to determine which parameters are the primary drivers of each model. We find large sensitivity and bias in component estimates that becomes mitigated when aggregated into a total ET estimate. The results also show that

the total ET of PT-JPL, PM-MOD, and GLEAM is most sensitive to NDVI, RH, and net radiation, respectively. The results of each study suggest that the soil evaporation component exhibits large errors and may be culpable for errors in ET partitioning. These results suggest that future improvements to remote sensing-based ET component estimates will vastly improve the confidence of the total ET estimates and provide greater understanding in how water interacts with vegetation, climate, and society.

Sensitivity and Partitioning in Remote Sensing Based Evapotranspiration Models

by
Carl J. Talsma

A THESIS

submitted to

Oregon State University

in partial fulfillment of
the requirements for the
degree of

Master of Science

Presented June 6, 2018
Commencement June 2018

Master of Science thesis of Carl J. Talsma presented on June 6, 2018

APPROVED:

Major Professor, representing Water Resources Engineering

Director of the Water Resources Graduate Program

Dean of the Graduate School

I understand that my thesis will become part of the permanent collection of Oregon State University libraries. My signature below authorizes release of my thesis to any reader upon request.

Carl J. Talsma, Author

ACKNOWLEDGEMENTS

This thesis would not have been possible without the support of the Betty & Ron Minor Memorial Fellowship. I would like to express my appreciation for the continual support offered to graduate students through this fellowship and my sincere thanks to Betty Minor and family.

I would like to express my sincerest appreciation to my advisor Steve Good, for offering unwavering encouragement and enthusiasm in my development both professionally and personally. Steve's eagerness and excitement to support my efforts and explore ideas make him the ideal exemplar of both a mentor and a scientist. I also appreciate the help and advice from each of my co-authors, teachers, and committee members who have been far more dedicated, informative, and patient than I could have hoped. I want to thank the Water Resources Graduate Program more broadly along with all of the staff, students, and administrators who make possible the devotion of so many resources to the study and research of water science.

I would also like to acknowledge the support of my family and friends, without whom I would never have made it to this point. I would especially like to thank my parents, Kelly and Carl, who have sacrificed and supported me to this point, and Lucy Keehn, who gives me the encouragement and the drive to realize my aspirations and to be a better person.

CONTRIBUTION OF AUTHORS

Steve Good was involved in the formulation of ideas and revision process for both manuscripts. Carlos Jimenez provided forcing data for both chapters, PM-MOD model code, and provided revisions to the first manuscript. Brecht Martens provided GLEAM model code, forcing data, and revisions to the first manuscript. Josh Fisher and Adam J. Purdy made available the PT-JPL model code and offered there insight throughout the editing and analysis process of the first manuscript. Diego Miralles aided in the revisions and offered input in the first manuscript. Matthew McCabe provided model forcing data and revisions for the first manuscript.

TABLE OF CONTENTS

LIST OF FIGURES

LIST OF FIGURES (Continued)

LIST OF TABLES

I. Introduction:

Evapotranspiration (ET), the process by which liquid water returns to the atmosphere as vapor, represents a central nexus at the intersection of the carbon, water, and energy cycles (Oki and Kanae, 2006). Terrestrial ET is traditionally partitioned into three components: transpiration of water through plant stomata, soil evaporation from the top layer of soil, and canopy interception and re-evaporation of rainfall. Each component represents an alternative pathway for water to return to the atmosphere via evaporation. The partitioning of ET between these pathways is controlled through a variety of competing factors including the productivity of vegetation, regional and local climatic factors, water table and rooting depth, groundwater connectivity to surface water, and phenology (Cavanaugh et al., 2011; Hu et al., 2009; Wang et al., 2014). How vegetation responds to a changing climate is one of the key uncertainties in climate forecasts, and partially depends on the magnitude of expected changes to transpiration rates and ET partitioning (Friedlingstein et al., 2014; Lawrence et al., 2007).

Remote sensing-based model estimates of ET have become ubiquitous in global climate research and often depend upon the aggregate of ET component estimates (Fisher et al., 2017; K. Zhang et al., 2016). While significant research has been done to enhance our ability to estimate total ET, our understanding of the components of ET remains critically limited (Miralles et al., 2016; Schlesinger and Jasechko, 2014). The development of accurate ET partitioning estimates has been hindered by the lack of a quality field dataset by which to validate modeled estimates. Remote sensing-based ET estimates have benefited from FLUXNET, the global network of eddy covariance tower sites used to validate modeled ET estimates (Baldocchi et al., 2001). Transpiration and soil evaporation fluxes are measured

using stable isotope techniques (Brunel et al., 1997; Gibson and Edwards, 2002; Jasechko et al., 2013), sap-flux probes (Fernández et al., 2006; Williams et al., 2004), and other methods (Gibson and Edwards, 2002; Lautz, 2008; McJannet et al., 2007), while interception is measured as the residual of rainfall captured above and below the canopy (Carlyle-Moses and Gash, 2011; Crockford and Richardson, 2000). ET partitioning data remains sparse and uncoordinated, and field methods lack the scale and quality that eddy covariance towers provide.

Furthermore, multiple models and forcing datasets exist to estimate ET and its components (Mccabe et al., 2016; Michel et al., 2016). Comparisons between models have shown large discrepancies in partitioning (Miralles et al., 2016), but these comparisons suffer from the unique data fields and parameters that each model requires. Model disparities can then result from both the formulation of the model and from error introduced by the uncertainty of a unique parameter within that model. Previous studies have attempted to force multiple models using the same dataset (Mccabe et al., 2016; Michel et al., 2016; Mueller et al., 2011), or to force the same model using multiple datasets to isolate sources of error (Badgley et al., 2015). However, models rarely share data requirements exactly and sources of error are more difficult to isolate when we assess the state of ET models more broadly.

This study attempts to assess the accuracy in the partitioning of three remote sensing-based ET models. First, we assess the performance of the modeled total ET and component estimates against a dataset of globally dispersed field estimates. We then conduct a sensitivity analysis on each of the models using the same forcing dataset. We contend that the field study estimates of ET, while containing errors of their own, can be aggregated to

provide information and trends against which to validate the remote sensing-based models. We can then assess the performance of the model across different metrics and parameters, and use the sensitivity analysis to determine if the model's sensitivity to a given parameter might explain the model component performance determined by the field studies.

The focus of the sensitivity analysis on the individual model components and their comparison against field derived values is novel. Few studies have explored the different partitioning strategies within these models, despite their importance to land surface feedbacks and to the model ET estimate itself. The ease and quantity at which remote sensing data is available will continue to create opportunities to refine and improve ET estimates. However, our poor understanding of the partitioning of ET will continue to limit those estimates. We hope that the following study provides insight into the performance of the partitioning strategies of the models as well as the broader challenges associated with determining ET partitioning and plant-water relations.

II. Partitioning of evapotranspiration in remote sensing-based models

Carl J. Talsma[1*], Stephen P. Good[1], Carlos Jimenez[2], Brecht Martens[3], Joshua B. Fisher[4], Diego G. Miralles[3], Matthew F. McCabe[5], Adam J. Purdy[6]

[1] *Department of Water Resources, Oregon State University, Corvallis, Oregon, USA*

[2]*Estellus, Paris, France*

[3]*Laboratory of Hydrology and Water Management, Ghent University, Ghent, Belgium*

[4]*Jet Propulsion Laboratory, California Institute of Technology, Pasadena, California, USA*

[5]*Division of Biological and Environmental Sciences and Engineering, King Abdullah University of Science and Technology, Thuwal, Saudi Arabia*

[6]*Department of Earth System Science, University of California, Irvine, California, USA*

**Corresponding author. E-mail address: talsmac83@gmail.com, Gilmore Hall, 124 SW 26th St, Corvallis, OR 97331*

Keywords: Evapotranspiration, Partitioning, Modeling, Remote Sensing, Transpiration, Soil Evaporation

Declarations of Interest: None

Abstract:

Satellite based retrievals of evapotranspiration (ET) are widely used for assessments of global and regional scale surface fluxes. However, the partitioning of the estimated ET between soil evaporation, transpiration, and canopy interception regularly shows strong divergence between models, and to date, remains largely unvalidated. To examine this problem, this paper considers three algorithms: the Penman-Monteith model from the Moderate Resolution Imaging Spectroradiometer (PM-MODIS), the Priestley-Taylor Jet Propulsion Laboratory model (PT-JPL), and the Global Land Evaporation Amsterdam Model (GLEAM). Surface flux estimates from these three models, obtained via the WACMOS-ET initiative, are compared against a comprehensive collection of field studies, spanning a wide range of climates and land cover types. Overall, we find errors between estimates of field and remote sensing-based soil evaporation (RMSD = 90-114%, r^2 = 0.14-0.25, N = 35), interception (RMSD = 62-181%, r^2 = 0.39-0.85, N = 13), and transpiration (RMSD = 54–114%, r^2 = 0.33-0.55, N = 35) are relatively large compared to the combined estimates of total ET (RMSD = 35-49%, r^2 = 0.61-0.75, N = 35). Errors in modeled ET components are compared between land cover types, field methods, and precipitation regimes. Modeled estimates of soil evaporation were found to have significant deviations from observed values across all three models, while the characterization of vegetation effects also influences errors in all three components. Improvements in these estimates, and other satellite based partitioning estimates are likely to lead to better understanding of the movement of water through the soil-plant-water continuum.

2.1 Introduction:

The evaporation of water from the Earth's surface to the atmosphere represents a critical link between the global water, carbon, and energy cycles (Oki and Kanae, 2006). An estimated two thirds of terrestrial rainfall returns to the atmosphere as evapotranspiration (*ET*) from the continents (Hobbins et al., 2004; Teuling et al., 2009) and the associated latent heat flux corresponds to a cooling of the Northern Hemisphere of about 15^{o}-25^{o}C (Shukla and Mintz, 1982). ET is a critical process governing water resource availability, agricultural productivity, and irrigation efficiency, as well as impacting the severity of droughts, floods, and wildfires (Littell et al., 2016; Molden et al., 2010; Trenberth, 2011; Wallace, 2000). Furthermore, the energy flux associated with ET fundamentally influences the development of the planetary boundary layer and the atmospheric processes contained within it (Ek and Holtslag, 2004; Pielke et al., 1998; Seneviratne et al., 2010). Future climate warming is expected to significantly alter the global water cycle, affecting regional and global rates of ET, precipitation, and streamflow (Huntington, 2006; Y. Zhang et al., 2016). Given the important role of ET in a variety of land surface processes, accurately estimating large-scale fluxes of ET is critical to our understanding of the earth system.

Spatially distributed, remote sensing-based ET models have become a dominant means to estimate catchment and global-scale ET fluxes (Anderson et al., 2007; Fisher et al., 2017; Schmugge et al., 2002). The large spatial extent and fine temporal resolution of these remote sensing products makes them perhaps the only observational means to assess global-scale impacts of changes in ET fluxes. These factors have made remote sensing-based models a powerful tool in both climate and large-scale hydrologic applications. Many of these remote sensing-based models estimate total ET via combination of its separate components:

transpiration through plant stomata, soil evaporation from the top layer of soil, and canopy rainfall interception. However, the wide array of algorithms and choice of forcing datasets have hampered the analysis of model results, as errors in model estimates may come from both forcing errors and/or errors in algorithms and parametrizations (Ershadi et al., 2015). Recent efforts have compared ET fluxes from several satellite-based ET models using a common forcing dataset, simplifying the comparison substantially (McCabe et al., 2016; Michel et al., 2016; Miralles et al., 2016).

These remote sensing-based ET estimates have shown good relative agreement in global estimates, but larger discrepancies regionally (Michel et al., 2016). Interestingly, the limited number of studies comparing individual ET components have shown that the global and regional contribution of transpiration, soil evaporation, and interception vary significantly between models, even where total ET estimates agree (Miralles et al., 2016). The divergence of ET partitioning estimates suggests that some models may contain large ET partitioning errors. Accurate partitioning estimates are highly desired for research related to agriculture, climate and land-use change, hydrology, and water resource availability. ET partitioning is also a crucial factor for global climate models as the partitioning of ET has proven to be a significant source of uncertainty for future climate projections (Lawrence et al., 2007). Incorrect parameterizations within ET models are likely to compromise the accuracy of estimates across ecoregions and through time. Furthermore, any divergence of ET partitioning is certainly an indicator that models may contain systematic errors in their formulations.

The mechanisms that govern the individual ET components of transpiration, soil evaporation, and canopy interception operate on varying spatial scales from relatively small (i.e. stomata, single plants) to larger regional scales (i.e. climate system) (Good et al., 2017;

Pieruschka et al., 2010; Wang and Dickinson, 2012; Wang et al., 2014). Field methods for measuring transpiration typically measure at the scale of an individual leaf or plant (Rana and Katerji, 2000; Schlesinger and Jasechko, 2014). Such field techniques include: sap-flow measurements, diurnal water table changes, water-balance approaches, and isotope based approaches (Gibson and Edwards, 2002; Lautz, 2008; McJannet et al., 2007; Nizinski et al., 2011). Measurements from such studies are extrapolated to larger spatial scales through assumptions about the variability of sap-flux densities (Dye et al., 1991; Fernández et al., 2006), changes in isotopic composition of water within the plant (Brunel et al., 1997), and general homogeneity of vegetation and stomatal response to environmental conditions. The spatial scale of these measurements remains a limitation for ET partitioning validation, as research into regional hydrologic and climatic processes often requires estimates of partitioned fluxes at much larger spatial scales.

Furthermore, field studies of ET partitioning often focus on a single component such as transpiration or interception, and rarely attempt to estimate all contributing ET components. Canopy interception, for instance, is a well-developed field of study (Carlyle-Moses and Gash, 2011; Crockford and Richardson, 2000; Levia and Frost, 2006; Muzylo et al., 2009), and is often estimated as the difference between rainfall above and below the canopy. However, few canopy interception studies attempt to quantify the role of interception as part of the ET flux. Similarly, transpiration studies are often focused on the physiologic processes of vegetation and disregard the role of transpiration in larger hydrologic and atmospheric cycles. Some field methods do not directly measure soil evaporation, and instead quantify it as the residual of ET and transpiration. Due to the fractured nature of the ET partitioning research, few field studies are available quantifying transpiration, soil evaporation, and interception simultaneously.

To address the uncertainty surrounding ET partitioning in remote sensing-based ET models, we evaluate three models and their partitioning strategies against a compilation of field studies. We hope to contextualize partitioning comparisons made by Miralles et al. (2016) using empirical field methods. While previous studies have attempted to compare specific model estimates of either canopy interception or transpiration against field data, few have jointly assessed errors in remote sensing-based estimates against transpiration, soil evaporation, and interception. In comparing model performance against compiled field estimates we hope to (1) reconcile the deviations between each model partition against a field standard, (2) determine if the modeled errors are consistent or vary across different land surface or climate conditions, (3) identify assumptions or parameters within the model that contribute to error, (4) and contextualize some of the partitioning comparisons made by Miralles et al. (2016).

2.2. METHODOLOGY:

We compared ET components from three remote sensing-based models against a compilation of field estimates of soil evaporation, transpiration, and interception. We assessed the Priestley-Taylor Jet Propulsion Lab model (PT-JPL)(Fisher et al., 2008), the Penman-Monteith MODerate Resolution Imaging Spectroradiometer (PM-MODIS) (Mu et al., 2011), and the Global Land Evaporation Amsterdam Model (GLEAM) (Martens et al., 2017; Miralles et al., 2011, 2010) model. Each model is widely used to estimate ET and provide relatively comparable estimates of the total ET flux (Miralles et al., 2016). Global annual mean values of ET for each model have been estimated at 54.9, 72.9, and 72.5 x 10^3 km^3 for PM-MOD, GLEAM, and PT-JPL respectively (*ibid.*).

2.2.1 Evaporation Models

Each model evaluated for this study adopts a similar structure to estimate total ET fluxes as well as the individual components of ET. The model structure may be categorized into three separate functions: (1) quantifying potential ET, (2) partitioning the potential ET into its given components to be aggregated as total ET, and (3) translating the potential ET into an actual ET based on the constraints of the component processes. Different models employ different strategies in accomplishing these basic functions but individual model parameters often fall into a single categorical function.

a. Priestley-Taylor Jet Propulsion Lab (PT-JPL)

The PT-JPL model utilizes the Priestley-Taylor equation (Priestley & Taylor, 1972) to estimate potential ET flux and is described in depth in Fisher et al. (2008). The model uses ecophysiological and atmospheric constraints to reduce the potential ET flux to an actual ET flux. The total ET is partitioned between soil evaporation, E_s [m/s], canopy transpiration, E_v [m/s], and canopy interception, E_i [m/s] as

(1a) $$E_s = \left(f_{wet} + f_{SM}(1 - f_{wet})\right)\alpha \frac{\Delta}{\lambda_v \rho_w (\Delta+\gamma)} (R_{ns} - G),$$

(1b) $$E_v = (1 - f_{wet}) f_g f_T f_M \alpha \frac{\Delta}{\lambda_v \rho_w (\Delta+\gamma)} R_{nc},$$

(1c) $$E_i = f_{wet} \alpha \frac{\Delta}{\lambda_v \rho_w (\Delta+\gamma)} R_{nc}$$

where a is the Priestley-Taylor coefficient (considered equal to 1.26), Δ is the slope of the vapor pressure curve [Pa/K], γ is the psychrometric constant [Pa/K], R_n is the net radiation [W/m^2], G is the energy flux into the ground [W/m^2], $\lambda_v$is the latent heat of vaporization[J/kg], f_{wet} is a relative surface wetness parameter (see below), f_{SM} is the soil moisture constraint, f_g

is the green canopy fraction, f_T is the plant temperature constraint, and f_M is the plant moisture constraint.

PT-JPL effectively accomplishes its partitioning using a canopy extinction equation to estimate the radiation penetrating through the canopy. This canopy extinction equation utilizes the leaf area index (LAI) in conjunction with the Beer-Lambert law of light attenuation (Norman Ay et al., 1995) to partition net radiation between the canopy and soil. Canopy processes (interception and transpiration) are determined using the radiation intercepted according to the Beer-Lambert equation, and soil evaporation is determined using the residual radiation penetrating the canopy.

PT-JPL scales each ET component by various scalars (f parameters) between 0 and 1 to account for environmental constraints on potential evaporation such as water and heat stress. Transpiration is constrained using four vegetation-based physiological parameters. Temperature and plant moisture effects on transpiration are calculated by normalizing phenological parameters by the maximum observed value per pixel. A canopy greenness fraction further constrains the transpiration flux based on the ratio between the fraction of absorbed photosynthetically active radiation ($fAPAR$) and the fraction of intercepted photosynthetically active radiation ($fIPAR$). The fourth constraint on transpiration is the surface wetness based on atmospheric relative humidity (f_{wet}). Soil evaporation constraints are determined by the surface wetness parameter (f_{wet}) and the available soil moisture (f_{sm}), the latter estimated by both relative humidity and vapor pressure deficit. Interception is estimated using the same f_{wet} parameter.

b. Penman-Monteith MODerate Resolution Imaging Spectroradiometer (PM-MODIS)

The PM-MOD model uses a framework based on the Penman-Monteith equation and utilizes specific conductance terms representing the vapor movement from the land surface to the overlying atmosphere. The model is described in depth by Mu et al. (2011) and estimates the components as:

(2a) $$E_i = f_{wet} f_c \frac{\Delta(R_n - G) + \rho c_p {}^{VPD}/_{r_a^{wc}}}{\lambda_v \rho_w (\Delta + \gamma \frac{r_s^{wc}}{r_a^{wc}})},$$

(2b) $$E_v = (1 - f_{wet}) f_c \frac{\Delta(R_n - G) + \rho c_p {}^{VPD}/_{r_a^{t}}}{\lambda_v \rho_w (\Delta + \gamma \frac{r_s^{t}}{r_a^{t}})},$$

(2c) $$E_s = [f_{wet} + (1 - f_{wet}) h^{{}^{VPD}/_{\beta}}] \frac{(s \times A_{soil} + \rho C_p (1 - f_c) {}^{VPD}/_{r_{as}})}{\lambda_v \rho_w (s + \gamma \frac{r_{tot}}{r_{as}})}.$$

Interception, transpiration, and soil evaporation are separated using fractional cover, f_c, calculated using $fAPAR$. The partitioned fluxes are constrained based on relative humidity (h), the fraction of wet surface (f_{wet}), and look-up table values of vegetation-dependent aerodynamic and surface resistances (r_a, r_s).

c. Global Land Evaporation Amsterdam Model (GLEAM)

Similarly to PT-JPL, GLEAM relies on a Priestley-Taylor framework to calculate potential ET. GLEAM uses a separate algorithm to calculate interception (E_i) based on a Gash analytical model (Gash, 1979; Valente et al., 1997) driven by precipitation observations. E_i estimates have been previously validated against field data independently (Miralles et al., 2010). The GLEAM model computes interception only for the tall canopy fraction within each pixel (see below).

Then soil evaporation (E_s), tall canopy transpiration (E_{tc}) and short canopy transpiration (E_{sc}) are calculated as

(3a) $$E_s = f_s S_s \alpha_s \frac{\Delta}{\lambda_v \rho_w (\Delta+\gamma)} (R_n^s - G_s)$$

(3b) $$E_{sc} = f_{sc} S_{sc} \alpha_{sc} \frac{\Delta}{\lambda_v \rho_w (\Delta+\gamma)} (R_n^{sc} - G_{sc}),$$

(3c) $$E_{tc} = f_{tc} S_{tc} \alpha_{tc} \frac{\Delta}{\lambda_v \rho_w (\Delta+\gamma)} (R_n^{tc} - G_{tc}) - E_i.$$

The transpiration (E_v) is then calculated as the sum of E_{sc} and E_{tc}. In equation (3a), (3b) and (3c), the partitioning of the evaporative flux into different components is based on the fractional vegetation cover (f). The fractional cover utilized is the MODIS Continuous Vegetation Fields product, MOD44B, which describes each pixel as a combination of bare soil, tall canopy, and short canopy vegetation (i.e. "s", "tc", and "sc", respectively). The model uses vegetation-dependent parameterizations of G as well as different values of α for each vegetation cover type. Characteristic albedo ratios per vegetation cover type come from look up tables and determine how R_n is distributed per cover fraction.

GLEAM model constrains the Priestley and Taylor potential evaporation estimates based on an evaporative stress factor. This stress factors, S, is parameterized separately for the bare soil, tall canopy, and short vegetation components based on soil moisture and vegetation phenology for the vegetated fractions (see Ss, Stc and Ssc in eq. (3a), (3b) and (3c), respectively).. The soil moisture is estimated based on a multilayer soil module driven by precipitation observations, and further optimized using a data assimilation system that incorporates observations of surface soil moisture (Martens et al., 2017, 2016). The transpiration stress associated with phenological changes is based on microwave vegetation optical depth, a proxy for vegetation water content (Miralles et al., 2011).

2.2.2 Field Validation Data

Field studies measuring the separate components of ET (i.e. soil evaporation, transpiration, and interception) are scarce. We utilized a set of studies previously consolidated by Schlesinger and Jasechko (2014) as well as additional studies containing annual values for transpiration and total ET. We then calculated soil evaporation as the residual of transpiration and total ET, assuming negligible interception. We compared the residual field estimate against modeled soil evaporation and the modeled residual (ET-T) and found that this assumption did not significantly influence the aggregate results of the study. These studies span several decades and use a variety of measurement techniques, primarily sap-flow measurements, isotope-based measurements, or meteorological models scaled using eddy-covariance and water balance models. Other studies have scaled measurements using biophysical models or through a water balance method to obtain canopy level values of transpiration and ET. Each field method suffers from their own set of assumption and is associated with some measurement error. Field study site locations are displayed in figure 2.1 and listed in table 2.1. Despite the range of spatial support and uncertainty related to each technique in the dataset, we believe that, in the aggregate, the field estimates offer a good means to evaluate the performance of the model estimates.

Some field studies within the dataset span only the growing season of a given year and may overestimate the ratio of transpiration to ET on an annual scale. Other studies span several years and report a single annual estimate for transpiration and ET fluxes. Field estimates are reported as annual values and are compared against the modeled annual means. Instances existed where separate field studies reported values for the same pixel, in which case the field estimates were averaged.

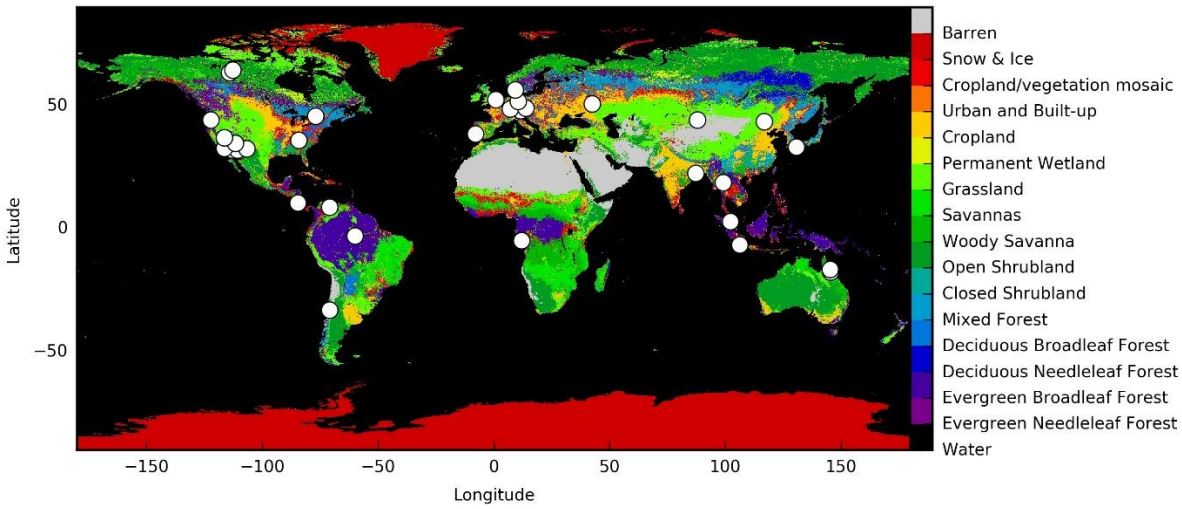

Figure 2.1: Map of field study locations (white circles) and associated IGBP land cover types. Land cover is derived from the MODIS-based MCD12Q1 product.

The field studies described above largely ignore evaporation of rainfall intercepted by the canopy. To validate the interception components of the models we used the dataset previously used in the validation of the GLEAM interception loss estimates (Miralles et al., 2010). This dataset includes studies estimating the interception of forested canopies and excludes field sites in grasslands or shrublands where herbaceous interception may occur. The field dataset describes the interception at a given site as a mean annual depth per area of canopy. In order to estimate the interception in a given pixel, we scaled each field value using the fraction of forested land cover described by the MCD12C1 land cover fraction product (NASA LP DAAC, Friedl, 2015). This does not account for the interception by herbaceous vegetation in non-forested areas, even though the rates of interception by short vegetation are expected to be comparatively much lower due to differences in aerodynamic conductance (David et al., 2005).

2.2.3 Model Forcing Data

For those input variables that are common to all three models, we used the WAter Cycle Observation Multi-mission Strategy - ET database (WACMOS-ET, http://wacmoset.estellus.eu/), which includes remote sensing derived surface meteorology and radiation fluxes (Michel et al., 2016; Miralles et al., 2016). In addition to the parameters already included in the WACMOS-ET forcing dataset, the PM-MOD model requires LAI, IGBP land cover, and $fAPAR$ as inputs while the PT-JPL model requires NDVI. The original WACMOS-ET dataset contains LAI and $fAPAR$ derived from the Joint Research Centre two-stream inversion package, but the values are not consistent with the MODIS derived LAI and $fAPAR$ that both PM-MOD and PT-JPL require. We used MODIS vegetation products (NASA LP DAAC, Didan, 2015) to supplement the WACMOS-ET data to force the PT-JPL and PM-MOD.

The input datasets vary in spatial and temporal resolution, but are re-sampled to a common 0.25° latitude x 0.25° longitude grid, and a 3-hourly temporal scale for PT-JPL and PM-MOD models, and a daily temporal scale for GLEAM. GLEAM no longer provides sub-daily estimates of ET, but PT-JPL requires maximum daily temperature and minimum daily humidity and is thus executed using the original 3-hourly forcing. In addition to the time variant fields, both GLEAM and PM-MOD require static fields. PM-MOD requires IGBP land cover values while GLEAM requires soil parameters derived from IGBP-DIS (Global Soil Task Group, 2014), and the MOD44B global vegetation continuous fields product.

2.3 Results:

We compared the modeled estimates for each ET component against the field study estimates at each location. Table 2.2 lists the r^2 correlation coefficient, the standard error, the percent mean bias deviation (% MBD), and the percent root mean squared deviation (% RMSD) across different models. Figure 2.2 shows linear regressions of the modeled estimates against the field estimates for each model and individual ET component.

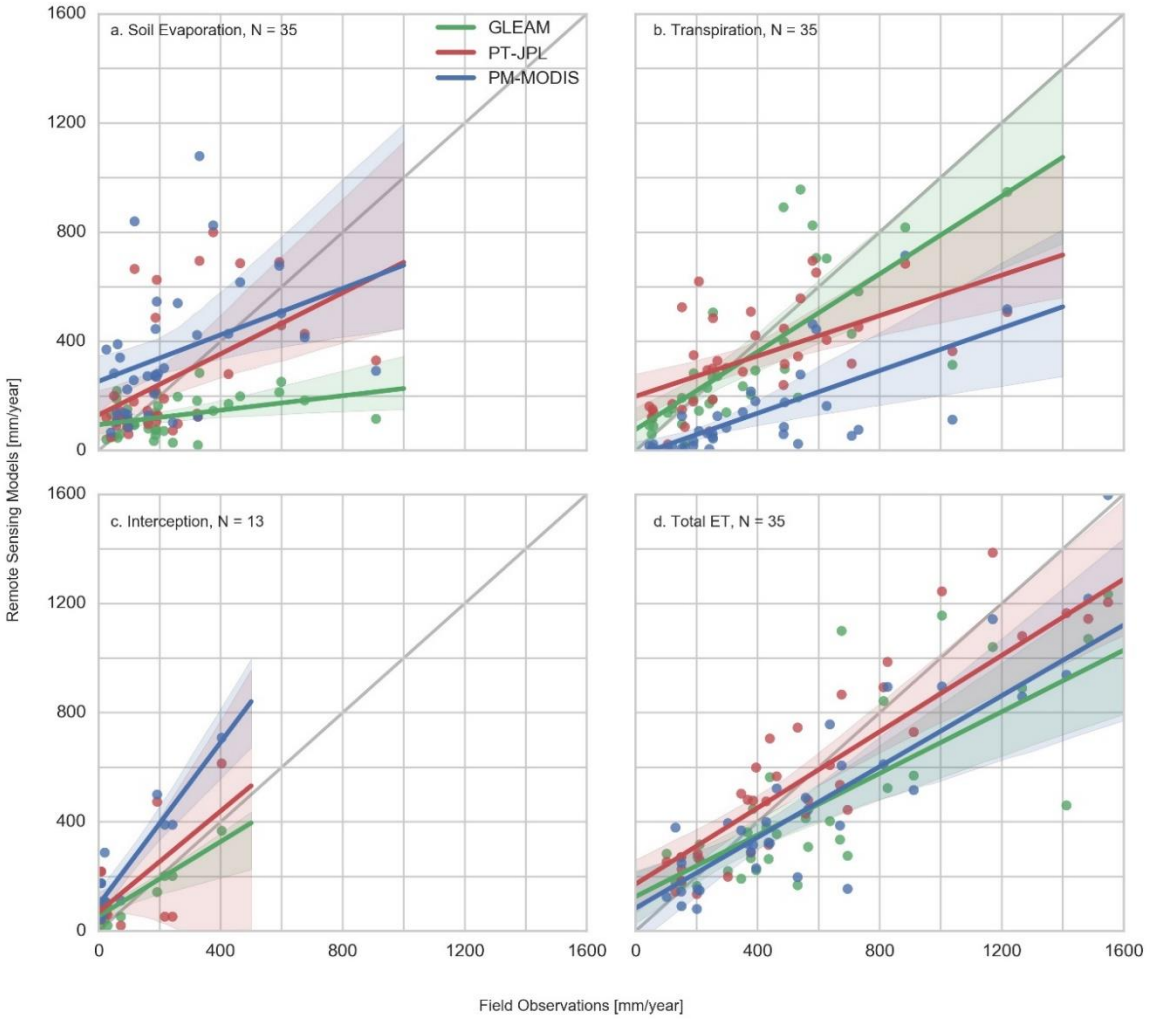

Figure 2.2: Comparison between modeled ET estimates and field observed estimates for (a) soil evaporation, (b) transpiration, (c) interception, and (d) total ET flux for each model. A regression is plotted with the 95% confidence interval for each model shaded. The grey line represents a perfect fit between field and modeled results.

Total ET results are comparable between models and show similar agreement with previous validations of total ET (Miralles et al., 2016). The modeled estimates generally overestimate the field estimates for small ET fluxes, and underestimate the field estimates at high values. Both PM-MOD and GLEAM show a tendency to underestimate the total flux, exhibiting a percent mean bias deviation (%MBD) of -21.6% and -20.9% respectively. PT-JPL ET estimates shows a %MBD of just -2.3%. The standard error exhibited by each model is very similar as are the overall trends. Comparatively, the modeled partitions show large discrepancies among themselves and agianst field data.

GLEAM offers the best results for estimating the transpiration flux, showing the lowest %RMSD, %MBD, and highest r^2 value. PT-JPL shows similar results to GLEAM for most statistics, except a lower correlation. The %MBD for the PM-MOD transpiration flux is -66.0%, which is substantially larger as compared to PT-JPL and GLEAM, where values of -10.7 % and -5.4 % are obtained respectively. The PT-JPL transpiration correlation ($r^2 = 0.33$) is much lower than previous validations of the transpiration component by Fisher et al. (2008) using sap flow estimates at three flux tower sites of alpine and sub-alpine climates. Compared to these three flux tower sites, our partitioning data spans a greater range of climate at a coarser temporal resolution. Recall that the slight underestimation of PT-JPL and GLEAM transpiration could be the result of certain field measurements reflecting only the growing season for a given year, rather than model deficiencies.

Both GLEAM ($r^2 = 0.82$) and PM-MOD ($r^2 = 0.85$) offer high correlations with field interception estimates. However, GLEAM shows lower RMSD (62.1%) and MBD (25.3%) as compared to PM-MOD (181.0% RMSD, 149.9% MBD). PT-JPL estimates of canopy interception compare poorly based on all statistical measures, resulting in an r^2 correlation of

only 0.39 and a RMSD of 157.4%. Overall, estimates of interception showed a large level of divergence with the field estimates for both PM-MOD and PT-JPL. Model estimates showed especially large errors where field estimates exhibited small fluxes or where the fraction of forest within the pixel was determined to be small. However, the small number of field interception studies (N=13) makes it difficult to definitively assess the model performance.

While the PT-JPL model provided the highest r^2 value and lowest RMSD for soil evaporation (89.8 %RMSD, r^2=0.25), the results are relatively poor compared to the transpiration estimates. Modeled estimates of soil evaporation were inaccurate across all models and displayed little agreement with the field estimates. GLEAM, while exhibiting a low standard error (0.05), consistently underestimated the flux of soil evaporation compared to the field results (-45.6 %MBD), which is mostly responsible for the bias in total ET exhibited by GLEAM. Conversely, PT-JPL estimates showed little bias (11.0 %MBD) and a relatively high standard error (0.17). PM-MOD performed poorly across all statistical measures, exhibiting a positive bias (49.4 %MBD).

Grouping the results by land cover type, water availability, and observational method allows us to identify how model performance changes across these groups. Figure 2.3 shows the relative error for each model estimate against field estimates categorized by land cover type. We consolidated IGBP land cover values into four new groupings: forests (IGBP #1-5), shrublands (IGBP #6-7), grasslands (IGBP #8-10), and cropland and urban (IGBP # 0, 11-16). An analysis of each IGBP classification individually was impractical given the small number of values in each land cover group.

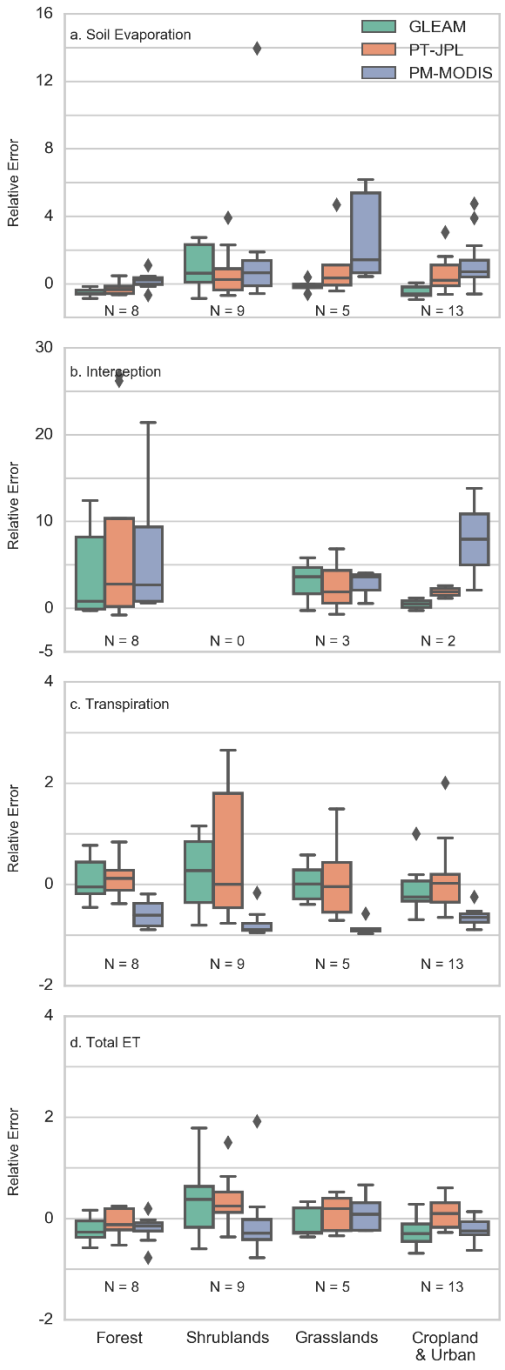

Figure 2.3: Relative error between modeled and field estimates based on IGBP land cover type classification from MODIS using the WACMOS-ET dataset. The original IGBP land cover types were consolidated into four groups: Forests (IGBP 1-5), Shrublands (6-7), Grasslands (8-10), and Cropland and Urban (0, 10-16).

GLEAM, when analyzed across land cover, generally shows more variance in shrublands and grasslands and comparatively little variance in forests. This is most evident in the GLEAM model estimates of soil evaporation, where the modeled estimates are extremely consistent in forests, less so in grasslands and croplands, and least in shrublands. As the GLEAM soil evaporation estimates become less consistent across these land cover types, the bias of these estimates shifts positively. A strong negative bias is evident in forests, and a positive one develops in shrublands. Similarly, the GLEAM model shows higher variance in its estimate errors of transpiration in shurblands and grasslands, and smaller variance in forests.

The differences between land cover types when considering interception become difficult to interpret because of the small amount of data in non-forested areas. The field interception dataset reports values exclusively from forests, so a non-forested land cover type for that location may suggest that the study site is not representative of the larger pixel. Apart from interception, PT-JPL and PM-MOD show little change in the bias of their estimates depending on land cover. Generally, all three models show a wider variation in estimate error in shrublands and grasslands than in forests.

Figure 2.4 shows the relative estimate error of each model across different precipitation regimes. Each model shows large errors in interception at low precipitation, with PM-MOD exhibiting large sensitivity to annual precipitation. The relative error of the GLEAM soil evaporation trends negatively with increasing precipitation as does the PT-JPL estimate of total ET.

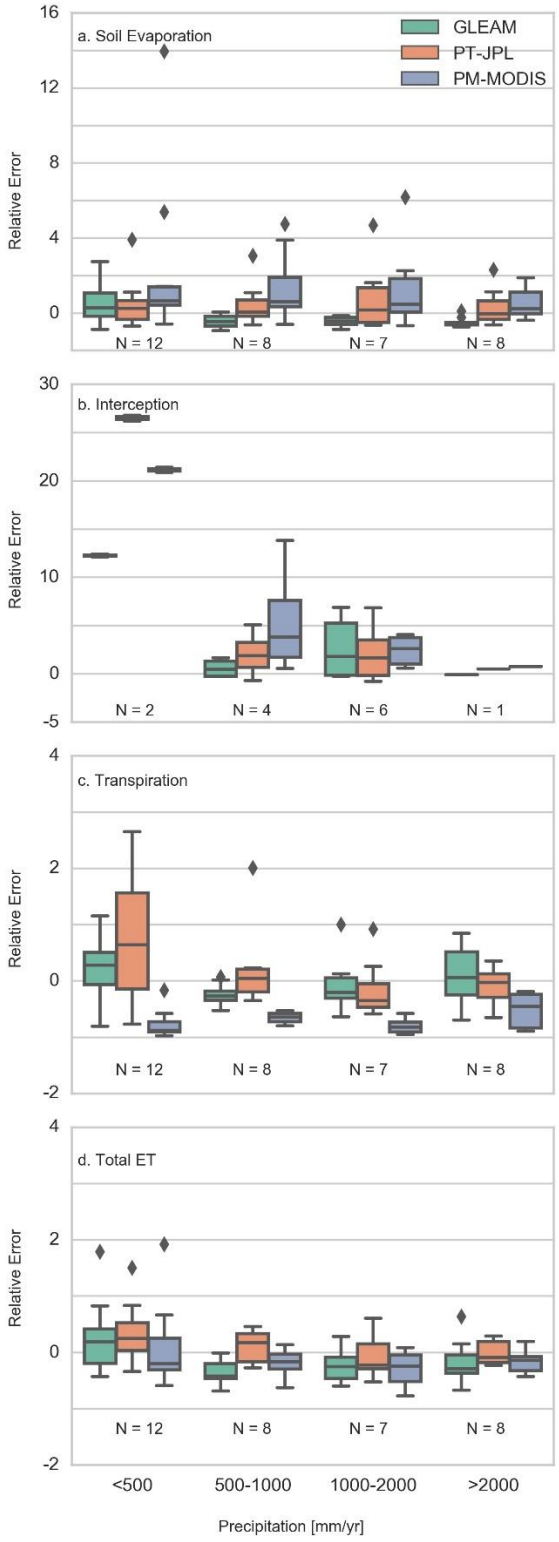

Figure 2.4: Relative error between modeled and field estimates separated into different precipitation regimes using the WACMOS-ET dataset.

Figure 2.5 shows the relative error of each model plotted by the field method used to partition ET. Estimates in soil evaporation are constant across field method, as are estimates in total ET to a lesser extent. Recall that soil evaporation is calculated as the residual of ET and transpiration, so that error in the observational method will be reflected in both transpiration and soil evaporation components. The PM-MOD transpiration estimates are also consistent, showing a clear negative bias regardless of field method. However, GLEAM and PT-JPL estimates vary slightly, while showing consistent estimates to one another.

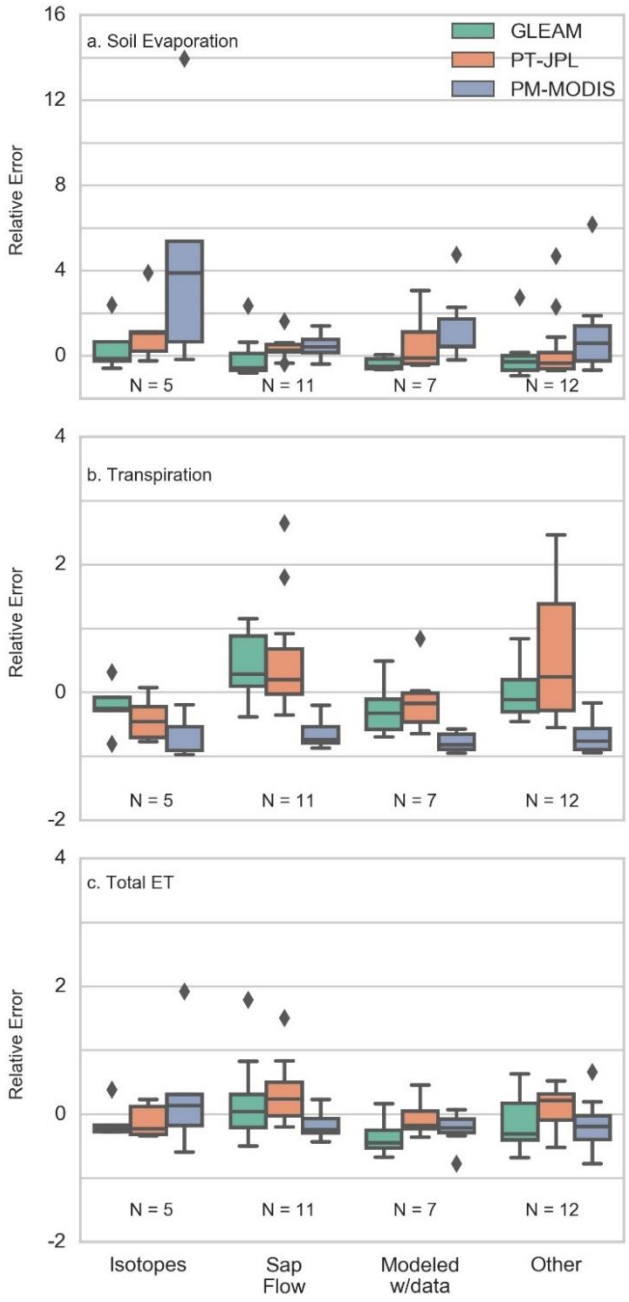

Figure 2.5: Relative error between field and modeled estimates separated by field method type. The field methods are discretized into five groups: Isotopes, Sap Flow, Modeled using collected and meteorological data, modeled using no meteorological data, and a miscellaneous group.

2.4 Discussion:

One of the inherent limitations in remote sensing-based evaluation studies is the challenge of acquiring independent observations that are representative of the scale of measurement. As such, we acknowledge that the spatial and temporal scale of the field-based estimates used in this study are not the ideal dataset for assessing the performance of these models, but few alternatives exists to estimate the individual components of ET. While eddy covariance observations are much better equipped for comparison with larger spatial fluxes and the finer temporal resolution of remote sensing-based ET products, they do not offer information regarding the individual components of ET. The field studies used in our analysis use a wide range of scaling techniques to acquire a canopy level ET measurement, and include eddy flux towers. Inevitably, some approaches are likely to be smaller in spatial scale than the satellite estimates, but, in the aggregate, still offer insight into how ET should be partitioned.

Our results show a moderate variation in total ET between each of the models, in agreement with previous studies (Michel et al., 2016; Miralles et al., 2016). However, the objective of this study is primarily the evaluation of the evaporation partitioning in these models. As large discrepancies exist between the separate fluxes estimated by different models, they are likely to overshadow the measurement error between field methods.

Clear patterns between modeled estimates are evident in the soil evaporation components of each model as well as the PM-MOD component of transpiration. This is illustrated in figure 2.5, where differences in modeled estimates are consistent regardless of the field method employed. PT-JPL and GLEAM estimates of transpiration show similar

results, while varying slightly across different field methods. This highlights the difficulties in disentangling the results of PT-JPL and GLEAM transpiration, given the errors that may exist in the field data. As such, we will only discuss where clear differences between models exist or where the models show large biases with respect to the field data.

Through rooting uptake, plants are able to utilize water for transpiration held in the soil long after rain events. Soil evaporation and interception are much more dependent on transient rain events, which increase water storage in the canopy or upper layer of soil that becomes available for fast evaporation (Williams et al., 2004; Yepez et al., 2005). The available water source for either flux also depends on the connectivity of that water to surface water or deeper soil stores (Good et al., 2015). The differences in water sources for separate evaporation components changes the fundamental nature of those processes and the modeling techniques and data required to capture these physical processes. While fine temporal sampling may be required to capture rain events contributing to soil evaporation and interception, it may not be required to capture transpiration rates.

The modeled soil evaporation shows little correlation with field estimates across all models. In addition, both PT-JPL and PM-MOD show large standard error in their estimates of soil evaporation. While the inability of model routines to fully capture the physical process of soil evaporation might be responsible for part of the total error, differences in the spatial and temporal scales of soil evaporation as compared to transpiration may contribute to larger standard error in the results of soil evaporation. Soil moisture dynamics have shown to vary significantly in time and space depending on the antecedent conditions (Grayson et al., 1997). Moreover, changes in the lateral or vertical movement of water in soil associated with these changes could affect the connectivity to surface water flows and the availability of water for

soil evaporation. Soil evaporation, being highly dependent on spatially variable soil moisture, could thus be disproportionately influenced by the differences in spatial scale between the field and modeled estimates. Additionally, different model representations of ground heat flux directly contribute to uncertainties in soil evaporation (Purdy et al., 2016).

Estimates of soil evaporation from GLEAM clearly underestimate the field measurements. The relative error in soil evaporation estimates is highly correlated with the MOD44B products, showing a tendency to underestimate field measurements corresponding with areas of higher fraction of vegetation and lower bare soil. This arises due to the fact that GLEAM only considers soil evaporation from bare soil and does not estimate the soil evaporation occurring under the canopy or under herbaceous vegetation. The higher correlation of the estimate error with herbaceous vegetation than tall canopy suggests that the underestimation of soil evaporation by GLEAM is more significant in areas of herbaceous vegetation. Figures 2.3 and 2.4 further corroborate this results. The underestimation in soil evaporation is most apparent in forested land cover and shows a negative relationship with increasing rainfall. As shown in Figure 2.2, this causes most of the underestimation in the GLEAM estimates of total ET.

PM-MOD and PT-JPL share their approach to scale the soil evaporation using observations of relative humidity and vapor pressure deficit. As a result, they largely show similar estimates of soil evaporation, and similar validation statistics. Therefore, different parameters must cause the divergences found in the soil evaporation products of PT-JPL and PM-MOD. Differences in the Penman-Monteith and Priestley-Taylor models often depend on the parametrization of α in the Priestley-Taylor equation and resistance factors in the Penman-Monteith equation. The largest deviations between Penman-Monteith and Priestley-Taylor ET

estimation occur when aerodynamic resistances and net radiation are small and VPD is high (Komatsu, 2005). Given the similarities between the model routines and output, it seems that the poor performance of the soil evaporation component likely stems from their shared assumptions.

PT-JPL and PM-MOD, by excluding precipitation and using relative humidity as a metric of a system's overall moisture, may see significant errors when soil and air moisture are in a state of disequilibrium. VPD and RH are correlated with soil moisture over weekly to seasonal time scales, but become decoupled over shorter time periods (Novick et al., 2016). Soil evaporation, more so than transpiration, may occur over shorter time periods following precipitation events. The use of humidity-based functions to account for water availability could explain the large standard error of the PM-MOD and PT-JPL soil evaporation component. However, spatial differences in the field and remote sensing-based products could also be culpable for the error. Higher frequency observations of ET partitioning are needed to better understand short-term dynamic changes in partitioning and how to reflect these dynamics within models.

Furthermore, soil moisture has been found to have a non-linear relationship with soil evaporation that can be characterized in two stages. The first stage is characterized by capillary transport, which sustains moisture at the soil surface. During the second stage, drying disrupts the hydraulic pathways within the soil and the vaporization plane moves below the soil surface, resulting in a significant reduction in soil evaporation (Haghighi and Or, 2013; Or et al., 2013). The point at which drying soils shift between stages of evaporation is largely dependent on physical soil characteristics and pore size and can cause dynamic shifts at hourly time scales in evaporation resistances (Aminzadeh and Or, 2017; Decker et al., 2017; Merlin et al., 2016).

Neither PT-JPL nor PM-MOD consider soil properties in their estimate of soil evaporation, while GLEAM uses field capacity and wilting point to determine stress factors. The non-consideration of soil properties could be contributing to the large standard error in those soil evaporation estimates.

The transpiration estimates of both PT-JPL and GLEAM show better agreement with field estimates than their respective soil evaporation estimates. Partitioning research has shown transpiration to be the dominate flux of total ET (Jasechko et al., 2013). Therefore, the transpiration estimate of the model is critical in the models' ability to estimate total ET. Transpiration estimation and vegetation modeling represent research areas where remote sensing provides tremendous utility. The large degree of variability in plant species and size make ground measurements of canopy scale interaction difficult. The use of vegetation indices derived from remotely sensed products are much more advantageous for measuring heterogeneous vegetation and biophysical processes such as transpiration (Glenn et al., 2008).

PM-MOD strongly underestimates the transpiration flux estimated by field techniques. The only vegetation parameter used by PM-MOD is the fraction of absorbed photosynthetically active radiation, $fAPAR$, along with surface and aerodynamic resistances from the literature based on IGBP land cover type. These resistances can be very difficult to parameterize, and look-up table values do not reflect the temporal variability in these resistances. However, since the underestimation is consistent across all land cover types, it seems more likely that the use of $fAPAR$ is driving the transpiration bias. Since PM-MOD uses $fAPAR$ to partition radiation, the accuracy of the model may vary seasonally as phenology changes.

GLEAM performed very well at capturing the field interception estimates, as shown in previous studies (Miralles, 2010). Interception has been studied extensively, but little information exists on interception rates outside of densely forested ecosystems. While GLEAM models interception only for the tall canopy fraction of the pixel, the other models estimate interception outside of forests based on leaf area index and $fAPAR$. Interception losses outside of forests are likely small relative to total ET fluxes (David et al., 2005), but the value of including this interception remains unknown, given that few field measurements exist outside of forests.

Comparisons of interception estimates across Amazonia conducted by Miralles et al. (2016) found that PT-JPL and PM-MOD estimates (based on the WACMOS-ET vegetation properties as input) nearly doubled the interception rates of GLEAM and field-measured values found in the literature. Furthermore, interception has been shown to correlate strongly with both rainfall intensity and volume as they relate to canopy storage capacity (Pypker et al., 2005). PM-MOD and PT-JPL lack a canopy storage parameter, instead electing to use humidity as a proxy for surface wetness, and do not use precipitation as a forcing parameter. By not defining a storage capacity for the vegetation in PM-MOD and PT-JPL, the models could overestimate the flux for rain events exceeding the canopy storage. While PM-MOD and PT-JPL rely heavily on radiation as main driver of interception, field studies have shown that the flux of interception loss is partly decoupled from the available energy (Holwerda et al., 2011). In that sense, GLEAM likely provides better remote sensing-based estimates of interception, as it builds upon the knowledge gained in ground-based research on interception, which identifies vegetation characteristics and rainfall properties as the main determinants of the flux (Gash, 1979).

2.5 Conclusion:

While this study attempted to validate the individual components of ET, little reliable data for these individual fluxes exists. Given the paucity of field datasets, it is difficult to draw definite conclusions on the sources of error within the modelled estimates of partitioned ET fluxes. While estimates diverge significantly between models, and modeled error is likely driving the bulk of the discrepancy with field partition estimates, the field methods themselves are also prone to errors. Furthermore, it is difficult to assess if the modeled estimates deviate due to the differences in model structure, or because of different forcing datasets and errors inherent in the forcing data. Given the multiple sources of potential error, it was challenging to determine to what magnitude we could attribute partitioning error to model methodology.

Remote sensing-based models will continue to play a dominant role in future ET research and its global implications (Fisher et al., 2017; Zhang et al., 2017). Improved spatial resolution and spectral availability of remote sensing products will undoubtedly provide a glut of modeled ET data for future researchers (Marshall et al., 2016; McCabe et al., 2017; Sun et al., 2017). However, the relative dearth of reliable field estimates for transpiration, soil evaporation, and interception inhibits quantifying the accuracy and applications of remote sensing-based ET estimates. Clearly, observations of the individual ET components are necessary to constrain ET models and improve ET accuracy for future research into climate and hydrologic dynamics. The consolidation of a global dataset of sap flux measurements (Poyatos et al., 2016) will undoubtedly present tremendous utility in validating remote sensing-based models and contribute to the advancement of ET science.

The results of this study present the first steps towards the validation of ET partitioning within remote sensing-based models. Our analysis shows that remote sensing-based ET

models, despite showing similar and quite accurate total ET retrievals, produce estimates of individual components that deviate significantly from field measurements. Even for locations where the total ET is accurately modeled, the modeled components show significant deviations from observations. The uncertainty of the ET partitioning may cause model estimates to deteriorate when applied more broadly across space and time.

In particular, we find that:

- PM-MOD showed a strong negative bias in its transpiration estimate that caused a negative bias in the total ET estimate. The bias is likely related to the scaling parameters of the canopy, as PM-MOD relates the absorbed PAR linearly to the transpiration rate.

- Model estimates of soil evaporation showed little correlation with field estimates across all models. GLEAM exhibited a strong negative bias likely due to the non-consideration of below-canopy soil evaporation. Both PM-MOD and PT-JPL also exhibited large standard error in their estimates of soil evaporation.

- The quality of the interception estimates outside of forests was not assessed. GLEAM showed good agreement with the field data over forests, while PT-JPL and PM-MOD showed larger divergences. The non-consideration of rainfall and canopy storage capacity in PT-JPL and PM-MOD, and the direct dependency of interception loss on radiation, are the most likely causes for the disagreement with the field data.

- Finally, our results confirm that caution should be taken when applying any of these models in isolation, as long as the goal of the study relies heavily on the models partitioning of ET fluxes.

Data Availability

The field observations and remote sensing datasets used in this study are all derived from previously published work.

The WACMOS-ET Reference Input Data Set was provided courtesy of the WACMOS-ET project and Estellus. http://wacmoset.estellus.eu/index.php?static9/data

The MOD12C1 data product was retrieved from the online Data Pool, courtesy of the NASA Land Processes Distributed Active Archive Center (LP DAAC), USGS/Earth Resources Observation and Science (EROS) Center, Sioux Falls, South Dakota, https://lpdaac.usgs.gov/data_access/data_pool

The MOD15A2 data product was retrieved from the AppEEARS data page, courtesy of the NASA Earth Observing System Data and Information System(EOSDIS) and the Land Processing Distributed Active Archive Center (LP DAAC), USGS/Earth Resources Observation and Science (EROS) Center, Sioux Falls, South Dakota, https://lpdaacsvc.cr.usgs.gov/appeears

Acknowledgements

CT and SPG acknowledge the support of the Betty Minor scholarship. JBF contributed to this research from the Jet Propulsion Laboratory, California Institute of Technology, under a contract with the National Aeronautics and Space Administration. California Institute of Technology. Government sponsorship acknowledged. JBF was supported in part by NASA's SUSMAP, INCA, IDS, GRACE, and ECOSTRESS programs. MFM was supported by the

King Abdullah University of Science and Technology. DGM acknowledges support from the European Research Council (ERC) under grant agreement n° 715254 (DRY–2–DRY).

References:

Adler, R.F., Huffman, G.J., Chang, A., Ferraro, R., Xie, P.-P., Janowiak, J., Rudolf, B., Schneider, U., Curtis, S., Bolvin, D., Gruber, A., Susskind, J., Arkin, P., Nelkin, E., Adler, R.F., Huffman, G.J., Chang, A., Ferraro, R., Xie, P.-P., Janowiak, J., Rudolf, B., Schneider, U., Curtis, S., Bolvin, D., Gruber, A., Susskind, J., Arkin, P., Nelkin, E., 2003. The Version-2 Global Precipitation Climatology Project (GPCP) Monthly Precipitation Analysis (1979–Present). J. Hydrometeorol. 4, 1147–1167. doi:10.1175/1525-7541(2003)004<1147:TVGPCP>2.0.CO;2

Allen, C.D., Macalady, A.K., Chenchouni, H., Bachelet, D., McDowell, N., Vennetier, M., Kitzberger, T., Rigling, A., Breshears, D.D., Hogg, E.H. (Ted), Gonzalez, P., Fensham, R., Zhang, Z., Castro, J., Demidova, N., Lim, J.-H., Allard, G., Running, S.W., Semerci, A., Cobb, N., 2010. A global overview of drought and heat-induced tree mortality reveals emerging climate change risks for forests. For. Ecol. Manage. 259, 660–684. doi:10.1016/J.FORECO.2009.09.001

Aminzadeh, M., Or, D., 2017. Pore-scale study of thermal fields during evaporation from drying porous surfaces. Int. J. Heat Mass Transf. 104, 1189–1201. doi:10.1016/J.IJHEATMASSTRANSFER.2016.09.039

Anderson, M.C., Norman, J.M., Mecikalski, J.R., Otkin, J.A., Kustas, W.P., 2007. A climatological study of evapotranspiration and moisture stress across the continental United States based on thermal remote sensing: 1. Model formulation. J. Geophys. Res. 112, D10117. doi:10.1029/2006JD007506

Badgley, G., Fisher, J.B., Jiménez, C., Tu, K.P., Vinukollu, R., Badgley, G., Fisher, J.B., Jiménez, C., Tu, K.P., Vinukollu, R., 2015. On Uncertainty in Global Terrestrial Evapotranspiration Estimates from Choice of Input Forcing Datasets*. J. Hydrometeorol. 16, 1449–1455. doi:10.1175/JHM-D-14-0040.1

Baldocchi, D., Falge, E., Gu, L., Olson, R., Hollinger, D., Running, S., Anthoni, P., Bernhofer, C., Davis, K., Evans, R., Fuentes, J., Goldstein, A., Katul, G., Law, B., Lee, X., Malhi, Y., Meyers, T., Munger, W., Oechel, W., Paw, K.T., Pilegaard, K., Schmid, H.P., Valentini, R., Verma, S., Vesala, T., Wilson, K., Wofsy, S., Hall, R., 2001. FLUXNET: A New Tool to Study the Temporal and Spatial Variability of Ecosystem-Scale Carbon Dioxide, Water Vapor, and Energy Flux Densities 82.

Bonan, G.B., 2008. Forests and climate change: forcings, feedbacks, and the climate benefits of forests. Science 320, 1444–9. doi:10.1126/science.1155121

Brunel, J.P., Walker, G.R., Dighton, J.C., Montenya, B., 1997. Use of stable isotopes of water to determine the origin of water used by the vegetation and to partition evapotranspiration. A case study from HAPEX-Sahel. J. Hydrol. 188–189, 466–481. doi:10.1016/S0022-1694(96)03188-5

Carlyle-Moses, D.E., Gash, J.H.C., 2011. Rainfall Interception Loss by Forest Canopies. Springer, Dordrecht, pp. 407–423. doi:10.1007/978-94-007-1363-5_20

Cavanaugh, M.L., Kurc, S.A., Scott, R.L., 2011. Evapotranspiration partitioning in semiarid shrubland ecosystems: a two-site evaluation of soil moisture control on transpiration. Ecohydrology 4, 671–681. doi:10.1002/eco.157

Ciais, P., Reichstein, M., Viovy, N., Granier, A., Ogée, J., Allard, V., Aubinet, M., Buchmann, N., Bernhofer, C., Carrara, A., Chevallier, F., De Noblet, N., Friend, A.D., Friedlingstein, P., Grünwald, T., Heinesch, B., Keronen, P., Knohl, A., Krinner, G., Loustau, D., Manca, G., Matteucci, G., Miglietta, F., Ourcival, J.M., Papale, D., Pilegaard, K., Rambal, S., Seufert, G., Soussana, J.F., Sanz, M.J., Schulze, E.D., Vesala, T., Valentini, R., 2005. Europe-wide reduction in primary productivity caused by the heat and drought in 2003. Nature 437, 529–533. doi:10.1038/nature03972

Crockford, R.H., Richardson, D.P., 2000. Partitioning of rainfall into throughfall, stemflow and interception: effect of forest type, ground cover and climate. Hydrol. Process. 14, 2903–2920. doi:10.1002/1099-1085(200011/12)14:16/17<2903::AID-HYP126>3.0.CO;2-6

David, J.S., Valente, F., Gash, J.H., 2005. Evaporation of Intercepted Rainfall, in: Encyclopedia of Hydrological Sciences. John Wiley & Sons, Ltd, Chichester, UK. doi:10.1002/0470848944.hsa046

Decker, M., Or, D., Pitman, A., Ukkola, A., 2017. New turbulent resistance parameterization for soil evaporation based on a pore-scale model: Impact on surface fluxes in CABLE. J. Adv. Model. Earth Syst. 9, 220–238. doi:10.1002/2016MS000832

Dee, D., Uppala, M.S., Simmons, J.A., Berrisford, P., Poli, P., Kobayashi, S., Andrae, U., Balmaseda, A.M., Balsamo, G., Bauer, P., Bechtold, P., Beljaars, M.A.C., van de Berg, L., Bidlot, J., Bormann, N., Delsol, C., Dragani, R., Fuentes, M., Geer, J.A., Haimberger, L., Healy, B.S., Hersbach, H., Holm, V.E., Isaksen, L., Kallberg, P., Khaler, M., Matricardi, M., McNally, P.A., Monge-Sanz, M.B., Morcrette, .J., Park, B.K., Peubey, C., de Rosnay, P., Tovolato, C., Thapaut, J.N., Vitart, F., 2011. The ERA-Interim reanalysis: configuration and performance of the data assimilation system. R. Meteorol. Soc. 137, 553–597. doi:10.1002/qj.828

Demaria, E.M., Nijssen, B., Wagener, T., 2007. Monte Carlo sensitivity analysis of land surface parameters using the Variable Infiltration Capacity model. J. Geophys. Res. 112, D11113. doi:10.1029/2006JD007534

Didan, K., 2015. MOD13A2 MODIS/Terra Vegetation Indices 16-Day L3 Global 1km SIN GRID V006 [Dataset]. doi:10.5067/MODIS/MOD13A2.006

Dolman, A.J., Miralles, D.G., de Jeu, R.A.M., 2014. Fifty years since Monteith's 1965 seminal paper: the emergence of global ecohydrology. Ecohydrology 7, 897–902. doi:10.1002/eco.1505

Dye, P.J., Olbrich, B.W., Poulter, A.G., 1991. The Influence of Growth Rings in Pinus patula on Heat Pulse Velocity and Sap Flow Measurement. J. Exp. Bot. 42, 867–870. doi:10.1093/jxb/42.7.867

Ek, M.B., Holtslag, A.A.M., 2004. Influence of Soil Moisture on Boundary Layer Cloud Development. J. Hydrometeorol. 5, 86–99. doi:10.1175/1525-7541(2004)005<0086:IOSMOB>2.0.CO;2

Ershadi, A., Mccabe, M.F., Evans, J.P., Wood, E.F., 2015. Impact of model structure and parameterization on Penman-Monteith type evaporation models. J. Hydrol. 525, 521–535. doi:10.1016/j.jhydrol.2015.04.008

Fernández, J.E., Durán, P.J., Palomo, M.J., Diaz-Espejo, A., Chamorro, V., Girón, I.F., 2006.

Calibration of sap flow estimated by the compensation heat pulse method in olive, plum and orange trees: relationships with xylem anatomy. Tree Physiol. 26, 719–28.
Fisher, J.B., Melton, F., Middleton, E., Hain, C., Anderson, M., Allen, R., McCabe, M.F., Hook, S., Baldocchi, D., Townsend, P.A., Kilic, A., Tu, K., Miralles, D.D., Perret, J., Lagouarde, J.-P., Waliser, D., Purdy, A.J., French, A., Schimel, D., Famiglietti, J.S., Stephens, G., Wood, E.F., 2017. The future of evapotranspiration: Global requirements for ecosystem functioning, carbon and climate feedbacks, agricultural management, and water resources. Water Resour. Res. 53, 2618–2626. doi:10.1002/2016WR020175
Fisher, J.B., Tu, K.P., Baldocchi, D.D., 2008. Global estimates of the land–atmosphere water flux based on monthly AVHRR and ISLSCP-II data, validated at 16 FLUXNET sites. Remote Sens. Environ. 112, 901–919. doi:10.1016/J.RSE.2007.06.025
Friedl, M.A., Sulla-Menashe, D., Tan, B., Schneider, A., Ramankutty, N., Sibley, A., Huang, X., 2009. MODIS Collection 5 global land cover: Algorithm refinements and characterization of new datasets. doi:10.1016/j.rse.2009.08.016
Friedlingstein, P., Meinshausen, M., Arora, V.K., Jones, C.D., Anav, A., Liddicoat, S.K., Knutti, R., Friedlingstein, P., Meinshausen, M., Arora, V.K., Jones, C.D., Anav, A., Liddicoat, S.K., Knutti, R., 2014. Uncertainties in CMIP5 Climate Projections due to Carbon Cycle Feedbacks. J. Clim. 27, 511–526. doi:10.1175/JCLI-D-12-00579.1
Gash, J.H.C., 1979. An analytical model of rainfall interception by forests. Q. J. R. Meteorol. Soc. 105, 43–55. doi:10.1002/qj.49710544304
Gibson, J.J., Edwards, T.W.D., 2002. Regional water balance trends and evaporation-transpiration partitioning from a stable isotope survey of lakes in northern Canada. Global Biogeochem. Cycles 16, 10-1-10–14. doi:10.1029/2001GB001839
Glenn, E.P., Huete, A.R., Nagler, P.L., Hirschboeck, K.K., Brown, P., 2007. Integrating Remote Sensing and Ground Methods to Estimate Evapotranspiration. CRC. Crit. Rev. Plant Sci. 26, 139–168. doi:10.1080/07352680701402503
Glenn, E.P., Huete, A.R., Nagler, P.L., Nelson, S.G., 2008. Relationship Between Remotely-sensed Vegetation Indices, Canopy Attributes and Plant Physiological Processes: What Vegetation Indices Can and Cannot Tell Us About the Landscape. Sensors 8, 2136–2160. doi:10.3390/s8042136
Good, S.P., Moore, G.W., Miralles, D.G., 2017. A mesic maximum in biological water use demarcates biome sensitivity to aridity shifts. Nat. Ecol. Evol. 1, 1883–1888. doi:10.1038/s41559-017-0371-8
Good, S.P., Noone, D., Bowen, G., 2015. Hydrologic connectivity constrains partitioning of global terrestrial water fluxes. Science 349, 175–7. doi:10.1126/science.aaa5931
Goulden, M.L., Bales, R.C., 2014. Mountain runoff vulnerability to increased evapotranspiration with vegetation expansion. Proc. Natl. Acad. Sci. U. S. A. 111, 14071–5. doi:10.1073/pnas.1319316111
Grayson, R.B., Western, A.W., Chiew, F.H.S., Bloschl, G., 1997. Preferred states in spatial soil moisture patterns: Local and nonlocal controls. Water Resour. Res. 33, 2897–2908.
Haghighi, E., Or, D., 2013. Evaporation from porous surfaces into turbulent airflows: Coupling eddy characteristics with pore scale vapor diffusion. Water Resour. Res. 49, 8432–8442. doi:10.1002/2012WR013324
Hammersley, J.M., Handscomb, D.C., 1964. General Principles of the Monte Carlo Method, in: Monte Carlo Methods. Springer Netherlands, Dordrecht, pp. 50–75. doi:10.1007/978-94-009-5819-7_5

Hobbins, M.T., Ramírez, J.A., Brown, T.C., 2004. Trends in pan evaporation and actual evapotranspiration across the conterminous U.S.: Paradoxical or complementary? Geophys. Res. Lett. doi:10.1029/2004GL019846

Holwerda, F., Bruijnzeel, L.A., Scatena, F.N., 2011. Comparison of passive fog gauges for determining fog duration and fog interception by a Puerto Rican elfin cloud forest. Hydrol. Process. 25, 367–373. doi:10.1002/hyp.7641

Hu, Z., Yu, G., Zhou, Y., Sun, X., Li, Y., Shi, P., Wang, Y., Song, X., Zheng, Z., Zhang, L., Li, S., 2009. Partitioning of evapotranspiration and its controls in four grassland ecosystems: Application of a two-source model. Agric. For. Meteorol. 149, 1410–1420. doi:10.1016/J.AGRFORMET.2009.03.014

Hulley, G., Hook, S., Fisher, J., Lee, C., 2017. ECOSTRESS, A NASA Earth-Ventures Instrument for studying links between the water cycle and plant health over the diurnal cycle, in: 2017 IEEE International Geoscience and Remote Sensing Symposium (IGARSS). IEEE, pp. 5494–5496. doi:10.1109/IGARSS.2017.8128248

Huntington, T.G., 2006. Evidence for intensification of the global water cycle: Review and synthesis. J. Hydrol. 319, 83–95. doi:10.1016/J.JHYDROL.2005.07.003

Jasechko, S., Sharp, Z.D., Gibson, J.J., Birks, S.J., Yi, Y., Fawcett, P.J., 2013. Terrestrial water fluxes dominated by transpiration. Nature 496, 347–350. doi:10.1038/nature11983

Komatsu, H., 2005. Forest categorization according to dry-canopy evaporation rates in the growing season: comparison of the Priestley-Taylor coefficient values from various observation sites. Hydrol. Process. 19, 3873–3896. doi:10.1002/hyp.5987

Kumar, S., Holmes, T., Mocko, D.M., Wang, S., Peters-Lidard, C., 2018. Attribution of Flux Partitioning Variations between Land Surface Models over the Continental U.S. Remote Sens. 10. doi:10.3390/rs10050751

Lautz, L.K., 2008. Estimating groundwater evapotranspiration rates using diurnal water-table fluctuations in a semi-arid riparian zone. Hydrogeol. J. 16, 483–497. doi:10.1007/s10040-007-0239-0

Lawrence, D.M., Thornton, P.E., Oleson, K.W., Bonan, G.B., Lawrence, D.M., Thornton, P.E., Oleson, K.W., Bonan, G.B., 2007. The Partitioning of Evapotranspiration into Transpiration, Soil Evaporation, and Canopy Evaporation in a GCM: Impacts on Land–Atmosphere Interaction. J. Hydrometeorol. 8, 862–880. doi:10.1175/JHM596.1

Levia, D.F., Frost, E.E., 2006. Variability of throughfall volume and solute inputs in wooded ecosystems. Prog. Phys. Geogr. 30, 605–632. doi:10.1177/0309133306071145

Littell, J.S., Peterson, D.L., Riley, K.L., Liu, Y., Luce, C.H., 2016. A review of the relationships between drought and forest fire in the United States. Glob. Chang. Biol. 22, 2353–2369. doi:10.1111/gcb.13275

Mancosu, N., Snyder, R., Kyriakakis, G., Spano, D., 2015. Water Scarcity and Future Challenges for Food Production. Water 7, 975–992. doi:10.3390/w7030975

Marshall, K.N., Cooper, D.J., Hobbs, N.T., 2014. Interactions among herbivory, climate, topography and plant age shape riparian willow dynamics in northern Yellowstone National Park, USA. J. Ecol. 102, 667–677. doi:10.1111/1365-2745.12225

Marshall, M., Thenkabail, P., Biggs, T., Post, K., 2016. Hyperspectral narrowband and multispectral broadband indices for remote sensing of crop evapotranspiration and its components (transpiration and soil evaporation). Agric. For. Meteorol. 218219, 122–134. doi:10.1016/j.agrformet.2015.12.025

Martens, B., Miralles, D., Lievens, H., Fernández-Prieto, D., Verhoest, N.E.C., 2016.

Improving terrestrial evaporation estimates over continental Australia through assimilation of SMOS soil moisture. Int. J. Appl. Earth Obs. Geoinf. 48, 146–162. doi:10.1016/J.JAG.2015.09.012

Martens, B., Miralles, D.G., Lievens, H., van der Schalie, R., de Jeu, R.A.M., Fernández-Prieto, D., Beck, H.E., Dorigo, W.A., Verhoest, N.E.C., 2017. GLEAM v3: satellite-based land evaporation and root-zone soil moisture. Geosci. Model Dev. 10, 1903–1925. doi:10.5194/gmd-10-1903-2017

McCabe, M.F., Aragon, B., Houborg, R., Mascaro, J., 2017. CubeSats in Hydrology: Ultrahigh-Resolution Insights Into Vegetation Dynamics and Terrestrial Evaporation. Water Resour. Res. 53, 10017–10024. doi:10.1002/2017WR022240

Mccabe, M.F., Ershadi, A., Jimenez, C., Miralles, D.G., Michel, D., Wood, E.F., 2016. The GEWEX LandFlux project: evaluation of model evaporation using tower-based and globally gridded forcing data. Geosci. Model Dev 9, 283–305. doi:10.5194/gmd-9-283-2016

Mccabe, M.F., Rodell, M., Alsdorf, D.E., Miralles, D.G., Uijlenhoet, R., Wagner, W., Lucieer, A., Houborg, R., Verhoest, N.E.C., Franz, T.E., Shi, J., Gao, H., Wood, E.F., 2017. The future of Earth observation in hydrology. Earth Syst. Sci 215194, 3879–3914. doi:10.5194/hess-21-3879-2017

McJannet, D., Fitch, P., Disher, M., Wallace, J., 2007. Measurements of transpiration in four tropical rainforest types of north Queensland, Australia. Hydrol. Process. 21, 3549–3564. doi:10.1002/hyp.6576

Meng, X.H., Evans, J.P., McCabe, M.F., Meng, X.H., Evans, J.P., McCabe, M.F., 2014. The Impact of Observed Vegetation Changes on Land–Atmosphere Feedbacks During Drought. J. Hydrometeorol. 15, 759–776. doi:10.1175/JHM-D-13-0130.1

Merlin, O., Stefan, V.G., Amazirh, A., Chanzy, A., Ceschia, E., Er-Raki, S., Gentine, P., Tallec, T., Ezzahar, J., Bircher, S., Beringer, J., Khabba, S., 2016. Modeling soil evaporation efficiency in a range of soil and atmospheric conditions using a meta-analysis approach. Water Resour. Res. doi:10.1002/2015WR018233

Michel, D., Jiménez, C., Miralles, D.G., Jung, M., Hirschi, M., Ershadi, A., Martens, B., Mccabe, M.F., Fisher, J.B., Mu, Q., Seneviratne, S.I., Wood, E.F., Fernández-Prieto, D., 2016. The WACMOS-ET project – Part 1: Tower-scale evaluation of four remote-sensing-based evapotranspiration algorithms. Hydrol. Earth Syst. Sci 20, 803–822. doi:10.5194/hess-20-803-2016

Miralles, D.G., Gash, J.H., Holmes, T.R.H., De Jeu, R.A.M., Dolman, A.J., 2010. Global canopy interception from satellite observations. J. Geophys. Res 115. doi:10.1029/2009JD013530

Miralles, D.G., Holmes, T.R.H., De Jeu, R.A.M., Gash, J.H., Meesters, A.G.C.A., Dolman, A.J., 2011. Global land-surface evaporation estimated from satellite-based observations. Hydrol. Earth Syst. Sci 15, 453–469. doi:10.5194/hess-15-453-2011

Miralles, D.G., Jiménez, C., Jung, M., Michel, D., Ershadi, A., McCabe, M.F., Hirschi, M., Martens, B., Dolman, A.J., Fisher, J.B., Mu, Q., Seneviratne, S.I., Wood, E.F., Fernaìndez-Prieto, D., 2016. The WACMOS-ET project – Part 2: Evaluation of global terrestrial evaporation data sets. Hydrol. Earth Syst. Sci. Discuss. 12, 10651–10700. doi:10.5194/hessd-12-10651-2015

Molden, D., Oweis, T., Steduto, P., Bindraban, P., Hanjra, M.A., Kijne, J., 2010. Improving agricultural water productivity: Between optimism and caution. Agric. Water Manag.

97, 528–535. doi:10.1016/J.AGWAT.2009.03.023
Mu, Q., Zhao, M., Running, S.W., 2011. Improvements to a MODIS global terrestrial evapotranspiration algorithm. Remote Sens. Environ. 115, 1781–1800. doi:10.1016/j.rse.2011.02.019
Mueller, B., Seneviratne, S.I., Jimenez, C., Corti, T., Hirschi, M., Balsamo, G., Ciais, P., Dirmeyer, P., Fisher, J.B., Guo, Z., Jung, M., Maignan, F., McCabe, M.F., Reichle, R., Reichstein, M., Rodell, M., Sheffield, J., Teuling, A.J., Wang, K., Wood, E.F., Zhang, Y., 2011. Evaluation of global observations-based evapotranspiration datasets and IPCC AR4 simulations. Geophys. Res. Lett. 38, n/a-n/a. doi:10.1029/2010GL046230
Muzylo, A., Llorens, P., Valente, F., Keizer, J.J., Domingo, F., Gash, J.H.C., 2009. A review of rainfall interception modelling. J. Hydrol. 370, 191–206. doi:10.1016/J.JHYDROL.2009.02.058
Nizinski, J.J., Galat, G., Galat-Luong, A., 2011. Water balance and sustainability of eucalyptus plantations in the Kouilou basin (Congo-Brazzaville). Russ. J. Ecol. 42, 305–314. doi:10.1134/S1067413611040126
Norman Ay, J.M., Kustas, W.P., Humes, K.S., 1995. Source approach for estimating soil and vegetation energy fluxes in observations of directional radiometric surface temperature. Agric. For. Meteorol. 77, 263–293.
Novick, K.A., Ficklin, D.L., Stoy, P.C., Williams, C.A., Bohrer, G., Oishi, A.C., Papuga, S.A., Blanken, P.D., Noormets, A., Sulman, B.N., Scott, R.L., Wang, L., Phillips, R.P., 2016. The increasing importance of atmospheric demand for ecosystem water and carbon fluxes. Nat. Clim. Chang. 6, 1023–1027. doi:10.1038/nclimate3114
Oki, T., Kanae, S., 2006. Global hydrological cycles and world water resources. Science 313, 1068–72. doi:10.1126/science.1128845
Or, D., Lehmann, P., Shahraeeni, E., Shokri, N., 2013. Advances in Soil Evaporation Physics—A Review. Vadose Zo. J. 12, 0. doi:10.2136/vzj2012.0163
Owe, M., de Jeu, R., Walker, J., 2001. A methodology for surface soil moisture and vegetation optical depth retrieval using the microwave polarization difference index. IEEE Trans. Geosci. Remote Sens. 39, 1643–1654. doi:10.1109/36.942542
Pielke, R.A., Sr, ., Avissar, R., Raupach, M., Dolman, A.J., Zeng, X., Denning, A.S., 1998. Interactions between the atmosphere and terrestrial ecosystems: influence on weather and climate. Glob. Chang. Biol. 4, 461–475. doi:10.1046/j.1365-2486.1998.t01-1-00176.x
Pieruschka, R., Huber, G., Berry, J.A., 2010. Control of transpiration by radiation. Proc. Natl. Acad. Sci. U. S. A. 107, 13372–7. doi:10.1073/pnas.0913177107
Porkka, M., Gerten, D., Schaphoff, S., Siebert, S., Kummu, M., 2016. Causes and trends of water scarcity in food production. Environ. Res. Lett. 11, 15001. doi:10.1088/1748-9326/11/1/015001
Poyatos, R., Granda, V., Molowny-Horas, R., Mencuccini, M., Steppe, K., Martínez-Vilalta, J., 2016. SAPFLUXNET: towards a global database of sap flow measurements. Tree Physiol. 36, 1449–1455. doi:10.1093/treephys/tpw110
Priestley, C.H.B., Taylor, R.J., 1972. On the assessment of sruface heat flux and evaporation using large scale parameters. Mon. Weather Rev. 81–92.
Purdy, A.J., Fisher, J.B., Goulden, M.L., Famiglietti, J.S., 2016. Ground heat flux: An analytical review of 6 models evaluated at 88 sites and globally. J. Geophys. Res. Biogeosciences 121, 3045–3059. doi:10.1002/2016JG003591

Pypker, T.G., Bond, B.J., Link, T.E., Marks, D., Unsworth, M.H., 2005. The importance of canopy structure in controlling the interception loss of rainfall: Examples from a young and an old-growth Douglas-fir forest. Agric. For. Meteorol. 130, 113–129. doi:10.1016/J.AGRFORMET.2005.03.003

R. Myneni, Y.K., n.d. MOD15A2H MODIS/Terra Leaf Area Index/FPAR 8-Day L4 Global 500m SIN Grid V006. doi.org. doi:10.5067/modis/mod15a2h.006

Rana, G., Katerji, N., 2000. Measurement and estimation of actual evapotranspiration in the field under Mediterranean climate: a review. Eur. J. Agron. 13, 125–153. doi:10.1016/S1161-0301(00)00070-8

Robert, C.P., 1995. Simulation of truncated normal variables. Stat. Comput. 5, 121–125. doi:10.1007/BF00143942

Schlesinger, W.H., Jasechko, S., 2014. Transpiration in the global water cycle. Agric. For. Meteorol. 189–190, 115–117. doi:10.1016/j.agrformet.2014.01.011

Schmugge, T.J., Kustas, W.P., Ritchie, J.C., Jackson, T.J., Rango, A., 2002. Remote sensing in hydrology. Adv. Water Resour. 25, 1367–1385. doi:10.1016/S0309-1708(02)00065-9

Seneviratne, S.I., Corti, T., Davin, E.L., Hirschi, M., Jaeger, E.B., Lehner, I., Orlowsky, B., Teuling, A.J., 2010. Investigating soil moisture–climate interactions in a changing climate: A review. Earth-Science Rev. 99, 125–161. doi:10.1016/J.EARSCIREV.2010.02.004

Shukla, J., Mintz, Y., 1982. Influence of Land-Surface Evapotranspiration on the Earth's Climate. Science 215, 1498–501. doi:10.1126/science.215.4539.1498

Spinoni, J., Naumann, G., Carrao, H., Barbosa, P., Vogt, J., 2014. World drought frequency, duration, and severity for 1951-2010. Int. J. Climatol. 34, 2792–2804. doi:10.1002/joc.3875

Stackhouse, P., Gupts, S., Cox, S., Mikovits, J., Zhang, T., Chiachiio, M., 2004. 12-year surface radiation budget data set. GEWEX News 14, 10–12.

Stone, P.H., Chow, S., Quirr, W.J., Stone, P.H., Chow, S., Quirr, W.J., 1977. The July Climate and a Comparison of the January and July Climates Simulated by the GISS General Circulation Model. Mon. Weather Rev. 105, 170–194. doi:10.1175/1520-0493(1977)105<0170:TJCAAC>2.0.CO;2

Sun, L., Anderson, M.C., Gao, F., Hain, C., Alfieri, J.G., Sharifi, A., McCarty, G.W., Yang, Y., Yang, Y., Kustas, W.P., McKee, L., 2017. Investigating water use over the Choptank River Watershed using a multisatellite data fusion approach. Water Resour. Res. 53, 5298–5319. doi:10.1002/2017WR020700

Talsma, C., Good, S.P., Jimenez, C., Martens, B., Fisher, J., 2017. Evaluation of Evapotranspiration Partitioning in Remote Sensing Models. Am. Geophys. Union, Fall Meet. 2017, Abstr. #H11M-08.

Talsma, C.J., Good, S.P., Jimenez, C., Martens, B., Fisher, J.B., Miralles, D.G., McCabe, M.F., Purdy, A.J., 2018. Partitioning of evapotranspiration in remote sensing-based models. Agric. For. Meteorol. doi:10.1016/j.agrformet.2018.05.010

Teuling, A.J., Hirschi, M., Ohmura, A., Wild, M., Reichstein, M., Ciais, P., Buchmann, N., Ammann, C., Montagnani, L., Richardson, A.D., Wohlfahrt, G., Seneviratne, S.I., 2009. A regional perspective on trends in continental evaporation. Geophys. Res. Lett. 36, n/a-n/a. doi:10.1029/2008GL036584

Trenberth, K.E., 2011. Changes in precipitation with climate change. Clim. Res. doi:10.2307/24872346

Valente, F., David, J.S., Gash, J.H.C., 1997. Modelling interception loss for two sparse eucalypt and pine forests in central Portugal using reformulated Rutter and Gash analytical models. J. Hydrol. 190, 141–162. doi:10.1016/S0022-1694(96)03066-1

Vinukollu, R.K., Meynadier, R., Sheffield, J., Wood, E.F., 2011. Multi-model, multi-sensor estimates of global evapotranspiration: climatology, uncertainties and trends. Hydrol. Process. 25, 3993–4010. doi:10.1002/hyp.8393

Wallace, J.., 2000. Increasing agricultural water use efficiency to meet future food production. Agric. Ecosyst. Environ. 82, 105–119. doi:10.1016/S0167-8809(00)00220-6

Wang, K., Dickinson, R.E., 2012. A review of global terrestrial evapotranspiration: Observation, modeling, climatology, and climatic variability. Rev. Geophys. 50. doi:10.1029/2011RG000373

Wang, L., Good, S.P., Caylor, K.K., 2014. Global synthesis of vegetation control on evapotranspiration partitioning. Geophys. Res. Lett. 41, 6753–6757. doi:10.1002/2014GL061439

Williams, D.G., Cable, W., Hultine, K., Hoedjes, J.C.B., Yepez, E.A., Simonneaux, V., Er-Raki, S., Boulet, G., de Bruin, H.A.R., Chehbouni, A., Hartogensis, O.K., Timouk, F., 2004. Evapotranspiration components determined by stable isotope, sap flow and eddy covariance techniques. Agric. For. Meteorol. 125, 241–258. doi:10.1016/J.AGRFORMET.2004.04.008

Yepez, E.A., Huxman, T.E., Ignace, D.D., English, N.B., Weltzin, J.F., Castellanos, A.E., Williams, D.G., 2005. Dynamics of transpiration and evaporation following a moisture pulse in semiarid grassland: A chamber-based isotope method for partitioning flux components. Agric. For. Meteorol. 132, 359–376. doi:10.1016/j.agrformet.2005.09.006

Zaitchik, B.F., Santanello, J.A., Kumar, S. V., Peters-Lidard, C.D., Zaitchik, B.F., Santanello, J.A., Kumar, S. V., Peters-Lidard, C.D., 2013. Representation of Soil Moisture Feedbacks during Drought in NASA Unified WRF (NU-WRF). J. Hydrometeorol. 14, 360–367. doi:10.1175/JHM-D-12-069.1

Zhang, K., Kimball, J.S., Running, S.W., 2016. A review of remote sensing based actual evapotranspiration estimation. Wiley Interdiscip. Rev. Water 3, 834–853. doi:10.1002/wat2.1168

Zhang, Y., Chiew, F.H.S., Peña-Arancibia, J., Sun, F., Li, H., Leuning, R., 2017. Global variation of transpiration and soil evaporation and the role of their major climate drivers. J. Geophys. Res. Atmos. 122, 6868–6881. doi:10.1002/2017JD027025

Zhang, Y., Peña-Arancibia, J.L., McVicar, T.R., Chiew, F.H.S., Vaze, J., Liu, C., Lu, X., Zheng, H., Wang, Y., Liu, Y.Y., Miralles, D.G., Pan, M., 2016. Multi-decadal trends in global terrestrial evapotranspiration and its components. Sci. Rep. 6, 19124. doi:10.1038/srep19124

Tables:

Reference	Start Date	End Date	Duration [days]	Location	Lat.	Long.	Forest Type	Method	Precip. [mm/yr]	E_v [mm/yr]	ET [mm/yr]	PET [mm/yr]	T/ET	Aridity
Poole t al. 1981	Annual Mean	-	-	Chile	-33.07	-71.00	Mediterranean Shrubland	Xylem pressure potential	590	206.5	531	1388	0.39	0.43
McJannet 2007	9/13/2003	6/30/2005	656	Queensland	-17.45	145.50	LMCF	Sapflow	2983	591	1445	1476	0.41	1.83
McJannet 2007	9/13/2003	6/30/2005	656	Queensland	-17.45	145.50	LMRF	Sapflow + other	2420	591	1087	1476	0.54	1.83
McJannet 2007	8/9/2002	1/23/2004	532	Queensland	-16.53	145.28	LMCF	Sapflow	3040	579	1459	1513	0.40	1.94
McJannet 2007	8/9/2002	1/23/2004	532	Queensland	-16.53	145.28	LMRF	Sapflow + other	2833	579	882	1513	0.66	1.94
Calder et al. 1986	4/6/1985	4/26/1985	20	Indonesia	-6.58	106.28	Tropical Rainforest	Model (with met. data), Isotopes	2851	883.81	1482.52	1591	0.60	1.79
Nizinski et al. 2011	-	-	-	D.R. Congo	-4.69	12.08	Tropical Rainforest	Radial flow meter	1019	825.39	947.67	1375	0.87	0.74
Nizinski et al. 2011	-	-	-	D.R. Congo	-4.69	12.08	Tropical Grassland	Radial flow meter	1019	591.02	703.11	1375	0.84	0.74
Leopoldo et al 1995	1/1/1981	12/31/1983	1094	Amazon	-3.13	-60.03	Tropical Rainforest	Model(with met. Data) Water Balance	2209	1243.7	1495	1612	0.83	1.29
Leopoldo et al. 1995	1/1/1981	12/31/1983	1094	Brazil	-3.13	-60.03	Tropical Rainforest	Model(with met. Data) Water Balance	2209	1237.04	1480.03	1612	0.84	1.29
Salati and Vose 1984	-	-	-	Brazil	-2.95	-59.95	Tropical Rainforest	Model(with met. Data) Water Balance	2000	1240	1620	1612	0.77	1.29

Salati and Vose 1984	-	-	-	Brazil	-2.95	-59.95	Tropical Rainforest	Model(with met. Data) Water Balance	2000	980	1500	1612	0.65	1.29
Shuttleworth 1988	9/1/1983	9/1/1985	731	Brazil	-2.95	-59.95	Tropical Rainforest	Model(with met. Data) Water Balance	2232	892.8	1116	1612	0.80	1.29
Tani et al 2003	1/1/1996	12/31/1999	1460	Malaysia	2.97	102.30	Tropical lowland forest	Model (with met. data) Water Balancd	1571	1218	1548	1689	0.79	0.93
Ataroff 2000	1/1/1996	12/31/1998	1095	Venezuela	8.63	-71.03	TMCF	Micromet	4450	484	674	1011	0.72	4.40
Aparecido 2016	1/1/2014	12/31/2014	364	Costa Rica	10.39	-84.63	TMRF	Sapflow + other	4200	540	1004	1543	0.54	2.72
Tanaka 2011	1/1/1999	11/4/2002	1403	Thailand	18.80	98.90	LMCF	Sapflow	1768	626	812	1743	0.77	1.01
Banerjee in Galoux et al. 1981	-	-	-	India	22.50	87.30	Tropical Rainforest	-	1623	730.35	1639.23	1617	0.45	1.00
Scott et al. 2006	10/1/2003	10/31/2007	1491	United States	31.70	-110.40	Desert	Sap Flow	322	119.14	202.86	1516	0.59	0.21
Cavanaugh et al. 2011	1/1/2008	12/31/2008	365	United States	31.74	-110.05	Desert	Model (with met. data), Sap flow	260	54.6	148.2	1567	0.42	0.17
Cavanaugh et al. 2011	1/1/2008	12/31/2008	365	United States	31.91	-110.84	Desert	Model (with met. data), Sap flow	212	44.52	101.76	1460	0.47	0.15
Liu et al. 1995	1/1/1992	12/31/1993	730	United States	31.95	-112.94	Desert	Model(with met. Data), Isotopes	200	160	200	1758	0.80	0.11

Schlesinger et al. 1987	8/27/1983	7/17/1984	325	United States	32.52	-106.80	Desert	Water-balance; control and bare plots	210	151.2	210	1519	0.72	0.14
Poole et al. 1981	9/1/1976	7/31/1977	333	United States	32.83	-116.43	Mediterranean Shrubland	Xylem pressure potential	475	152	394.25	1441	0.39	0.33
Kumagai et al., (in press)	4/1/2007	6/30/2008	456	Japan	33.13	130.72	Temperate Forest	Model (with met. data), sap flow	2128	486.2	911.4	949	0.53	2.24
McNulty 1996	Annual Mean	-	-	United States	34.00	-85.80	Temperate Forest	Xylem pressure potential	1225	600.25	784	1334	0.77	0.92
Waring et al. 1981	-	-	-	United States	34.64	-111.78	Temperate Forest	Xylem pressure potential	1085	531.65	694.4	1349	0.76	0.80
Flore et al. 1982	-	-	-	Tunisia	35.80	9.20	Steppe	Model (with met. data)	144	64.8	144	1533	0.45	0.11
Wilson et al. 2001	1/1/1998	12/31/1998	364	United States	35.96	-84.29	Temperate Deciduous Forests	Model (with met. data), sap flow	1333	253.27	439.89	1242	0.58	1.07
Smith et al. 1995	1/1/1988	12/31/1988	365	United States	36.93	-116.56	Desert	Xylem pressure potential	150	52.5	150	1431	0.35	0.10
Paco et al. 2009	1/1/2005	12/31/2005	364	Portugal	38.50	-8.00	Temperate Deciduous Forests	Sap flow	669	488.37	669	1165	0.73	0.57
Huang et al. 2010	1/1/2003	12/31/2006	1460	China	43.53	116.67	Steppe	Model (with met. data)	275	151.25	244.75	814	0.62	0.53
Hu et al. 2009	1/1/2003	12/31/2005	1095	China	43.55	116.67	Temperate Grassland	Model (with met. data)	580	226.2	510.4	814	0.44	0.53
Waring et al. 1981	10/1/1973	9/30/1974	364	United States	44.20	-122.30	Temperate Forest	Xylem pressure potential	2355	376.8	635.85	855	0.59	2.75

Liu et al. 2012	1/1/2009	12/31/2009	364	China	44.28	87.93	Desert	Energy balance model	150	57	150	996	0.38	0.15
Telmer and Veizer 2000	9/1/1991	9/30/1992	395	Canada	45.70	-76.90	Boreal Forest	Isotope-based (catchment)	872	392.4	462.16	842	0.85	1.04
Tajchman 1972	1/1/1965	12/31/1965	364	Germany	48.04	11.56	Temperate Forest	Energy balance model	725	268.25	427.75	757	0.63	0.96
Granier et al. 2000	1/1/1995	12/31/1995	364	France	48.67	7.08	Temperate Deciduous Forests	Sap flow	763	251.79	366.24	774	0.69	0.99
Prazak et al. 1994	1/1/1985	12/31/1989	1825	Czech Republic	49.06	13.66	Temperate Forest	Model (with met. data)	366	190.32	384.3	739	0.52	0.50
Molchanov cited in Galoux et al. 1981	-	-	-	Russia	50.75	42.50	Temperate Deciduous Forests	-	513	251.37	436.05	800	0.58	0.64
Two studies by Delfs (1967), cited by Choudhury et al. 1998	-	-	-	Germany	51.76	10.51	Boreal Forest	-	1237	235.03	556.65	675	0.42	1.83
Hudson 1988	Annual Mean	-	-	United Kingdom	52.00	-3.50	Temperate Forest	Model (with met. data)	2620	183.4	786	566	0.23	4.63
Gash and Stewart 1997	1/1/1975	12/31/1975	364	United Kingdom	52.42	0.67	Temperate Forest	Model (with met. data)	595	351.05	565.25	655	0.55	0.91
Ladekari 1998	7/1/1992	12/31/1994	913	Denmark	56.41	9.35	Temperate Deciduous Forests	Model (with met. data)	549	296.46	345.87	560	0.86	0.98
Gibson and Edwards, 2002	1/1/1993	12/31/1994	729	Canada	63.41	-114.26	Boreal Forest	Isotope-based (catchment)	340	241.4	302.6	423	0.81	0.80

Gibson and Edwards, 2002	1/1/1993	12/31/1994	729	Canada	64.50	-112.70	Tundra	Isotope-based(catchment)	310	105.4	130.2	354	0.81	0.88

Table 2.1: List of field studies used to validate the remote sensing model partitions. Shown are the study location, date, duration, and biome type along with the precipitation, transpiration, and evapotranspiration measured by each study. The potential evapotranspiration (PET), T/ET ratio, and aridity index are also listed. For each study, soil evaporation was calculated as the residual between the total ET and transpiration estimate of each study.

		Wacmos Models 0.25° 2005-2007		
		PM-MOD	**PT-JPL**	**GLEAM**
r^2	E_s	0.14	0.25	0.14
	E_v	0.45	0.33	0.55
	E_i	0.85	0.39	0.82
	ET	0.64	0.75	0.61
Standard Error	E_s	0.19	0.17	0.05
	E_v	0.08	0.09	0.12
	E_i	0.19	0.34	0.09
	ET	0.09	0.07	0.08
% MBD	E_s	49.4	11.0	-45.6
	E_v	-66.0	-10.7	-5.4
	E_i	149.9	65.1	25.3
	ET	-21.6	-2.3	-20.9
% RMSD	E_s	114.2	89.8	90.6
	E_v	86.1	61.6	54.0
	E_i	181.0	157.4	62.1
	ET	45.1	35.1	48.5

Table 2.2: Validation statistics for different satellite-based ET datasets. The r^2 correlation coefficient describes the percent variability of the field data that the models were able to capture. The standard error describes the spread or standard deviation of the data. The mean bias error (MBD) describes the bias of the modeled estimate to either over- or under-estimate the field data. The root mean square deviation (RMSD) describes the accuracy of the model representing both the size and variation of the gross error. MBD and RMSD are reported as a percentage of the average field estimate for each partition. Blue represents good performance, while orange represents poor performance.

III. Sensitivity of transpiration, soil evaporation, and interception in remote sensing based evapotranspiration models using a Monte Carlo analysis

Carl J. Talsma[1*], Stephen P. Good[1], Carlos Jimenez[2], Brecht Martens[3], Joshua B. Fisher[4], Diego G. Miralles[3], Adam J. Purdy[4]

[1] *Department of Water Resources, Oregon State University, Corvallis, Oregon, USA*

[2]*Estellus, Paris, France*

[3]*Laboratory of Hydrology and Water Management, Ghent University, Ghent, Belgium*

[4]*Jet Propulsion Laboratory, California Institute of Technology, Pasadena, California, USA*

**Corresponding author. E-mail address: talsmac83@gmail.com, Gilmore Hall, 124 SW 26th St, Corvallis, OR 97331*

Abstract:

Accurately estimating evapotranspiration (ET) at large spatial scales is essential to our understanding of land-atmosphere coupling and the surface balance of water, energy, and carbon. Comparisons between remote sensing-based ET models are difficult due to diversity in model formulation, parametrization, and data requirements. The constituent components of ET have been shown to deviate substantially among models and between models and field estimates. This study analyzes the sensitivity of three global ET remote sensing models in an attempt to isolate the error associated with input variable uncertainty and reveal the underlying drivers of the model components. We examine the transpiration, soil evaporation, interception, and total ET estimates of the Penman-Montieth model from the Moderate Resolution Imaging Spectroradiometer (PM-MOD), the Priestley-Taylor Jet Propulsion Laboratory model (PT-JPL), and the Global Land Evaporation Amsterdam Model (GLEAM). We analyze the sensitivity of the models based on the uncertainty of the input variables and as a function of the raw value of the input variables themselves. We find that, at σ=10% added uncertainty levels, the total ET estimates from PT-JPL, PM-MOD, and GLEAM are most sensitive to Normalized Difference Vegetation Index (NDVI), relative humidity, and net radiation, respectively. Consistently, systemic bias introduced by variable uncertainty in the component estimates is mitigated when components are aggregated to a total ET estimate. Additionally, the GLEAM model was found to have far less sensitivity to the input variables and is likely more sensitive to model constants and parameterization. These results suggest that slight changes to input variables may result in outsized variation in ET partitioning, and relatively smaller changes to the total ET estimates. Our results help to explain why model

estimates of total ET perform relatively well despite large deviations in the individual ET component estimates. Improving the ET partitioning within these models will help to further our understanding of the global relationships between water, climate, and vegetation.

3.1 Introduction:

Evapotranspiration (ET) is a critical component to the cycling of water, carbon, and energy throughout the land and atmosphere and represents a crucial juncture for feedbacks and interactions between those cycles (Fisher et al., 2017; Oki and Kanae, 2006). Future changes to regional and global climate are expected to significantly alter both the supply (precipitation, snow, and groundwater) and demand (ET) side of the hydrological cycle (Huntington, 2006; Y. Zhang et al., 2016). These hydrological impacts are projected to involve increased drought severity, frequency, and duration (Allen et al., 2010; Spinoni et al., 2014; Zaitchik et al., 2013). Furthermore, the response of vegetation to these changes in climate is a large uncertainty in both climate projections and in global food security (Ciais et al., 2005; Friedlingstein et al., 2014; Mancosu et al., 2015).

The atmospheric demand of water through ET controls soil moisture, agricultural drought, and hydrological drought and is a key variable for climate prediction, water resources management, and agricultural food production (Fisher et al., 2017; Goulden and Bales, 2014; Meng et al., 2014; Porkka et al., 2016). Due to the spatial and temporal scales at which estimates of ET are meaningful for climate research, remote sensing-based models have become the dominant means to obtain ET fluxes at the relevant spatio-temporal scales (Dolman et al., 2014; Fisher et al., 2017; Mccabe et al., 2017). Relatively accurate satellite-

based estimates of ET now exist with global coverage at several spatial and temporal scales (Mccabe et al., 2017; Miralles et al., 2016).

While remote sensing-based models have vastly improved our ability to estimate ET globally, the accurate estimation of ET components lags behind. ET is composed of three main fluxes: transpiration from plant stomata, soil evaporation from the top layer of soil, and rainfall interception. Though each of these components is often calculated within remote sensing-based ET models, comparisons have shown that although the total evaporative flux from different models agrees relatively well, the different components diverge substantially (Miralles et al., 2016). Furthermore, recent comparisons against in situ component data show large biases in remote sensing-based estimates of ET components even where total ET is accurate (Talsma et al., 2018).

How ET is partitioned into transpiration, soil evaporation, and interception remains an important topic for remote sensing research. Transpiration represents a crucial link between the carbon and water cycle and is a key component in determining how the terrestrial biosphere will respond to a changing climate (Bonan, 2008; Lawrence et al., 2007). Furthermore, changes to climate and the corresponding effect on the evaporation demand are likely to alter the partitioning of ET in the future (Good et al., 2017; Wang et al., 2014). Given the large observed discrepancies between modeled and field-based components of ET, along with the use of such ET models in climate forecasting and non-stationary systems, the partitioning strategies employed by these models may be inadequate in monitoring future changes in total ET.

However, comparing ET models becomes difficult to interpret as each model requires its specific set of forcing variables. As such, discrepancies between model estimates can be

attributed to assumed model formulations, parameterizations of model constants, and the propagation of error associated with different forcing data. Previous studies have attempted to use similar forcing data where possible to isolate differences in model formulations (Mccabe et al., 2017; Michel et al., 2016; Miralles et al., 2016), while other studies have forced the same model with different forcing data, attributing errors as large as 20% of the global mean ET to forcing data alone (Badgley et al., 2015; Vinukollu et al., 2011). Still, due to the large diversity of models and data requirements, it is difficult to directly compare model estimates, or to attribute errors to specific model variables or formulations. Furthermore, studies have largely focused on the total ET estimates of these models and have largely ignored how dataset uncertainty might affect the estimates of transpiration, soil evaporation, and interception separately of total ET.

This study uses a Monte Carlo sensitivity analysis to explore how the uncertainty of individual variables within three remote sensing-based models introduces errors into the component estimates of ET. The analysis allows us to unravel how changes in variable uncertainty, changes to climatic and biophysical conditions, and the use of different model formulation influences differences in modeled estimates. To date, no study has attempted to assess the sensitivity of the individual components within these models to their forcing variables. The goal of this study is to (1) determine to which model input variables the ET components are most sensitive, (2) determine if non-linearity in model formulation introduces significant bias in the ET components due to variable uncertainty, (3) and analyze model sensitivity across a range of input conditions.

3.2 Methods:

3.2.1 Models and Data

Three remote sensing-based evapotranspiration models were selected for this study: the Priestley-Taylor Jet Propulstion Lab (PT-JPL) model (Fisher et al., 2008), the Penman-Monteith MODerate Resolution Imaging Spectroradiometer (PM-MOD) model (Mu et al., 2011), and the Global Land Evaporation Amsterdam Model v3.1 (GLEAM) (Martens et al., 2017). The outputs for each of these models have previously been compared against globally distributed eddy flux ET measurements (Ershadi et al., 2015; Mccabe et al., 2016; Michel et al., 2016), as well as ET partitioning estimates from isotopes, sap flux, and other methods (Talsma et al., 2018). Each model is widely used to estimate evapotranspiration and outputs the individual components of ET: transpiration, soil evaporation, and interception loss. Both PT-JPL and GLEAM rely on the Priestley-Taylor equation to estimate a potential ET value (Priestley and Taylor, 1972) and then constrain that potential value to an actual estimate using an estimate of evaporative stress based on ancillary data. A detailed description of PT-JPL may be found in Fischer et al. (2008), while GLEAM is described in Miralles et al. (2011) and Martens et al. (2017, 2016). PM-MOD on the other hand uses a Penman-Monteith estimate of potential ET and then similarly constrains the potential value to an actual estimate. PM-MOD is described in depth by Mu et al. (2011).

We used the WACMOS-ET forcing database (http://wacmoset.estellus.eu/) to run the three models, which includes remote sensing-based and reanalysis meteorology and radiation flux products (Michel et al., 2016; Miralles et al., 2016). We also used MODIS vegetation and land cover products (NASA LP DAAC, Friedl et al., 2009; Didan, 2015) to force PT-JPL and PM-MOD. The WACMOS database does contain the vegetation products necessary to

force the PT-JPL and PM-MOD models, but those products are developed using a two-stream inversion package and are dimensionally inconsistent with the MODIS products that PT-JPL and PM-MOD are developed to use.

The WACMOS forcing dataset consists of various re-analysis and remote sensing based products that have been aggregated to a common 0.25^{o} longitudinal x 0.25^{o} latitudinal grid, at 3-hourly temporal scale. However, GLEAM no longer provides sub-daily estimates of ET, while PT-JPL remains sensitive to maximum daily temperature and minimum daily humidity estimates. Thus, the two models cannot be run on a common temporal scale. As such, we run the GLEAM model at a daily resolution using the mean value of the sub-daily dataset, and run both PT-JPL and PM-MOD at the original 3-hourly scale.

Due to computational power and data availability, we force each model with a dataset of 47 pixel locations over three years (2003-2005), rather than the global dataset. These locations span a large range of ecoregions across the Earth, and have previously been used to compare modeled output against field based ET component estimates (Talsma et al., 2017). While limiting the dataset to these specific locations may neglect the model sensitivity in regions not represented in the data, it allows us to more directly compare the results of this study to the results of Talsma et al. (2017). To further examine how our results might be affected by the specific locations, we also analyze the sensitivity results categorized by the unperturbed forcing data values.

While some variables within the forcing dataset are shared among all three models, each model also requires unique input variables. Table 3.1 shows the dynamic variables that force each model and lists the original source product. However, both PM-MOD and GLEAM require additional spatially-varying static variables. PM-MOD relies on the MODIS

IGBP landcover type product to determine canopy resistances, while GLEAM uses static variables to describe soil properties (Global Soil Task Group, 2014) and vegetation fractions at the sub-pixel level (MOD44B). The latter is expected to be very important for the ET portioning in GLEAM , as the model uses the fractional canopy covers from the MOD44B product to directly partition the ET flux between soil and canopy.

Variable	Product	PT-JPL	PM-MOD	GLEAM
Surface Radiation	SRB (Stackhouse et al., 2004)	✓	✓	✓
Temperature	ERA-Interim (Dee et al., 2011)	✓	✓	✓
Relative Humidity	ERA-Interim (Dee et al., 2011)	✓	✓	
Precipitation	SFR-GPCP (Adler et al., 2003)			✓
***f*APAR**	MODIS (Didan, 2015)		✓	
LAI	MODIS (Didan, 2015)		✓	
NDVI	MODIS (Didan, 2015)	✓		
Vegetation Optical Depth	LRPM (Owe et al., 2001)			✓

Table 3.1: Dynamic forcing variables for each of the three models.

3.2.2 Monte Carlo Sensitivity Analysis

To assess each model's relative sensitivity to the forcing, we use a Monte Carlo style simulation (Demaria et al., 2007; Hammersley and Handscomb, 1964). This approach involves perturbing input variables by some random uncertainty drawn from a predetermined probability distribution and analyzing how the final model output changes in reference to the perturbation. We can then compare the model sensitivity across variables, within variable ranges, and across models.

This study examines the sensitivity of the models to temporally variable input variables (Table 3.1). GLEAM, and, to a lesser extent, PM-MOD also use static parameters and constants that vary in space but do not vary in time. While these values are important to the partitioning within the models, this study does not consider the sensitivity of the models to these parameters and constants.

Many of the products shown in Table 3.1 are re-analysis products that are the result of model simulations which incorporate observations from balloon soundings, satellite data, and in situ measurements in a data assimilation system. Furthermore, the original products have been manipulated further to create a common spatial and temporal scale. As such, data quality will change in time and space (Dee et al., 2011), and an accurate estimate of the product uncertainty is difficult to determine. To account for potential changes in forcing uncertainty, we analyzed the sensitivity to each input variable at a range of uncertainties.

The required input variables for each model contains both naturally bounded and unbounded variables. For unbounded variables such as net radiation and temperature, a Gaussian error distribution is assumed. We use a truncated-normal distribution to describe the errors of the bounded variables. Bounded variables included relative humidity (RH, 0-1), leaf area index (LAI, 0-∞ m2/m2), normalized difference vegetation index (NDVI, -1.0-1.0), fraction of absorbed photosynthetically active radiation (fAPAR, 0-1), precipitation (P, 0-∞ mm/day), and Vegetation Optical Depth (VOD, 0-∞). For both cases, the expected mean value is the raw data input and the standard deviation of the distribution is a predetermined fraction of the raw value ranging from 0.01% to 40%. At an uncertainty level of 40% many of the variables have collapsed to distributions in which further added uncertainty would not

results in significant changes. Meanwhile, the boundary effects of bounded variables could skew model sensitivity at large uncertainty.

The Gaussian distribution allows us to perturb the data while conserving the original unperturbed value as the mean of the distribution. Thus, any bias found in the distribution of the sensitivity results will reflect non-linear formulations within the model. While this distribution may not reflect the reality of the uncertainty contained within the data, it allows us to observe how the model formulation and parameterization might propagate error in a way that would introduce bias to the estimate. Thus, we assume that the forcing does not contain any systematic error or bias.

The truncated-normal distribution is a combination of a mean conserving distribution with a mean changing shift, so that bounded variables may not preserve the original mean (Robert, 1995). The truncated-normal distribution is advantageous over a beta or gamma distribution because we can specify large uncertainties without the distribution collapsing toward probability masses located only at one or both bounds. If a variable is bounded on one side or if the original mean is closer to one of the bounds, then the expected mean of the resulting distribution will shift away from that bound. The resulting magnitude of the shift is a function of the difference between the bound and the original mean and the level of added uncertainty. The resulting shift is therefore more likely to influence the results found here if the added uncertainty is high or if the original variable is closer to one of the bounds.

Figures 3.1-3.3 shows the joint probability distribution functions for the entire study period over all sites. The distributions show both the raw unperturbed data and the distribution of data after perturbation at various uncertainty levels. Note that these figures show the distributions of the original and perturbed data and not the theoretical distributions

used to generate random error. PT-JPL and PM-MOD show identical distributions for common forcing variables. For forcing variables common to the GLEAM model, such as net radiation, the distributions are slightly different due to the difference in temporal resolution.

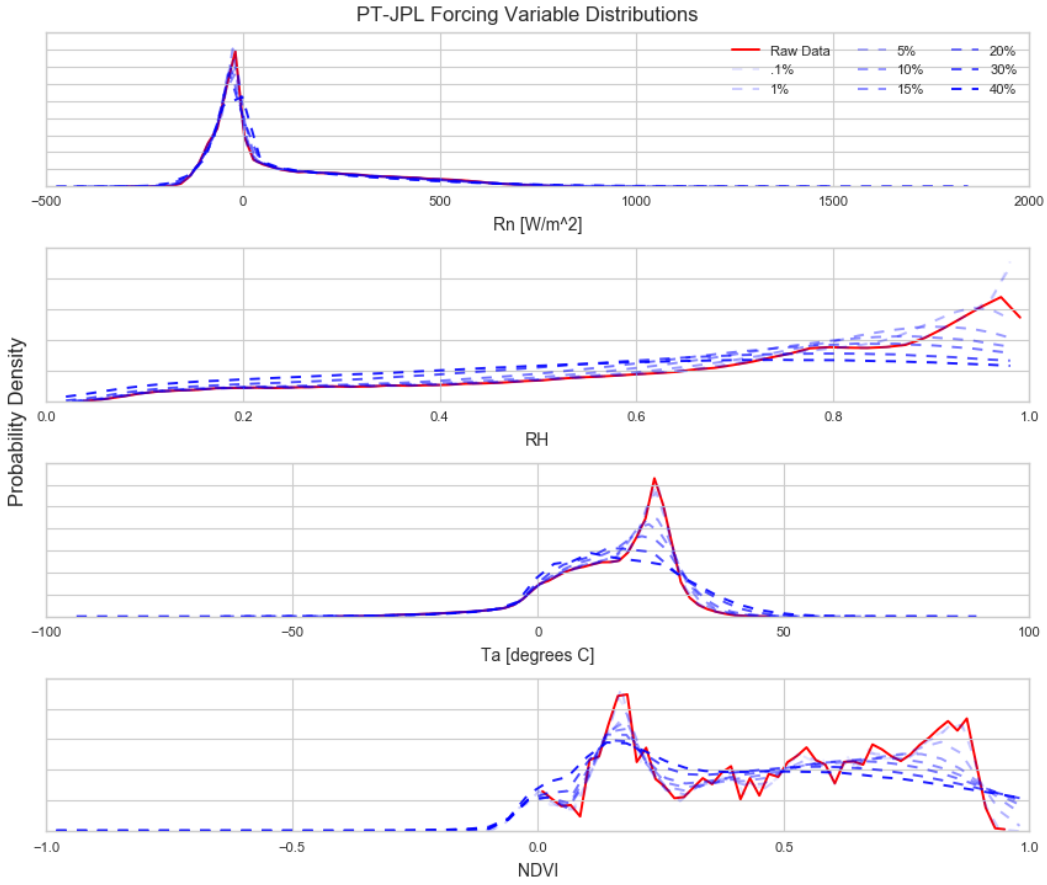

Figure 3.1: Raw and perturbed data at varying added uncertainty for PT-JPL forcing.

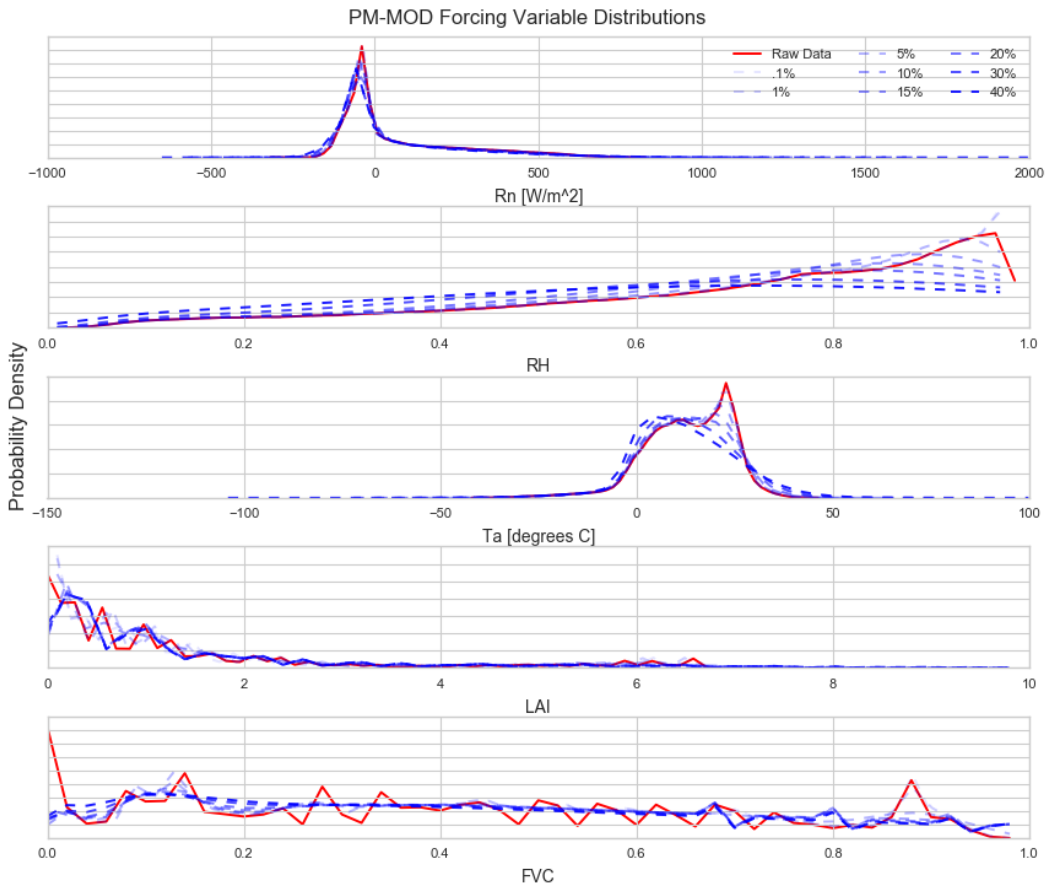

Figure 3.2: Raw and perturbed data at varying added uncertainty for PM-MOD forcing.

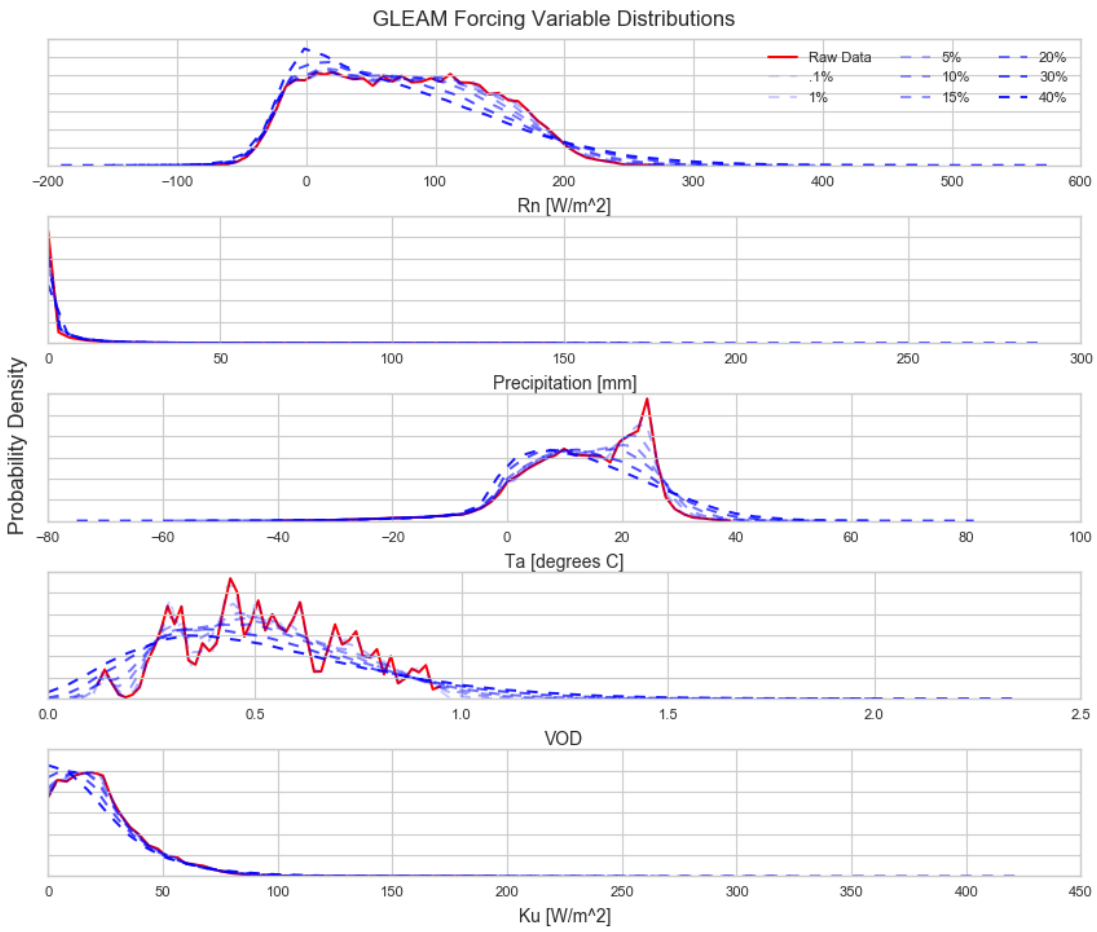

Figure 3.3: Raw and perturbed data at varying added uncertainty for GLEAM forcing.

3.2.3 Error and Bias Assessment

As previously stated, we forced the model for three years (2003-2005) at 47 locations. Random error was added to each forcing variable based on the described probability distributions and each data point was sampled 100 times. This process was repeated at each assumed uncertainty level and for each variable field. This resulted in approximately 62 x 10^6 data values at the 3 hourly time scale and 7.8 x 10^6 values at the daily time scale for each variable and each uncertainty level. Given that we cannot determine the exact uncertainty for each forcing variable, we perturb only one variable at a time.

We then describe the results of each model estimate using the relative error:

$$\delta = \frac{x_i - x_0}{x_0} \quad (1)$$

Where x_i is the perturbed estimate and x_0 is the unperturbed estimate. We then aggregate the results at each time and location and analyze the results as a distribution of the relative error. We analyze the resulting distribution of the simulations using two objective functions: root mean squared deviation (RMSD, Eq. (2)) and mean bias deviation (MBD, Eq. (3)). Both functions are calculated at an added uncertainty of σ=10%, and are normalized by the mean total ET estimate for the model across all data points with no added uncertainty:

$$RMSD = \sqrt{\frac{\sum_{i,x}^{N}(\dot{y}_{i,x} - y_{i,x})^2}{N}} \Big/ \overline{ET}, \quad (2)$$

and

$$MBD = \frac{\sum_{i,x}^{N} \dot{y_{i,x}} - y_{i,x}}{N} \Big/ \overline{ET}. \quad (3)$$

Where $\dot{y}_{i,x}$ represents the estimated value after perturbation, $y_{i,x}$ is the original estimate, N is the total number of estimates, x is the specific location and i the specific time, and $\overline{ET}$ is the model-specific mean ET over all locations and time.

3.3 RESULTS:

3.3.1 Model Sensitivity

Figures 3.4-3.6 show the sensitivity of the model output to each of the forcing variables for different uncertainty levels. The plots show the interquartile range of the relative error distribution for each uncertainty level, as well as the mode of the distribution. Generally, a greater interquartile range signifies that the model is more sensitive to that forcing variable.

The deviation of the mode from a relative error 0 signifies how much bias is introduced to the model estimate because of variable uncertainty.

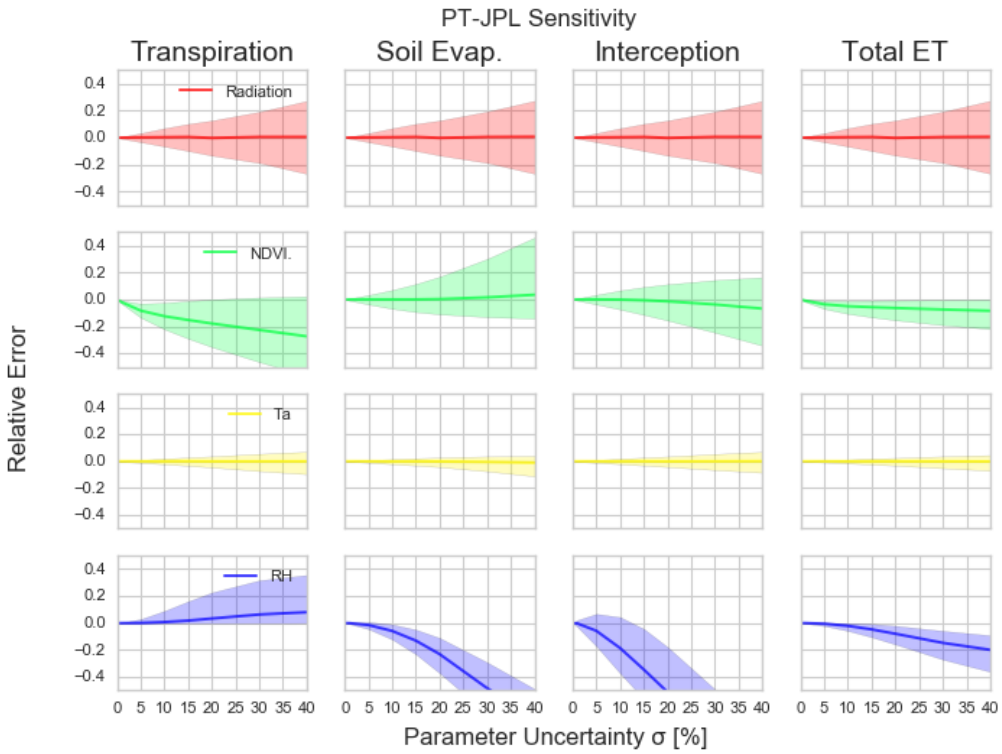

Figure 3.4: The sensitivity of PT-JPL to forcing variables at a range of added random uncertainty. Relative error is used to measure the difference in model output before and after perturbing the input variable. The shaded region represents the area contained within the 25th and 75th percentile of resulting error distribution while the line represents the mode.

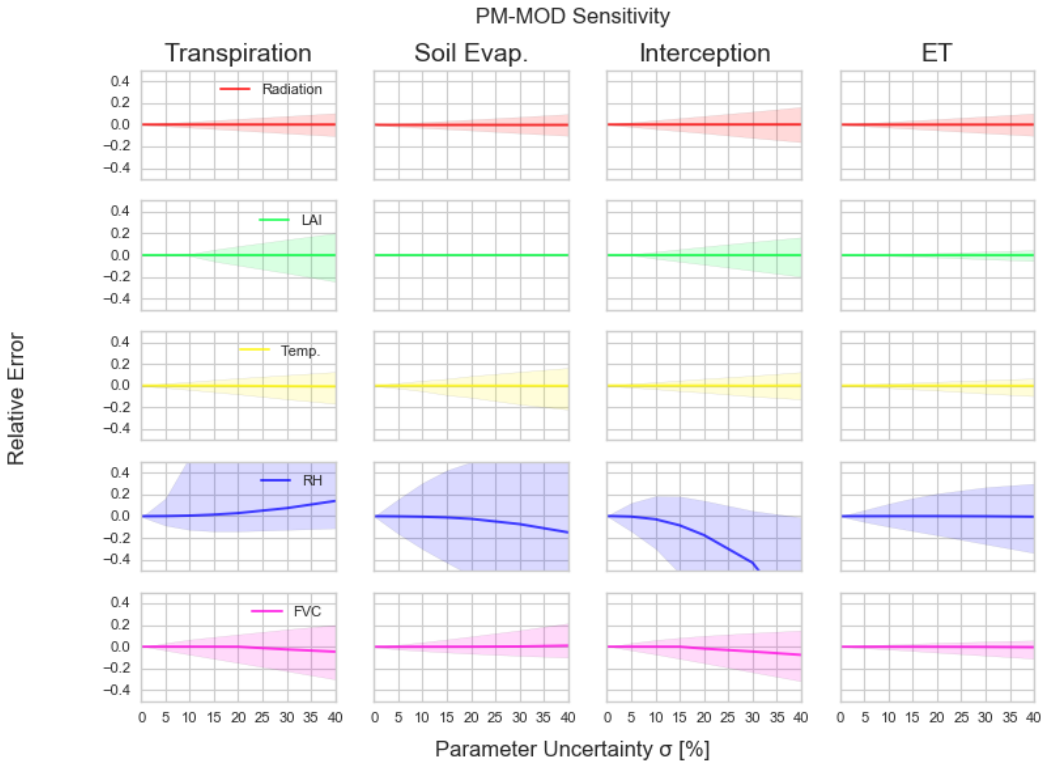

Figure 3.5: The sensitivity of PM-MOD to forcing variables at a range of added random uncertainty. Relative error is used to measure the difference in model output before and after perturbing the input variable. The shaded region represents the area contained within the 25th and 75th percentile of resulting error distribution while the line represents the mode.

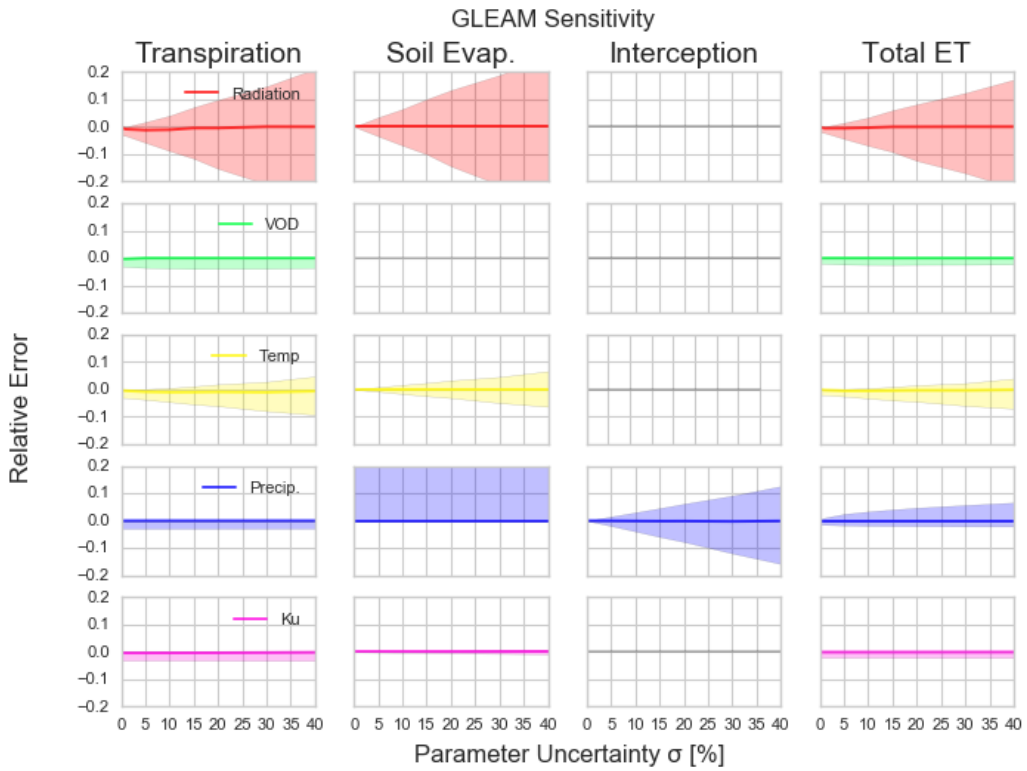

Figure 3.6: The sensitivity of GLEAM to forcing variables at a range of added random uncertainty. Relative error is used to measure the difference in model output before and after perturbing the input variable. The shaded region represents the area contained within the 25th and 75th percentile of resulting error distribution while the line represents the mode.

While the interquartile range and mode give us an idea of the distribution of error at each uncertainty, they do not represent the entire distribution. Figures 3.7-3.9 show the probability distributions of the relative error for each forcing variable and each modeled ET component at an added uncertainty of σ=10%. 10% was chosen because it represents significant added uncertainty while avoiding the boundary effects of larger uncertainties. Table 3.2 shows the root mean squared deviations (RMSD) and mean biased deviation (MBD) for each of the variables and each modeled ET component at this uncertainty level. The values in table 3.2 are expressed as a percentage of the mean ET estimate across all data points.

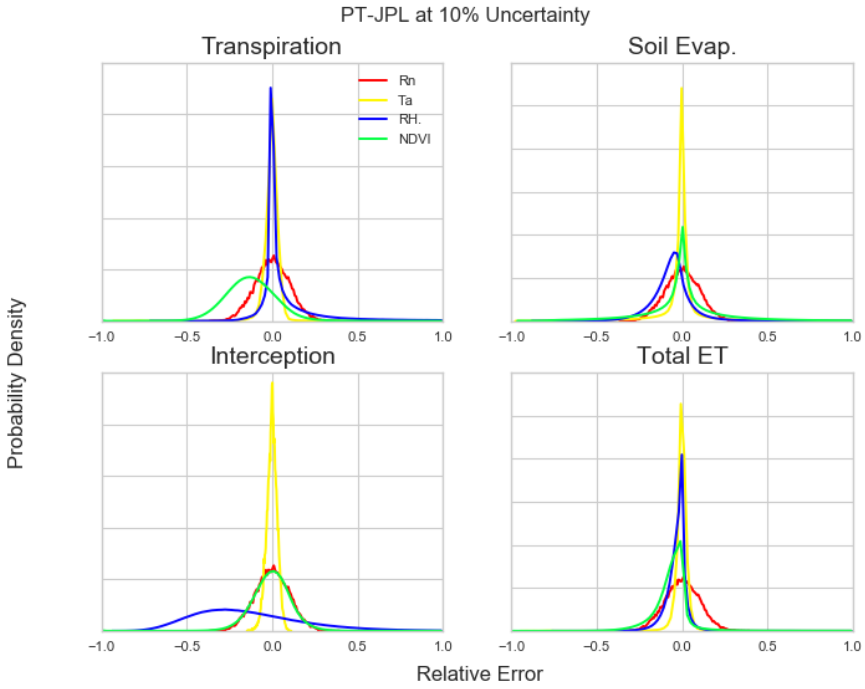

Figure 3.7: PT-JPL model probability density of the relative error for each input variable with σ = 10% added uncertainty.

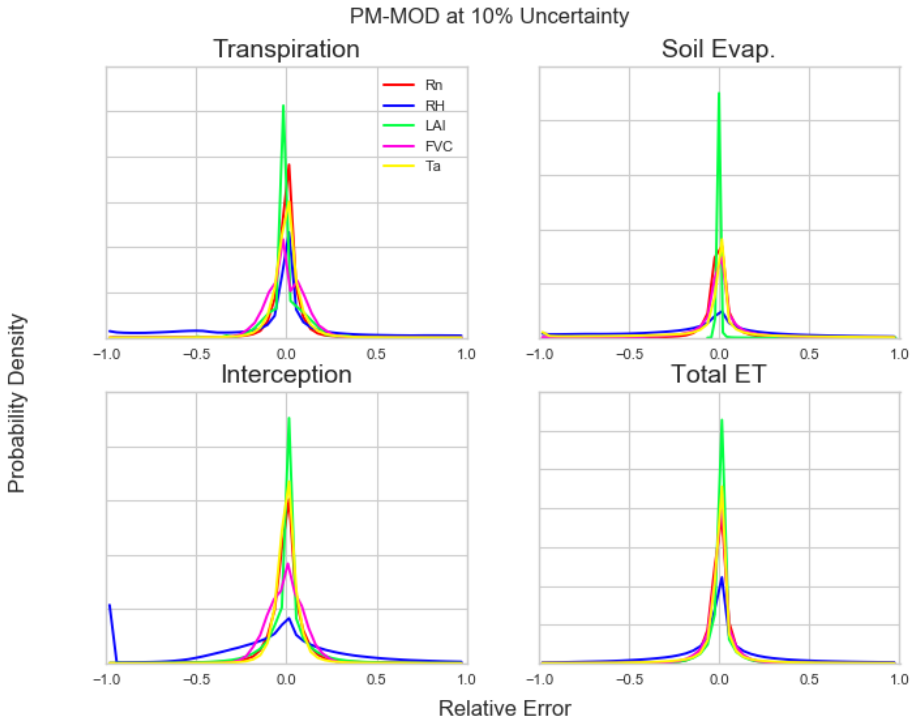

Figure 3.8: PM-MOD model probability density of the relative error for each input variable with σ = 10% added uncertainty.

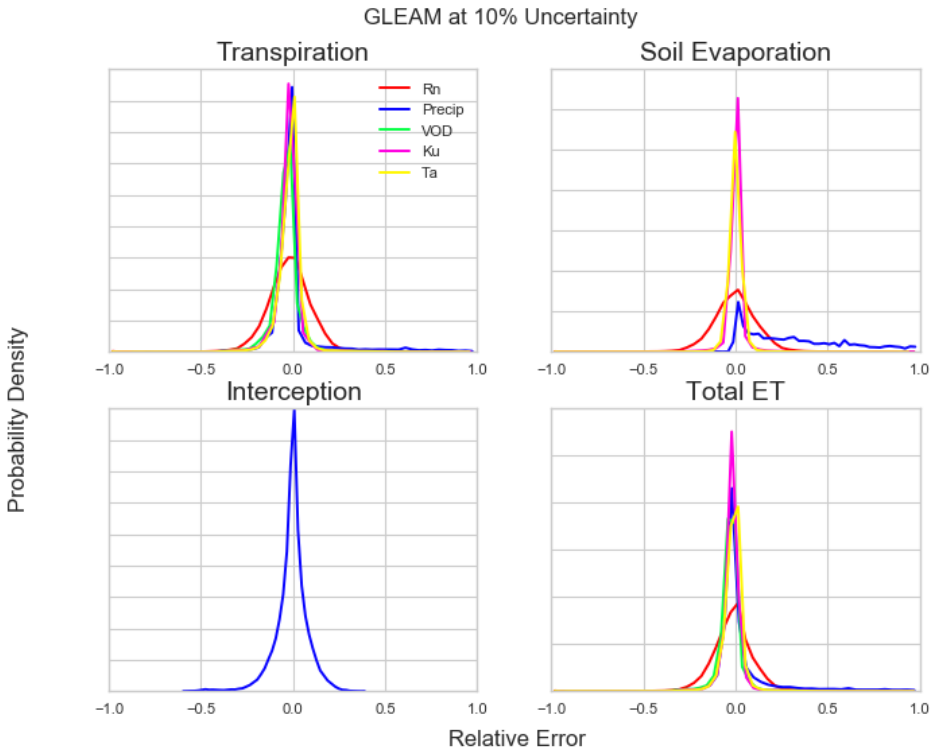

Figure 3.9: GLEAM model probability density of the relative error for each input variable with σ = 10% added uncertainty.

	PT-JPL 10% Uncertainty							
	RMSD				MBD			
	E_{veg}	E_{soil}	E_{int}	E_{total}	E_{veg}	E_{soil}	E_{int}	E_{total}
Rn	38.8	38.8	38.8	38.8	1.4	1.4	1.4	1.4
RH	122.6	60.6	151.4	33.1	41.9	-26.1	-59.0	-12.9
Ta	32.3	71.3	13.6	35.9	0.9	-2.3	0.5	0.5
NDVI	91.0	112.0	51.4	100.0	-51.4	5.1	-1.4	-20.0
	PM-MOD 10% Uncertainty							
	RMSD				MBD			
	E_{veg}	E_{soil}	E_{int}	E_{total}	E_{veg}	E_{soil}	E_{int}	E_{total}
Rn	47.4	49.6	42.4	49.1	-0.3	-2.3	0.2	-0.5
RH	144.5	174.2	129.3	122.3	-25.3	-33.7	-19.2	-2.7
Ta	48.3	125.7	28.0	68.1	1.0	-18.6	1.3	1.2
FVC	44.2	83.3	30.8	44.0	-0.6	-0.8	-0.6	-1.1
LAI	37.7	8.7	45.5	38.6	0.4	-0.4	0.3	0.4
	GLEAM 10% Uncertainty							
	RMSD				MBD			
	E_{veg}	E_{soil}	E_{int}	E_{total}	E_{veg}	E_{soil}	E_{int}	E_{total}
Rn	8.07	8.15		7.49	-1.16	-0.03		-0.83
P	4.54	4.07	4.10	4.82	-0.74	0.80	-0.14	0.02
Ta	4.49	2.79		3.88	-1.14	0.00		-0.80
Ku	3.96	2.69		3.28	-1.13	0.02		-0.78
VOD	3.94			3.21	-1.16			-0.85

Table 3.2: Root mean squared deviation (RMSD) and mean bias deviation (MBD) of the distribution of deviation in model estimates due to variable perturbations. Each value is normalized by the mean ET estimate across the raw dataset for that model. Blank cells represent instances where the input variable for a model is not an input of the specific model component.

PT-JPL takes four input variables: net radiation, NDVI, temperature, and RH. Each of the modeled ET components varies linearly with net radiation. Figure 3.4 shows that the relative error also increases linearly with increasing uncertainty in the net radiation term. Due to this linear relationship, there is little to no bias in the model output associated with uncertainty in net radiation evidenced by a MBD of 1% for all ET components. Similarly, the sensitivity of the model is unbiased to uncertainties in temperature. For RH and NDVI, however, the model shows strong bias in relative error due to forcing uncertainty. The transpiration component of PT-JPL shows a strong negative bias (MBD = -51%) due to uncertainty in NDVI, while showing a positive bias (MBD = 42%) due to uncertainty in RH. The soil

evaporation and interception components show a strong negative bias (MBD = -26%, -59%, respectively) due to uncertainty in RH. Interestingly, the contrasting biases in the ET components due to uncertainty in the RH term only result in a slight negative bias (MBD = -13%) in the total ET term and a much smaller RMSD (33%) compared to the components RMSD, wich typically ranges between61 and151%. Figure 3.7 also helps to illustrate the biases in the distribution of error associated with NDVI and RH, while the net radiation and temperature distributions tend to be much more unbiased and symmetrical.

PM-MOD has five temporally variable forcings: net radiation, RH, temperature, fraction of absorbed photosynthetically active radiation (FAPAR), and leaf are index (LAI). Additionally, PM-MOD uses IGBP land cover type to determine look up table values for aerodynamic and stomatal resistances. Each of the ET components estimated by PM-MOD is exceedingly sensitive to RH and has negative bias associated with RH. Figure 3.5 shows that as uncertainty increases, the RH, and the FVC term to a lesser extent, the component estimates tend to collapse in either direction. The total ET estimate is similarly sensitive to RH (RMSD = 122%), while the bias becomes somewhat mitigated when the components are aggregated (MBD = -3%). Figure 3.8 shows that large masses of probabilities associated with RH aggregate in the transpiration and interception terms at a relative error of -1, signifying that a change to RH caused the new model estimate to collapse to 0 flux. The soil evaporation estimate appears to be particularly sensitive to changes in the input variables, as perturbations to RH (RMSD = 174%), temperature (RMSD = 132%), net radiation (RMSD = 50%), and FAPAR (RMSD = 84%) each exhibit their largest MBD and RMSD in the soil evaporation term.

GLEAM has five temporally variable forcings: net radiation, temperature, precipitation, vegetation optical depth (VOD), and shortwave outgoing radiation (Ku). Additionally, GLEAM has several static variables including MOD44B canopy fraction which is the primary value used to partition the total ET flux into separate ET components. GLEAM, among the three models, shows the least sensitivity to its inputs, as evidenced by the low RMSD and MBD. Each of the inputs show a slight negative bias in the transpiration estimate, and precipitation shows a negative bias in the total ET estimate. Figure 3.9 shows a curious distribution of error associated with precipitation in the soil evaporation term with a large positive tail. The interquartile range for several variables look quite skewed in figure 3.6, including VOD, Ku, and precipitation in many cases. While the skew appears quite severe, the mode remains near zero and the MBD remains quite small. Precipitation is the only variable influencing the GLEAM interception estimate while soil evaporation, transpiration, and the overall ET estimates are primarily influenced by net radiation (RMSD = 8.2, 8.2, and 7.6% respectively).

PM-MOD and PT-JPL share many similarities in their results from this analysis. Both models show large biases and uncertainty in their components associated with RH. However, in both models these biases do not manifest to the same extent in the total ET estimate. A similar pattern is also evident for both models in their vegetation inputs. Both NDVI in PT-JPL and FAPAR in PM-MOD show large uncertainties with some bias in their component terms, while the total ET term exhibits far less sensitivity. Perhaps expectedly, temperature and radiation also show similar sensitivity for each model. Both models show an increased sensitivity to temperature in the soil evaporation term and both have similar ranges of RMSD associated with net radiation.

Figures 3.10-3.12 show the sensitivity of each model to perturbations in the forcing categorized as a function of the forcing (without perturbation) itself. The figures show the interquartile range and mode of the relative error associated with an uncertainty of 10%. These figures allow us to analyze how the model sensitivity changes based on the physical conditions at a given location. The figures shows trends in both the bias of the percentile values and in the interquartile range as well.

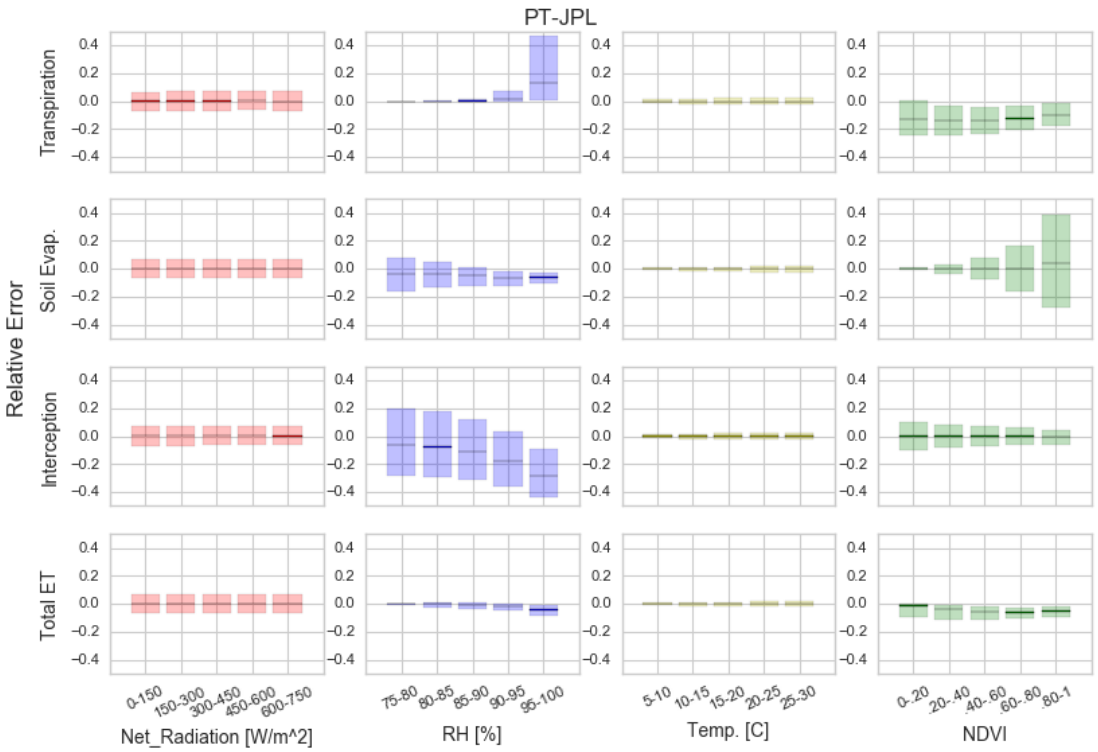

Figure 3.10: Relative error due to added uncertainty (σ = 10%) for each input variable of PT-JPL categorized by the raw value of the variable itself. The colored box represents the interquartile range of the distribution with the mode plotted as a line within the box.

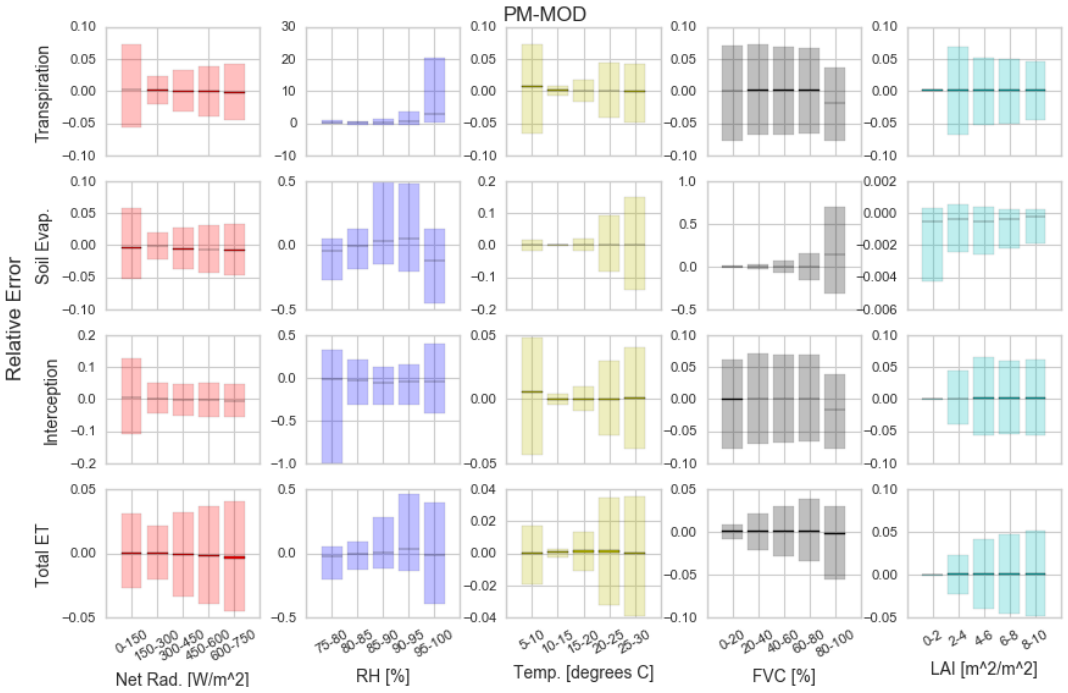

Figure 3.11: Relative error due to added uncertainty (σ = 10%) for each input variable of PM-MOD categorized by the raw value of the variable itself. The colored box represents the interquartile range of the distribution with the mode plotted as a line within the box.

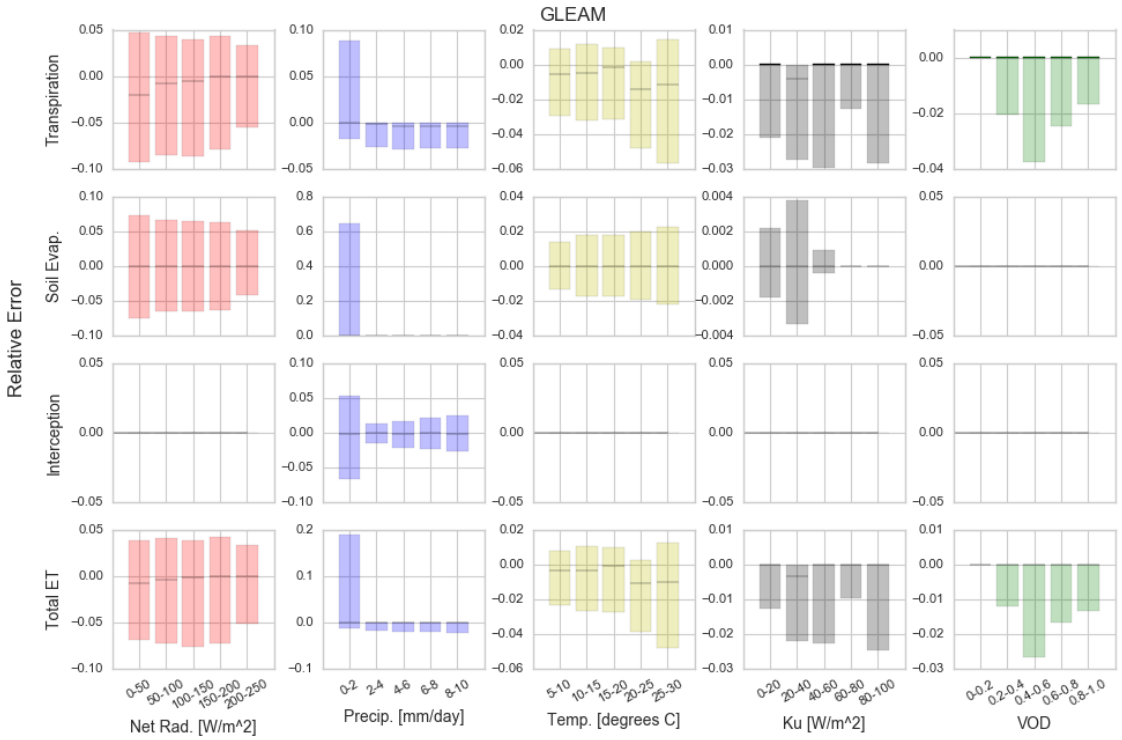

Figure 3.12: Relative error due to added uncertainty ($\sigma = 10\%$) for each input variable of GLEAM categorized by the raw value of the variable itself. The colored box represents the interquartile range of the distribution with the mode plotted as a line within the box.

PT-JPL shows a steady distribution with changing net radiation and temperature, while both the bias and range of the error distribution changes with RH and NDVI. However, the changes to uncertainty in the estimated ET components again contrast each other and as such limit the uncertainty in the total ET estimate at each of the ranges in input values. Both PM-MOD and PT-JPL exhibit the same increasing uncertainty with increasing RH in their transpiration component and again show similar increasing uncertainty in soil evaporation with increasing vegetation indices. PM-MOD, shown in figure 3.11, appears to be more sensitive to changes at extreme temperatures than to changes at more moderate temperatures. Interestingly, PM-MOD soil evaporation appears to be more sensitive to lower LAI values, but also more sensitive to higher values of FAPAR. GLEAM, shown in figure 3.12, is overwhelmingly more sensitive to changes in low precipitation events than larger events. Net

radiation and temperature show relatively unbiased and consistent distributions in error as those variables change, while VOD and Ku show somewhat more asymmetric distributions with an unbiased mode.

3.4 Discussion:

Because the uncertainty of the re-analysis products used to force the models is often difficult to determine, it is difficult to quantify the absolute error that forcing uncertainty might have on the estimates of ET and its components. The models also rely on temporally static parameters and constants that are not analyzed here. Despite these limitations, we are still able to offer insights into how the temporally variable inputs influence the model estimates. Of particular interest are the differences in how the forcing affects the component estimates as compared to the total ET estimate, and how uncertainty in the input variables can introduce bias into estimates.

The bias in relative error due to uncertainty in RH in both PT-JPL and PM-MOD is expected due to the non-linear dependence of the ET components to RH within these models. In both models, the model parameter f_{wet} - parameterized as a function of RH^4- is used to approximate surface wetness. It is important to consider that the relationship between humidity and a given ET component is very likely to be non-linear, making non-linear parameterizations, as in PT-JPL and PM-MOD, appropriate (Fisher et al., 2008; Stone et al., 1977). However, large forcing uncertainties in non-linear models can introduce large biases to the model estimate, and thus might debilitate the usefulness of the model. Figure 3.4 shows how increasing uncertainty in the RH introduces growing bias in the component estimates of PT-JPL and PM-MOD. The point at which this bias becomes detrimental is

determined by the uncertainty of the input variable. It should be noted that bias could also be introduced to RH by the use of the truncated-normal distribution, although only near the upper bound.

Despite the similar use of RH in PT-JPL and PM-MOD, both models do have slightly different error distributions. PM-MOD filters RH values less than 0.70 and masks them with a value of 0, while PT-JPL does not. This filter is likely responsible for the large probability mass in the interception component shown in figure 3.8 at a relative error of -1 where added uncertainty has RH values greater than 0.70 to become filtered. Both models are also dependent on vapor pressure deficit (VPD), a function of RH and temperature. PM-MOD is dependent on VPD as part of the Penman-Monteith equation and both models incorporate VPD into their soil evaporation estimates. Notice that both PT-JPL and PM-MOD soil evaporation estimates are very sensitive to both RH and temperature, and PM-MOD is generally more sensitive than PT-JPL to both RH and temperature, likely due to the employment of VPD.

The soil evaporation term of PT-JPL and PM-MOD when compared to field estimates shows very little agreement (Talsma et al., 2018). Here, we find soil evaporation for those models to be generally quite sensitive to uncertainty in the inputs of RH, temperature, NDVI, and FAPAR. Furthermore, the sensitivity of the soil evaporation estimate appears to vary depending on the value of the input variable itself. These factors could explain the large variance in their agreement with the field studies.

Given the high sensitivity of soil evaporation to forcing uncertainty in each of the models, this component could be responsible for a large portion of the partitioning divergence between models. Improvement of the soil evaporation term, therefore, offers a

potential area in which to focus efforts in order to improve model partitioning. Similarly, a study of North American Land Data Assimaltion System (NLDAS) ET models shows that soil evaporation contributes relatively more to the uncertainty in the partitioning of the ET flux, than it does to the ET flux itself (Kumar et al., 2018). Those results also demonstrate that the ability of the model to estimate transpiration is largely responsible for its ability to estimate the total flux. Despite the inability to estimate soil evaporation or correctly partition the flux, the total ET estimate remained reasonably accurate. Furthermore, counteracting biases in the ET components from PT-JPL and PM-MOD show a decreased sensitivity of the total ET estimate to forcing as compared to the component estimates.

Interestingly, in many of the instances where bias is exhibited in the modeled components, the biases counteract each other in the aggregate total ET estimate. This is especially true for the terms used to partition the available water or radiation between ET components (RH, NDVI, FAPAR). This could help to explain some of the divergences in partitioning between models as well as the negative bias previously found in the PT-JPL and PM-MOD transpiration estimates when compared to field estimates of transpiration. This also suggests that uncertainty in the estimated ET components is likely larger than in the total ET estimates. Our results suggest that, in the cases of PT-JPL and PM-MOD, slight changes in input variables have the potential to vastly change the partitioning of ET while resulting in only modest changes to the overall ET estimate.

GLEAM, however, appears to be much more reliant on the underlying formulation of the model and model constants than on its input variables. The RMSD and MBD exhibited by GLEAM is roughly an order of magnitude smaller than that of PM-MOD and PT-JPL. Given the complexity of GLEAM compared to the other two models, it might be expected that

GLEAM would be more sensitive to model formulations and constants. This complexity also makes interpreting the biases of the error distributions in the model more difficult. Precipitation, Ku, and VOD exhibit very asymmetric distributions in both figures 3.6 and 3.9. The complexity of GLEAM results in very few truly linear relationships, as the model relies on water balances, storage capacities, and stress factors to account for the water available to various evaporative pathways. Here it results in somewhat skewed distributions in estimates, but the various parameterizations within the model can likely be adjusted to accommodate those errors. The distribution of precipitation is also characterized by a large frequency of very small events, which may be prone to biases introduced by the truncated-normal distribution. When perturbed by an increasing level of uncertainty, the distribution collapses so that these small events become less frequent. Given the greater sensitivity to these smaller events shown in figure 3.12, the distribution of error then becomes skewed for the various components.

Despite similar underlying formulations, each model exhibits large sensitivity to different forcings. GLEAM interception is exclusively sensitive to precipitation, while the remainder of the GLEAM components are largely sensitive to net radiation. While PT-JPL and PM-MOD are also sensitive to net radiation, they are far more sensitive in each of their component estimates to RH and vegetation forcings. The PT-JPL ET estimate appears to be very sensitive to changes in NDVI (RMSD = 1.01), suggesting that changes to vegetation patterns due to climate change could coincide with large changes to the ET estimate. Similarly, the PM-MOD ET estimate is most sensitive to changes in RH (RMSD = 1.22) largely driven by the soil evaporation term.

Furthermore, models may be more sensitive to forcing errors at various extremes of that variable. The GLEAM model's sensitivity to low precipitation events opposed to larger events is likely due to various water storage factors and the large frequency of low rainfall events. Both PM-MOD and PT-JPL transpiration components are more sensitive at high RH values than at lower values. This is due to the f_{wet} term, which exhibits a much higher slope as a function of humidity at high RH values and due to the negative bias introduced by the truncated-normal distribution. PM-MOD ET also shows increasing uncertainty at increasing values of both LAI and FVC. In case of FVC, the relationship appears to be driven by the soil evaporation term, which is substantially more uncertain at high FVC values. PT-JPL exhibits a similar trend in soil evaporation, but in the NDVI term.

Where trends exist in the uncertainty of the model with changing ambient conditions informs where these model estimates may be vulnerable to large uncertainties. The partitioning of both PM-MOD and PT-JPL seems particularly sensitive to extremes in vegetation and RH forcing, although RH could be influenced by the distributions used in this analysis. Again, the trends in component uncertainty tend to mitigate one another when aggregated in the total ET estimate of PT-JPL. However, PM-MOD exhibits larger uncertainty in its total ET estimate at elevated values of radiation, vegetation indices, and temperature. This is somewhat worrisome considering that the largest fluxes coincide with large values of these variables and represent areas where accurate estimates of ET are exceedingly important to climate forecasts. The utility of global scale ET models is predicated on their ability to measure large fluxes and, ideally, the model would exhibit higher certainty in its estimation at elevated fluxes.

3.5 Conclusion:

The demand for research and data concerning ET and ET components will continue to fuel efforts into various remote sensing-based models (Fisher et al., 2017; Zhang et al., 2017). However, changes in climate and its related feedbacks will require models to show correct sensitivity to many input variables (Friedlingstein et al., 2014; Lawrence et al., 2007). Furthermore, the rapid expansion in remote sensing products, data, and techniques (Marshall et al., 2016; McCabe et al., 2017; Sun et al., 2017) presents challenges in understanding and quantifying how errors and uncertainty within the forcing data will propagate to model estimates (Badgley et al., 2015; Vinukollu et al., 2011). As large datasets and modeled products become ubiquitous, so will the need to thoroughly validate, test, and explore those products.

While ET based science has progressed to the point of offering relatively accurate estimates of total ET at a global extent and various scales, the various components of ET, transpiration, soil evaporation, and interception, remain difficult to evaluate. The existence of strong divergences in modeled ET components suggests that some models' total ET estimates may be prone to future inaccuracies as climate and the observed partitioning of ET chagnes. The results found here offer further evidence that estimates of the ET components are subject to greater uncertainty than the total ET estimate. The partitioning of ET remains a key question in both climate and ET research and further examination of modeled components is needed.

While some studies have attempted to intercompare models using a similar forcing dataset (McCabe et al., 2016; Michel et al., 2016; Mueller et al., 2011; Vinukollu et al., 2011), others have compared a single model output using multiple data sources (Badgley et

al., 2015). We instead intercompare models at a range of forcing uncertainties. This approach ignores systematic errors in the forcing products, but allows for a conceptual framework to assess how improvements to forcing products might improve model performance. The sensitivity analyses in this study allow us to determine what variables drive the individual component estimates and helps to explain why the models achieve vastly different ET partitioning strategies. We can also assess if the uncertainty of the forcing data introduces significant bias into the ET estimate based on the non-linearity of the model formulation. The results of the study present a means to assess the strategies of each model, and to compare those strategies against our theoretical understanding of ET and its components.

Some of the main findings of this study are:

- GLEAM is primarily sensitive to net radiation, except for the interception component, which is exclusively driven by precipitation.
- GLEAM is much more sensitive to variability in low precipitation events as compared to larger events.
- GLEAM is comparatively less sensitive to changes in its input variables than PM-MOD and PT-JPL. The complexity of the GLEAM model likely means that it is much more sensitive to the model formulations and parameterizations.
- The non-linear use of RH in both PT-JPL and PM-MOD results in large biases in the component estimates associated with the uncertainty of the RH product.
- Both PT-JPL and PM-MOD soil evaporation show large sensitivity to inputs, perhaps creating greater overall uncertainty in the soil evaporation estimate.
- Variables associated with large biases in component estimates often counteract each other to limit bias and uncertainty in the total ET estimate. Changes to forcing could

cause large changes to ET partitioning within the model with comparatively smaller changes to the overall ET estimate.

- Both PM-MOD and PT-JPL soil evaporation are much more sensitive to changes in vegetation when vegetation indices are high. This suggests larger uncertainties in the soil evaporation estimate in forests. PM-MOD's ET estimate is also more sensitive to larger values of net radiation, vegetation indices, and temperature.

Data Availability

The WACMOS-ET Reference Input Data Set was provided courtesy of the WACMOS-ET project and Estellus. http://wacmoset.estellus.eu/index.php?static9/data

The MOD12C1 data product was retrieved from the online Data Pool, courtesy of the NASA Land Processes Distributed Active Archive Center (LP DAAC), USGS/Earth Resources Observation and Science (EROS) Center, Sioux Falls, South Dakota, https://lpdaac.usgs.gov/data_access/data_pool

The MOD15A2 data product was retrieved from the AppEEARS data page, courtesy of the NASA Earth Observing System Data and Information System(EOSDIS) and the Land Processing Distributed Active Archive Center (LP DAAC), USGS/Earth Resources Observation and Science (EROS) Center, Sioux Falls, South Dakota, https://lpdaacsvc.cr.usgs.gov/appeears

References:

Adler, R.F., Huffman, G.J., Chang, A., Ferraro, R., Xie, P.-P., Janowiak, J., Rudolf, B., Schneider, U., Curtis, S., Bolvin, D., Gruber, A., Susskind, J., Arkin, P., Nelkin, E., Adler, R.F., Huffman, G.J., Chang, A., Ferraro, R., Xie, P.-P., Janowiak, J., Rudolf, B., Schneider, U., Curtis, S., Bolvin, D., Gruber, A., Susskind, J., Arkin, P., Nelkin, E., 2003. The Version-2 Global Precipitation Climatology Project (GPCP) Monthly Precipitation Analysis (1979–Present). J. Hydrometeorol. 4, 1147–1167. doi:10.1175/1525-7541(2003)004<1147:TVGPCP>2.0.CO;2

Allen, C.D., Macalady, A.K., Chenchouni, H., Bachelet, D., McDowell, N., Vennetier, M., Kitzberger, T., Rigling, A., Breshears, D.D., Hogg, E.H. (Ted), Gonzalez, P., Fensham, R., Zhang, Z., Castro, J., Demidova, N., Lim, J.-H., Allard, G., Running, S.W., Semerci, A., Cobb, N., 2010. A global overview of drought and heat-induced tree mortality reveals emerging climate change risks for forests. For. Ecol. Manage. 259, 660–684. doi:10.1016/J.FORECO.2009.09.001

Aminzadeh, M., Or, D., 2017. Pore-scale study of thermal fields during evaporation from drying porous surfaces. Int. J. Heat Mass Transf. 104, 1189–1201. doi:10.1016/J.IJHEATMASSTRANSFER.2016.09.039

Anderson, M.C., Norman, J.M., Mecikalski, J.R., Otkin, J.A., Kustas, W.P., 2007. A climatological study of evapotranspiration and moisture stress across the continental United States based on thermal remote sensing: 1. Model formulation. J. Geophys. Res. 112, D10117. doi:10.1029/2006JD007506

Badgley, G., Fisher, J.B., Jiménez, C., Tu, K.P., Vinukollu, R., Badgley, G., Fisher, J.B., Jiménez, C., Tu, K.P., Vinukollu, R., 2015. On Uncertainty in Global Terrestrial Evapotranspiration Estimates from Choice of Input Forcing Datasets*. J. Hydrometeorol. 16, 1449–1455. doi:10.1175/JHM-D-14-0040.1

Baldocchi, D., Falge, E., Gu, L., Olson, R., Hollinger, D., Running, S., Anthoni, P., Bernhofer, C., Davis, K., Evans, R., Fuentes, J., Goldstein, A., Katul, G., Law, B., Lee, X., Malhi, Y., Meyers, T., Munger, W., Oechel, W., Paw, K.T., Pilegaard, K., Schmid, H.P., Valentini, R., Verma, S., Vesala, T., Wilson, K., Wofsy, S., Hall, R., 2001. FLUXNET: A New Tool to Study the Temporal and Spatial Variability of Ecosystem-Scale Carbon Dioxide, Water Vapor, and Energy Flux Densities 82.

Bonan, G.B., 2008. Forests and climate change: forcings, feedbacks, and the climate benefits of forests. Science 320, 1444–9. doi:10.1126/science.1155121

Brunel, J.P., Walker, G.R., Dighton, J.C., Montenya, B., 1997. Use of stable isotopes of water to determine the origin of water used by the vegetation and to partition evapotranspiration. A case study from HAPEX-Sahel. J. Hydrol. 188–189, 466–481. doi:10.1016/S0022-1694(96)03188-5

Carlyle-Moses, D.E., Gash, J.H.C., 2011. Rainfall Interception Loss by Forest Canopies. Springer, Dordrecht, pp. 407–423. doi:10.1007/978-94-007-1363-5_20

Cavanaugh, M.L., Kurc, S.A., Scott, R.L., 2011. Evapotranspiration partitioning in semiarid shrubland ecosystems: a two-site evaluation of soil moisture control on transpiration. Ecohydrology 4, 671–681. doi:10.1002/eco.157

Ciais, P., Reichstein, M., Viovy, N., Granier, A., Ogée, J., Allard, V., Aubinet, M., Buchmann, N., Bernhofer, C., Carrara, A., Chevallier, F., De Noblet, N., Friend, A.D., Friedlingstein, P., Grünwald, T., Heinesch, B., Keronen, P., Knohl, A., Krinner, G.,

Loustau, D., Manca, G., Matteucci, G., Miglietta, F., Ourcival, J.M., Papale, D., Pilegaard, K., Rambal, S., Seufert, G., Soussana, J.F., Sanz, M.J., Schulze, E.D., Vesala, T., Valentini, R., 2005. Europe-wide reduction in primary productivity caused by the heat and drought in 2003. Nature 437, 529–533. doi:10.1038/nature03972

Crockford, R.H., Richardson, D.P., 2000. Partitioning of rainfall into throughfall, stemflow and interception: effect of forest type, ground cover and climate. Hydrol. Process. 14, 2903–2920. doi:10.1002/1099-1085(200011/12)14:16/17<2903::AID-HYP126>3.0.CO;2-6

David, J.S., Valente, F., Gash, J.H., 2005. Evaporation of Intercepted Rainfall, in: Encyclopedia of Hydrological Sciences. John Wiley & Sons, Ltd, Chichester, UK. doi:10.1002/0470848944.hsa046

Decker, M., Or, D., Pitman, A., Ukkola, A., 2017. New turbulent resistance parameterization for soil evaporation based on a pore-scale model: Impact on surface fluxes in CABLE. J. Adv. Model. Earth Syst. 9, 220–238. doi:10.1002/2016MS000832

Dee, D., Uppala, M.S., Simmons, J.A., Berrisford, P., Poli, P., Kobayashi, S., Andrae, U., Balmaseda, A.M., Balsamo, G., Bauer, P., Bechtold, P., Beljaars, M.A.C., van de Berg, L., Bidlot, J., Bormann, N., Delsol, C., Dragani, R., Fuentes, M., Geer, J.A., Haimberger, L., Healy, B.S., Hersbach, H., Holm, V.E., Isaksen, L., Kallberg, P., Khaler, M., Matricardi, M., McNally, P.A., Monge-Sanz, M.B., Morcrette, .J., Park, B.K., Peubey, C., de Rosnay, P., Tovolato, C., Thapaut, J.N., Vitart, F., 2011. The ERA-Interim reanalysis: configuration and performance of the data assimilation system. R. Meteorol. Soc. 137, 553–597. doi:10.1002/qj.828

Demaria, E.M., Nijssen, B., Wagener, T., 2007. Monte Carlo sensitivity analysis of land surface parameters using the Variable Infiltration Capacity model. J. Geophys. Res. 112, D11113. doi:10.1029/2006JD007534

Didan, K., 2015. MOD13A2 MODIS/Terra Vegetation Indices 16-Day L3 Global 1km SIN GRID V006 [Dataset]. doi:10.5067/MODIS/MOD13A2.006

Dolman, A.J., Miralles, D.G., de Jeu, R.A.M., 2014. Fifty years since Monteith's 1965 seminal paper: the emergence of global ecohydrology. Ecohydrology 7, 897–902. doi:10.1002/eco.1505

Dye, P.J., Olbrich, B.W., Poulter, A.G., 1991. The Influence of Growth Rings in Pinus patula on Heat Pulse Velocity and Sap Flow Measurement. J. Exp. Bot. 42, 867–870. doi:10.1093/jxb/42.7.867

Ek, M.B., Holtslag, A.A.M., 2004. Influence of Soil Moisture on Boundary Layer Cloud Development. J. Hydrometeorol. 5, 86–99. doi:10.1175/1525-7541(2004)005<0086:IOSMOB>2.0.CO;2

Ershadi, A., Mccabe, M.F., Evans, J.P., Wood, E.F., 2015. Impact of model structure and parameterization on Penman-Monteith type evaporation models. J. Hydrol. 525, 521–535. doi:10.1016/j.jhydrol.2015.04.008

Fernández, J.E., Durán, P.J., Palomo, M.J., Diaz-Espejo, A., Chamorro, V., Girón, I.F., 2006. Calibration of sap flow estimated by the compensation heat pulse method in olive, plum and orange trees: relationships with xylem anatomy. Tree Physiol. 26, 719–28.

Fisher, J.B., Melton, F., Middleton, E., Hain, C., Anderson, M., Allen, R., McCabe, M.F., Hook, S., Baldocchi, D., Townsend, P.A., Kilic, A., Tu, K., Miralles, D.D., Perret, J., Lagouarde, J.-P., Waliser, D., Purdy, A.J., French, A., Schimel, D., Famiglietti, J.S., Stephens, G., Wood, E.F., 2017. The future of evapotranspiration: Global requirements

for ecosystem functioning, carbon and climate feedbacks, agricultural management, and water resources. Water Resour. Res. 53, 2618–2626. doi:10.1002/2016WR020175

Fisher, J.B., Tu, K.P., Baldocchi, D.D., 2008. Global estimates of the land–atmosphere water flux based on monthly AVHRR and ISLSCP-II data, validated at 16 FLUXNET sites. Remote Sens. Environ. 112, 901–919. doi:10.1016/J.RSE.2007.06.025

Friedl, M.A., Sulla-Menashe, D., Tan, B., Schneider, A., Ramankutty, N., Sibley, A., Huang, X., 2009. MODIS Collection 5 global land cover: Algorithm refinements and characterization of new datasets. doi:10.1016/j.rse.2009.08.016

Friedlingstein, P., Meinshausen, M., Arora, V.K., Jones, C.D., Anav, A., Liddicoat, S.K., Knutti, R., Friedlingstein, P., Meinshausen, M., Arora, V.K., Jones, C.D., Anav, A., Liddicoat, S.K., Knutti, R., 2014. Uncertainties in CMIP5 Climate Projections due to Carbon Cycle Feedbacks. J. Clim. 27, 511–526. doi:10.1175/JCLI-D-12-00579.1

Gash, J.H.C., 1979. An analytical model of rainfall interception by forests. Q. J. R. Meteorol. Soc. 105, 43–55. doi:10.1002/qj.49710544304

Gibson, J.J., Edwards, T.W.D., 2002. Regional water balance trends and evaporation-transpiration partitioning from a stable isotope survey of lakes in northern Canada. Global Biogeochem. Cycles 16, 10-1-10–14. doi:10.1029/2001GB001839

Glenn, E.P., Huete, A.R., Nagler, P.L., Hirschboeck, K.K., Brown, P., 2007. Integrating Remote Sensing and Ground Methods to Estimate Evapotranspiration. CRC. Crit. Rev. Plant Sci. 26, 139–168. doi:10.1080/07352680701402503

Glenn, E.P., Huete, A.R., Nagler, P.L., Nelson, S.G., 2008. Relationship Between Remotely-sensed Vegetation Indices, Canopy Attributes and Plant Physiological Processes: What Vegetation Indices Can and Cannot Tell Us About the Landscape. Sensors 8, 2136–2160. doi:10.3390/s8042136

Good, S.P., Moore, G.W., Miralles, D.G., 2017. A mesic maximum in biological water use demarcates biome sensitivity to aridity shifts. Nat. Ecol. Evol. 1, 1883–1888. doi:10.1038/s41559-017-0371-8

Good, S.P., Noone, D., Bowen, G., 2015. Hydrologic connectivity constrains partitioning of global terrestrial water fluxes. Science 349, 175–7. doi:10.1126/science.aaa5931

Goulden, M.L., Bales, R.C., 2014. Mountain runoff vulnerability to increased evapotranspiration with vegetation expansion. Proc. Natl. Acad. Sci. U. S. A. 111, 14071–5. doi:10.1073/pnas.1319316111

Grayson, R.B., Western, A.W., Chiew, F.H.S., Bloschl, G., 1997. Preferred states in spatial soil moisture patterns: Local and nonlocal controls. Water Resour. Res. 33, 2897–2908.

Haghighi, E., Or, D., 2013. Evaporation from porous surfaces into turbulent airflows: Coupling eddy characteristics with pore scale vapor diffusion. Water Resour. Res. 49, 8432–8442. doi:10.1002/2012WR013324

Hammersley, J.M., Handscomb, D.C., 1964. General Principles of the Monte Carlo Method, in: Monte Carlo Methods. Springer Netherlands, Dordrecht, pp. 50–75. doi:10.1007/978-94-009-5819-7_5

Hobbins, M.T., Ramírez, J.A., Brown, T.C., 2004. Trends in pan evaporation and actual evapotranspiration across the conterminous U.S.: Paradoxical or complementary? Geophys. Res. Lett. doi:10.1029/2004GL019846

Holwerda, F., Bruijnzeel, L.A., Scatena, F.N., 2011. Comparison of passive fog gauges for determining fog duration and fog interception by a Puerto Rican elfin cloud forest. Hydrol. Process. 25, 367–373. doi:10.1002/hyp.7641

Hu, Z., Yu, G., Zhou, Y., Sun, X., Li, Y., Shi, P., Wang, Y., Song, X., Zheng, Z., Zhang, L., Li, S., 2009. Partitioning of evapotranspiration and its controls in four grassland ecosystems: Application of a two-source model. Agric. For. Meteorol. 149, 1410–1420. doi:10.1016/J.AGRFORMET.2009.03.014

Hulley, G., Hook, S., Fisher, J., Lee, C., 2017. ECOSTRESS, A NASA Earth-Ventures Instrument for studying links between the water cycle and plant health over the diurnal cycle, in: 2017 IEEE International Geoscience and Remote Sensing Symposium (IGARSS). IEEE, pp. 5494–5496. doi:10.1109/IGARSS.2017.8128248

Huntington, T.G., 2006. Evidence for intensification of the global water cycle: Review and synthesis. J. Hydrol. 319, 83–95. doi:10.1016/J.JHYDROL.2005.07.003

Jasechko, S., Sharp, Z.D., Gibson, J.J., Birks, S.J., Yi, Y., Fawcett, P.J., 2013. Terrestrial water fluxes dominated by transpiration. Nature 496, 347–350. doi:10.1038/nature11983

Komatsu, H., 2005. Forest categorization according to dry-canopy evaporation rates in the growing season: comparison of the Priestley-Taylor coefficient values from various observation sites. Hydrol. Process. 19, 3873–3896. doi:10.1002/hyp.5987

Kumar, S., Holmes, T., Mocko, D.M., Wang, S., Peters-Lidard, C., 2018. Attribution of Flux Partitioning Variations between Land Surface Models over the Continental U.S. Remote Sens. 10. doi:10.3390/rs10050751

Lautz, L.K., 2008. Estimating groundwater evapotranspiration rates using diurnal water-table fluctuations in a semi-arid riparian zone. Hydrogeol. J. 16, 483–497. doi:10.1007/s10040-007-0239-0

Lawrence, D.M., Thornton, P.E., Oleson, K.W., Bonan, G.B., Lawrence, D.M., Thornton, P.E., Oleson, K.W., Bonan, G.B., 2007. The Partitioning of Evapotranspiration into Transpiration, Soil Evaporation, and Canopy Evaporation in a GCM: Impacts on Land–Atmosphere Interaction. J. Hydrometeorol. 8, 862–880. doi:10.1175/JHM596.1

Levia, D.F., Frost, E.E., 2006. Variability of throughfall volume and solute inputs in wooded ecosystems. Prog. Phys. Geogr. 30, 605–632. doi:10.1177/0309133306071145

Littell, J.S., Peterson, D.L., Riley, K.L., Liu, Y., Luce, C.H., 2016. A review of the relationships between drought and forest fire in the United States. Glob. Chang. Biol. 22, 2353–2369. doi:10.1111/gcb.13275

Mancosu, N., Snyder, R., Kyriakakis, G., Spano, D., 2015. Water Scarcity and Future Challenges for Food Production. Water 7, 975–992. doi:10.3390/w7030975

Marshall, K.N., Cooper, D.J., Hobbs, N.T., 2014. Interactions among herbivory, climate, topography and plant age shape riparian willow dynamics in northern Yellowstone National Park, USA. J. Ecol. 102, 667–677. doi:10.1111/1365-2745.12225

Marshall, M., Thenkabail, P., Biggs, T., Post, K., 2016. Hyperspectral narrowband and multispectral broadband indices for remote sensing of crop evapotranspiration and its components (transpiration and soil evaporation). Agric. For. Meteorol. 218219, 122–134. doi:10.1016/j.agrformet.2015.12.025

Martens, B., Miralles, D., Lievens, H., Fernández-Prieto, D., Verhoest, N.E.C., 2016. Improving terrestrial evaporation estimates over continental Australia through assimilation of SMOS soil moisture. Int. J. Appl. Earth Obs. Geoinf. 48, 146–162. doi:10.1016/J.JAG.2015.09.012

Martens, B., Miralles, D.G., Lievens, H., van der Schalie, R., de Jeu, R.A.M., Fernández-Prieto, D., Beck, H.E., Dorigo, W.A., Verhoest, N.E.C., 2017. GLEAM v3: satellite-based land evaporation and root-zone soil moisture. Geosci. Model Dev. 10, 1903–1925.

doi:10.5194/gmd-10-1903-2017
McCabe, M.F., Aragon, B., Houborg, R., Mascaro, J., 2017. CubeSats in Hydrology: Ultrahigh-Resolution Insights Into Vegetation Dynamics and Terrestrial Evaporation. Water Resour. Res. 53, 10017–10024. doi:10.1002/2017WR022240
Mccabe, M.F., Ershadi, A., Jimenez, C., Miralles, D.G., Michel, D., Wood, E.F., 2016. The GEWEX LandFlux project: evaluation of model evaporation using tower-based and globally gridded forcing data. Geosci. Model Dev 9, 283–305. doi:10.5194/gmd-9-283-2016
Mccabe, M.F., Rodell, M., Alsdorf, D.E., Miralles, D.G., Uijlenhoet, R., Wagner, W., Lucieer, A., Houborg, R., Verhoest, N.E.C., Franz, T.E., Shi, J., Gao, H., Wood, E.F., 2017. The future of Earth observation in hydrology. Earth Syst. Sci 215194, 3879–3914. doi:10.5194/hess-21-3879-2017
McJannet, D., Fitch, P., Disher, M., Wallace, J., 2007. Measurements of transpiration in four tropical rainforest types of north Queensland, Australia. Hydrol. Process. 21, 3549–3564. doi:10.1002/hyp.6576
Meng, X.H., Evans, J.P., McCabe, M.F., Meng, X.H., Evans, J.P., McCabe, M.F., 2014. The Impact of Observed Vegetation Changes on Land–Atmosphere Feedbacks During Drought. J. Hydrometeorol. 15, 759–776. doi:10.1175/JHM-D-13-0130.1
Merlin, O., Stefan, V.G., Amazirh, A., Chanzy, A., Ceschia, E., Er-Raki, S., Gentine, P., Tallec, T., Ezzahar, J., Bircher, S., Beringer, J., Khabba, S., 2016. Modeling soil evaporation efficiency in a range of soil and atmospheric conditions using a meta-analysis approach. Water Resour. Res. doi:10.1002/2015WR018233
Michel, D., Jiménez, C., Miralles, D.G., Jung, M., Hirschi, M., Ershadi, A., Martens, B., Mccabe, M.F., Fisher, J.B., Mu, Q., Seneviratne, S.I., Wood, E.F., Fernández-Prieto, D., 2016. The WACMOS-ET project – Part 1: Tower-scale evaluation of four remote-sensing-based evapotranspiration algorithms. Hydrol. Earth Syst. Sci 20, 803–822. doi:10.5194/hess-20-803-2016
Miralles, D.G., Gash, J.H., Holmes, T.R.H., De Jeu, R.A.M., Dolman, A.J., 2010. Global canopy interception from satellite observations. J. Geophys. Res 115. doi:10.1029/2009JD013530
Miralles, D.G., Holmes, T.R.H., De Jeu, R.A.M., Gash, J.H., Meesters, A.G.C.A., Dolman, A.J., 2011. Global land-surface evaporation estimated from satellite-based observations. Hydrol. Earth Syst. Sci 15, 453–469. doi:10.5194/hess-15-453-2011
Miralles, D.G., Jiménez, C., Jung, M., Michel, D., Ershadi, A., McCabe, M.F., Hirschi, M., Martens, B., Dolman, A.J., Fisher, J.B., Mu, Q., Seneviratne, S.I., Wood, E.F., Fernaìndez-Prieto, D., 2016. The WACMOS-ET project – Part 2: Evaluation of global terrestrial evaporation data sets. Hydrol. Earth Syst. Sci. Discuss. 12, 10651–10700. doi:10.5194/hessd-12-10651-2015
Molden, D., Oweis, T., Steduto, P., Bindraban, P., Hanjra, M.A., Kijne, J., 2010. Improving agricultural water productivity: Between optimism and caution. Agric. Water Manag. 97, 528–535. doi:10.1016/J.AGWAT.2009.03.023
Mu, Q., Zhao, M., Running, S.W., 2011. Improvements to a MODIS global terrestrial evapotranspiration algorithm. Remote Sens. Environ. 115, 1781–1800. doi:10.1016/j.rse.2011.02.019
Mueller, B., Seneviratne, S.I., Jimenez, C., Corti, T., Hirschi, M., Balsamo, G., Ciais, P., Dirmeyer, P., Fisher, J.B., Guo, Z., Jung, M., Maignan, F., McCabe, M.F., Reichle, R.,

Reichstein, M., Rodell, M., Sheffield, J., Teuling, A.J., Wang, K., Wood, E.F., Zhang, Y., 2011. Evaluation of global observations-based evapotranspiration datasets and IPCC AR4 simulations. Geophys. Res. Lett. 38, n/a-n/a. doi:10.1029/2010GL046230

Muzylo, A., Llorens, P., Valente, F., Keizer, J.J., Domingo, F., Gash, J.H.C., 2009. A review of rainfall interception modelling. J. Hydrol. 370, 191–206. doi:10.1016/J.JHYDROL.2009.02.058

Nizinski, J.J., Galat, G., Galat-Luong, A., 2011. Water balance and sustainability of eucalyptus plantations in the Kouilou basin (Congo-Brazzaville). Russ. J. Ecol. 42, 305–314. doi:10.1134/S1067413611040126

Norman Ay, J.M., Kustas, W.P., Humes, K.S., 1995. Source approach for estimating soil and vegetation energy fluxes in observations of directional radiometric surface temperature. Agric. For. Meteorol. 77, 263–293.

Novick, K.A., Ficklin, D.L., Stoy, P.C., Williams, C.A., Bohrer, G., Oishi, A.C., Papuga, S.A., Blanken, P.D., Noormets, A., Sulman, B.N., Scott, R.L., Wang, L., Phillips, R.P., 2016. The increasing importance of atmospheric demand for ecosystem water and carbon fluxes. Nat. Clim. Chang. 6, 1023–1027. doi:10.1038/nclimate3114

Oki, T., Kanae, S., 2006. Global hydrological cycles and world water resources. Science 313, 1068–72. doi:10.1126/science.1128845

Or, D., Lehmann, P., Shahraeeni, E., Shokri, N., 2013. Advances in Soil Evaporation Physics—A Review. Vadose Zo. J. 12, 0. doi:10.2136/vzj2012.0163

Owe, M., de Jeu, R., Walker, J., 2001. A methodology for surface soil moisture and vegetation optical depth retrieval using the microwave polarization difference index. IEEE Trans. Geosci. Remote Sens. 39, 1643–1654. doi:10.1109/36.942542

Pielke, R.A., Sr, ., Avissar, R., Raupach, M., Dolman, A.J., Zeng, X., Denning, A.S., 1998. Interactions between the atmosphere and terrestrial ecosystems: influence on weather and climate. Glob. Chang. Biol. 4, 461–475. doi:10.1046/j.1365-2486.1998.t01-1-00176.x

Pieruschka, R., Huber, G., Berry, J.A., 2010. Control of transpiration by radiation. Proc. Natl. Acad. Sci. U. S. A. 107, 13372–7. doi:10.1073/pnas.0913177107

Porkka, M., Gerten, D., Schaphoff, S., Siebert, S., Kummu, M., 2016. Causes and trends of water scarcity in food production. Environ. Res. Lett. 11, 15001. doi:10.1088/1748-9326/11/1/015001

Poyatos, R., Granda, V., Molowny-Horas, R., Mencuccini, M., Steppe, K., Martínez-Vilalta, J., 2016. SAPFLUXNET: towards a global database of sap flow measurements. Tree Physiol. 36, 1449–1455. doi:10.1093/treephys/tpw110

Priestley, C.H.B., Taylor, R.J., 1972. On the assessment of sruface heat flux and evaporation using large scale parameters. Mon. Weather Rev. 81–92.

Purdy, A.J., Fisher, J.B., Goulden, M.L., Famiglietti, J.S., 2016. Ground heat flux: An analytical review of 6 models evaluated at 88 sites and globally. J. Geophys. Res. Biogeosciences 121, 3045–3059. doi:10.1002/2016JG003591

Pypker, T.G., Bond, B.J., Link, T.E., Marks, D., Unsworth, M.H., 2005. The importance of canopy structure in controlling the interception loss of rainfall: Examples from a young and an old-growth Douglas-fir forest. Agric. For. Meteorol. 130, 113–129. doi:10.1016/J.AGRFORMET.2005.03.003

R. Myneni, Y.K., n.d. MOD15A2H MODIS/Terra Leaf Area Index/FPAR 8-Day L4 Global 500m SIN Grid V006. doi.org. doi:10.5067/modis/mod15a2h.006

Rana, G., Katerji, N., 2000. Measurement and estimation of actual evapotranspiration in the field under Mediterranean climate: a review. Eur. J. Agron. 13, 125–153. doi:10.1016/S1161-0301(00)00070-8

Robert, C.P., 1995. Simulation of truncated normal variables. Stat. Comput. 5, 121–125. doi:10.1007/BF00143942

Schlesinger, W.H., Jasechko, S., 2014. Transpiration in the global water cycle. Agric. For. Meteorol. 189–190, 115–117. doi:10.1016/j.agrformet.2014.01.011

Schmugge, T.J., Kustas, W.P., Ritchie, J.C., Jackson, T.J., Rango, A., 2002. Remote sensing in hydrology. Adv. Water Resour. 25, 1367–1385. doi:10.1016/S0309-1708(02)00065-9

Seneviratne, S.I., Corti, T., Davin, E.L., Hirschi, M., Jaeger, E.B., Lehner, I., Orlowsky, B., Teuling, A.J., 2010. Investigating soil moisture–climate interactions in a changing climate: A review. Earth-Science Rev. 99, 125–161. doi:10.1016/J.EARSCIREV.2010.02.004

Shukla, J., Mintz, Y., 1982. Influence of Land-Surface Evapotranspiration on the Earth's Climate. Science 215, 1498–501. doi:10.1126/science.215.4539.1498

Spinoni, J., Naumann, G., Carrao, H., Barbosa, P., Vogt, J., 2014. World drought frequency, duration, and severity for 1951-2010. Int. J. Climatol. 34, 2792–2804. doi:10.1002/joc.3875

Stackhouse, P., Gupts, S., Cox, S., Mikovits, J., Zhang, T., Chiachiio, M., 2004. 12-year surface radiation budget data set. GEWEX News 14, 10–12.

Stone, P.H., Chow, S., Quirr, W.J., Stone, P.H., Chow, S., Quirr, W.J., 1977. The July Climate and a Comparison of the January and July Climates Simulated by the GISS General Circulation Model. Mon. Weather Rev. 105, 170–194. doi:10.1175/1520-0493(1977)105<0170:TJCAAC>2.0.CO;2

Sun, L., Anderson, M.C., Gao, F., Hain, C., Alfieri, J.G., Sharifi, A., McCarty, G.W., Yang, Y., Yang, Y., Kustas, W.P., McKee, L., 2017. Investigating water use over the Choptank River Watershed using a multisatellite data fusion approach. Water Resour. Res. 53, 5298–5319. doi:10.1002/2017WR020700

Talsma, C., Good, S.P., Jimenez, C., Martens, B., Fisher, J., 2017. Evaluation of Evapotranspiration Partitioning in Remote Sensing Models. Am. Geophys. Union, Fall Meet. 2017, Abstr. #H11M-08.

Talsma, C.J., Good, S.P., Jimenez, C., Martens, B., Fisher, J.B., Miralles, D.G., McCabe, M.F., Purdy, A.J., 2018. Partitioning of evapotranspiration in remote sensing-based models. Agric. For. Meteorol. doi:10.1016/j.agrformet.2018.05.010

Teuling, A.J., Hirschi, M., Ohmura, A., Wild, M., Reichstein, M., Ciais, P., Buchmann, N., Ammann, C., Montagnani, L., Richardson, A.D., Wohlfahrt, G., Seneviratne, S.I., 2009. A regional perspective on trends in continental evaporation. Geophys. Res. Lett. 36, n/a-n/a. doi:10.1029/2008GL036584

Trenberth, K.E., 2011. Changes in precipitation with climate change. Clim. Res. doi:10.2307/24872346

Valente, F., David, J.S., Gash, J.H.C., 1997. Modelling interception loss for two sparse eucalypt and pine forests in central Portugal using reformulated Rutter and Gash analytical models. J. Hydrol. 190, 141–162. doi:10.1016/S0022-1694(96)03066-1

Vinukollu, R.K., Meynadier, R., Sheffield, J., Wood, E.F., 2011. Multi-model, multi-sensor estimates of global evapotranspiration: climatology, uncertainties and trends. Hydrol. Process. 25, 3993–4010. doi:10.1002/hyp.8393

Wallace, J.., 2000. Increasing agricultural water use efficiency to meet future food production. Agric. Ecosyst. Environ. 82, 105–119. doi:10.1016/S0167-8809(00)00220-6

Wang, K., Dickinson, R.E., 2012. A review of global terrestrial evapotranspiration: Observation, modeling, climatology, and climatic variability. Rev. Geophys. 50. doi:10.1029/2011RG000373

Wang, L., Good, S.P., Caylor, K.K., 2014. Global synthesis of vegetation control on evapotranspiration partitioning. Geophys. Res. Lett. 41, 6753–6757. doi:10.1002/2014GL061439

Williams, D.G., Cable, W., Hultine, K., Hoedjes, J.C.B., Yepez, E.A., Simonneaux, V., Er-Raki, S., Boulet, G., de Bruin, H.A.R., Chehbouni, A., Hartogensis, O.K., Timouk, F., 2004. Evapotranspiration components determined by stable isotope, sap flow and eddy covariance techniques. Agric. For. Meteorol. 125, 241–258. doi:10.1016/J.AGRFORMET.2004.04.008

Yepez, E.A., Huxman, T.E., Ignace, D.D., English, N.B., Weltzin, J.F., Castellanos, A.E., Williams, D.G., 2005. Dynamics of transpiration and evaporation following a moisture pulse in semiarid grassland: A chamber-based isotope method for partitioning flux components. Agric. For. Meteorol. 132, 359–376. doi:10.1016/j.agrformet.2005.09.006

Zaitchik, B.F., Santanello, J.A., Kumar, S. V., Peters-Lidard, C.D., Zaitchik, B.F., Santanello, J.A., Kumar, S. V., Peters-Lidard, C.D., 2013. Representation of Soil Moisture Feedbacks during Drought in NASA Unified WRF (NU-WRF). J. Hydrometeorol. 14, 360–367. doi:10.1175/JHM-D-12-069.1

Zhang, K., Kimball, J.S., Running, S.W., 2016. A review of remote sensing based actual evapotranspiration estimation. Wiley Interdiscip. Rev. Water 3, 834–853. doi:10.1002/wat2.1168

Zhang, Y., Chiew, F.H.S., Peña-Arancibia, J., Sun, F., Li, H., Leuning, R., 2017. Global variation of transpiration and soil evaporation and the role of their major climate drivers. J. Geophys. Res. Atmos. 122, 6868–6881. doi:10.1002/2017JD027025

Zhang, Y., Peña-Arancibia, J.L., McVicar, T.R., Chiew, F.H.S., Vaze, J., Liu, C., Lu, X., Zheng, H., Wang, Y., Liu, Y.Y., Miralles, D.G., Pan, M., 2016. Multi-decadal trends in global terrestrial evapotranspiration and its components. Sci. Rep. 6, 19124. doi:10.1038/srep19124

IV. Conclusion:

Remote sensing efforts into estimating ET are increasing, as is the amount of remote sensing data available. Recent advances in thermal infrared, microwave, hyperspectral, as well as the spatial and temporal scale of remote sensing products will undoubtedly serve to improve ET estimates (Hulley et al., 2017; Marshall et al., 2014; Martens et al., 2016; Sun et al., 2017). However, some of the key questions remaining in ET science involve the partitioning of ET into transpiration, soil evaporation, and interception (Fisher et al., 2017; Lawrence et al., 2007). Limited field data confines our understanding of those processes and the challenge for ET scientists will be in connecting the burgeoning amount of remote sensing data with the relative scarcity of field partitioning data.

Efforts have begun, including in this study, to coordinate field data into a larger dataset that would allow us to compare partitioning studies across various ecological parameters and remote sensing-based metrics (Schlesinger and Jasechko, 2014; Talsma et al., 2018). The SAPFLUXnet project is in the process of combining hundreds of sap flux measurements across different species and biomes (Poyatos et al., 2016). Still, remote sensing products will continue to outpace the field products and are much better suited for global long term monitoring of ET (Glenn et al., 2007; K. Zhang et al., 2016). Inferences regarding patterns and trends observed in remote sensing data may inform research with little field validation to back it.

Here, we attempt to reconcile differences found between modeled and field derived estimates of ET components. Several challenges arise in making these comparisons and multiple sources of error are discussed and explored. We use a Monte Carlo sensitivity

analysis to determine how dataset error might influence model estimates and to further explore which parameters might be responsible for partitioning errors. While some potential sources of error remain unaccounted for, the two studies found here are able to explore the role of both model formulation and dataset uncertainty in previously observed model divergences. The main findings of this study are that…

- Relatively large deviations from field methods exist in the component estimates of the ET models while showing relative agreement in total ET estimates.
- Large biases and deviations emerge as a result of the uncertainty of the forcing data. Bias found due to parameter uncertainty in the opposite direction of the observed bias with field estimates suggests that model formulation or systemic dataset error is responsible for significant error.
- The soil evaporation term of both PM-MOD and PT-JPL shows large variance in its agreement with the field estimates. Both model components also show large sensitivity to the input parameters including RH and temperature.
- Soil evaporation appears to be the worst performing component across each of the models. The mis-parameterization of the soil evaporation term is likely driving a proportionally large amount of the partitioning error.

V. Bibliography:

Adler, R.F., Huffman, G.J., Chang, A., Ferraro, R., Xie, P.-P., Janowiak, J., Rudolf, B., Schneider, U., Curtis, S., Bolvin, D., Gruber, A., Susskind, J., Arkin, P., Nelkin, E., Adler, R.F., Huffman, G.J., Chang, A., Ferraro, R., Xie, P.-P., Janowiak, J., Rudolf, B., Schneider, U., Curtis, S., Bolvin, D., Gruber, A., Susskind, J., Arkin, P., Nelkin, E., 2003. The Version-2 Global Precipitation Climatology Project (GPCP) Monthly Precipitation Analysis (1979–Present). J. Hydrometeorol. 4, 1147–1167. doi:10.1175/1525-7541(2003)004<1147:TVGPCP>2.0.CO;2

Allen, C.D., Macalady, A.K., Chenchouni, H., Bachelet, D., McDowell, N., Vennetier, M., Kitzberger, T., Rigling, A., Breshears, D.D., Hogg, E.H. (Ted), Gonzalez, P., Fensham, R., Zhang, Z., Castro, J., Demidova, N., Lim, J.-H., Allard, G., Running, S.W., Semerci, A., Cobb, N., 2010. A global overview of drought and heat-induced tree mortality reveals emerging climate change risks for forests. For. Ecol. Manage. 259, 660–684. doi:10.1016/J.FORECO.2009.09.001

Aminzadeh, M., Or, D., 2017. Pore-scale study of thermal fields during evaporation from drying porous surfaces. Int. J. Heat Mass Transf. 104, 1189–1201. doi:10.1016/J.IJHEATMASSTRANSFER.2016.09.039

Anderson, M.C., Norman, J.M., Mecikalski, J.R., Otkin, J.A., Kustas, W.P., 2007. A climatological study of evapotranspiration and moisture stress across the continental United States based on thermal remote sensing: 1. Model formulation. J. Geophys. Res. 112, D10117. doi:10.1029/2006JD007506

Badgley, G., Fisher, J.B., Jiménez, C., Tu, K.P., Vinukollu, R., Badgley, G., Fisher, J.B., Jiménez, C., Tu, K.P., Vinukollu, R., 2015. On Uncertainty in Global Terrestrial Evapotranspiration Estimates from Choice of Input Forcing Datasets*. J. Hydrometeorol. 16, 1449–1455. doi:10.1175/JHM-D-14-0040.1

Baldocchi, D., Falge, E., Gu, L., Olson, R., Hollinger, D., Running, S., Anthoni, P., Bernhofer, C., Davis, K., Evans, R., Fuentes, J., Goldstein, A., Katul, G., Law, B., Lee, X., Malhi, Y., Meyers, T., Munger, W., Oechel, W., Paw, K.T., Pilegaard, K., Schmid, H.P., Valentini, R., Verma, S., Vesala, T., Wilson, K., Wofsy, S., Hall, R., 2001. FLUXNET: A New Tool to Study the Temporal and Spatial Variability of Ecosystem-Scale Carbon Dioxide, Water Vapor, and Energy Flux Densities 82.

Bonan, G.B., 2008. Forests and climate change: forcings, feedbacks, and the climate benefits of forests. Science 320, 1444–9. doi:10.1126/science.1155121

Brunel, J.P., Walker, G.R., Dighton, J.C., Montenya, B., 1997. Use of stable isotopes of water to determine the origin of water used by the vegetation and to partition evapotranspiration. A case study from HAPEX-Sahel. J. Hydrol. 188–189, 466–481. doi:10.1016/S0022-1694(96)03188-5

Carlyle-Moses, D.E., Gash, J.H.C., 2011. Rainfall Interception Loss by Forest Canopies. Springer, Dordrecht, pp. 407–423. doi:10.1007/978-94-007-1363-5_20

Cavanaugh, M.L., Kurc, S.A., Scott, R.L., 2011. Evapotranspiration partitioning in semiarid shrubland ecosystems: a two-site evaluation of soil moisture control on transpiration. Ecohydrology 4, 671–681. doi:10.1002/eco.157

Ciais, P., Reichstein, M., Viovy, N., Granier, A., Ogée, J., Allard, V., Aubinet, M., Buchmann, N., Bernhofer, C., Carrara, A., Chevallier, F., De Noblet, N., Friend, A.D., Friedlingstein, P., Grünwald, T., Heinesch, B., Keronen, P., Knohl, A., Krinner, G.,

Loustau, D., Manca, G., Matteucci, G., Miglietta, F., Ourcival, J.M., Papale, D., Pilegaard, K., Rambal, S., Seufert, G., Soussana, J.F., Sanz, M.J., Schulze, E.D., Vesala, T., Valentini, R., 2005. Europe-wide reduction in primary productivity caused by the heat and drought in 2003. Nature 437, 529–533. doi:10.1038/nature03972

Crockford, R.H., Richardson, D.P., 2000. Partitioning of rainfall into throughfall, stemflow and interception: effect of forest type, ground cover and climate. Hydrol. Process. 14, 2903–2920. doi:10.1002/1099-1085(200011/12)14:16/17<2903::AID-HYP126>3.0.CO;2-6

David, J.S., Valente, F., Gash, J.H., 2005. Evaporation of Intercepted Rainfall, in: Encyclopedia of Hydrological Sciences. John Wiley & Sons, Ltd, Chichester, UK. doi:10.1002/0470848944.hsa046

Decker, M., Or, D., Pitman, A., Ukkola, A., 2017. New turbulent resistance parameterization for soil evaporation based on a pore-scale model: Impact on surface fluxes in CABLE. J. Adv. Model. Earth Syst. 9, 220–238. doi:10.1002/2016MS000832

Dee, D., Uppala, M.S., Simmons, J.A., Berrisford, P., Poli, P., Kobayashi, S., Andrae, U., Balmaseda, A.M., Balsamo, G., Bauer, P., Bechtold, P., Beljaars, M.A.C., van de Berg, L., Bidlot, J., Bormann, N., Delsol, C., Dragani, R., Fuentes, M., Geer, J.A., Haimberger, L., Healy, B.S., Hersbach, H., Holm, V.E., Isaksen, L., Kallberg, P., Khaler, M., Matricardi, M., McNally, P.A., Monge-Sanz, M.B., Morcrette, .J., Park, B.K., Peubey, C., de Rosnay, P., Tovolato, C., Thapaut, J.N., Vitart, F., 2011. The ERA-Interim reanalysis: configuration and performance of the data assimilation system. R. Meteorol. Soc. 137, 553–597. doi:10.1002/qj.828

Demaria, E.M., Nijssen, B., Wagener, T., 2007. Monte Carlo sensitivity analysis of land surface parameters using the Variable Infiltration Capacity model. J. Geophys. Res. 112, D11113. doi:10.1029/2006JD007534

Didan, K., 2015. MOD13A2 MODIS/Terra Vegetation Indices 16-Day L3 Global 1km SIN GRID V006 [Dataset]. doi:10.5067/MODIS/MOD13A2.006

Dolman, A.J., Miralles, D.G., de Jeu, R.A.M., 2014. Fifty years since Monteith's 1965 seminal paper: the emergence of global ecohydrology. Ecohydrology 7, 897–902. doi:10.1002/eco.1505

Dye, P.J., Olbrich, B.W., Poulter, A.G., 1991. The Influence of Growth Rings in Pinus patula on Heat Pulse Velocity and Sap Flow Measurement. J. Exp. Bot. 42, 867–870. doi:10.1093/jxb/42.7.867

Ek, M.B., Holtslag, A.A.M., 2004. Influence of Soil Moisture on Boundary Layer Cloud Development. J. Hydrometeorol. 5, 86–99. doi:10.1175/1525-7541(2004)005<0086:IOSMOB>2.0.CO;2

Ershadi, A., Mccabe, M.F., Evans, J.P., Wood, E.F., 2015. Impact of model structure and parameterization on Penman-Monteith type evaporation models. J. Hydrol. 525, 521–535. doi:10.1016/j.jhydrol.2015.04.008

Fernández, J.E., Durán, P.J., Palomo, M.J., Diaz-Espejo, A., Chamorro, V., Girón, I.F., 2006. Calibration of sap flow estimated by the compensation heat pulse method in olive, plum and orange trees: relationships with xylem anatomy. Tree Physiol. 26, 719–28.

Fisher, J.B., Melton, F., Middleton, E., Hain, C., Anderson, M., Allen, R., McCabe, M.F., Hook, S., Baldocchi, D., Townsend, P.A., Kilic, A., Tu, K., Miralles, D.D., Perret, J., Lagouarde, J.-P., Waliser, D., Purdy, A.J., French, A., Schimel, D., Famiglietti, J.S., Stephens, G., Wood, E.F., 2017. The future of evapotranspiration: Global requirements

for ecosystem functioning, carbon and climate feedbacks, agricultural management, and water resources. Water Resour. Res. 53, 2618–2626. doi:10.1002/2016WR020175

Fisher, J.B., Tu, K.P., Baldocchi, D.D., 2008. Global estimates of the land–atmosphere water flux based on monthly AVHRR and ISLSCP-II data, validated at 16 FLUXNET sites. Remote Sens. Environ. 112, 901–919. doi:10.1016/J.RSE.2007.06.025

Friedl, M.A., Sulla-Menashe, D., Tan, B., Schneider, A., Ramankutty, N., Sibley, A., Huang, X., 2009. MODIS Collection 5 global land cover: Algorithm refinements and characterization of new datasets. doi:10.1016/j.rse.2009.08.016

Friedlingstein, P., Meinshausen, M., Arora, V.K., Jones, C.D., Anav, A., Liddicoat, S.K., Knutti, R., Friedlingstein, P., Meinshausen, M., Arora, V.K., Jones, C.D., Anav, A., Liddicoat, S.K., Knutti, R., 2014. Uncertainties in CMIP5 Climate Projections due to Carbon Cycle Feedbacks. J. Clim. 27, 511–526. doi:10.1175/JCLI-D-12-00579.1

Gash, J.H.C., 1979. An analytical model of rainfall interception by forests. Q. J. R. Meteorol. Soc. 105, 43–55. doi:10.1002/qj.49710544304

Gibson, J.J., Edwards, T.W.D., 2002. Regional water balance trends and evaporation-transpiration partitioning from a stable isotope survey of lakes in northern Canada. Global Biogeochem. Cycles 16, 10-1-10–14. doi:10.1029/2001GB001839

Glenn, E.P., Huete, A.R., Nagler, P.L., Hirschboeck, K.K., Brown, P., 2007. Integrating Remote Sensing and Ground Methods to Estimate Evapotranspiration. CRC. Crit. Rev. Plant Sci. 26, 139–168. doi:10.1080/07352680701402503

Glenn, E.P., Huete, A.R., Nagler, P.L., Nelson, S.G., 2008. Relationship Between Remotely-sensed Vegetation Indices, Canopy Attributes and Plant Physiological Processes: What Vegetation Indices Can and Cannot Tell Us About the Landscape. Sensors 8, 2136–2160. doi:10.3390/s8042136

Good, S.P., Moore, G.W., Miralles, D.G., 2017. A mesic maximum in biological water use demarcates biome sensitivity to aridity shifts. Nat. Ecol. Evol. 1, 1883–1888. doi:10.1038/s41559-017-0371-8

Good, S.P., Noone, D., Bowen, G., 2015. Hydrologic connectivity constrains partitioning of global terrestrial water fluxes. Science 349, 175–7. doi:10.1126/science.aaa5931

Goulden, M.L., Bales, R.C., 2014. Mountain runoff vulnerability to increased evapotranspiration with vegetation expansion. Proc. Natl. Acad. Sci. U. S. A. 111, 14071–5. doi:10.1073/pnas.1319316111

Grayson, R.B., Western, A.W., Chiew, F.H.S., Bloschl, G., 1997. Preferred states in spatial soil moisture patterns: Local and nonlocal controls. Water Resour. Res. 33, 2897–2908.

Haghighi, E., Or, D., 2013. Evaporation from porous surfaces into turbulent airflows: Coupling eddy characteristics with pore scale vapor diffusion. Water Resour. Res. 49, 8432–8442. doi:10.1002/2012WR013324

Hammersley, J.M., Handscomb, D.C., 1964. General Principles of the Monte Carlo Method, in: Monte Carlo Methods. Springer Netherlands, Dordrecht, pp. 50–75. doi:10.1007/978-94-009-5819-7_5

Hobbins, M.T., Ramírez, J.A., Brown, T.C., 2004. Trends in pan evaporation and actual evapotranspiration across the conterminous U.S.: Paradoxical or complementary? Geophys. Res. Lett. doi:10.1029/2004GL019846

Holwerda, F., Bruijnzeel, L.A., Scatena, F.N., 2011. Comparison of passive fog gauges for determining fog duration and fog interception by a Puerto Rican elfin cloud forest. Hydrol. Process. 25, 367–373. doi:10.1002/hyp.7641

Hu, Z., Yu, G., Zhou, Y., Sun, X., Li, Y., Shi, P., Wang, Y., Song, X., Zheng, Z., Zhang, L., Li, S., 2009. Partitioning of evapotranspiration and its controls in four grassland ecosystems: Application of a two-source model. Agric. For. Meteorol. 149, 1410–1420. doi:10.1016/J.AGRFORMET.2009.03.014

Hulley, G., Hook, S., Fisher, J., Lee, C., 2017. ECOSTRESS, A NASA Earth-Ventures Instrument for studying links between the water cycle and plant health over the diurnal cycle, in: 2017 IEEE International Geoscience and Remote Sensing Symposium (IGARSS). IEEE, pp. 5494–5496. doi:10.1109/IGARSS.2017.8128248

Huntington, T.G., 2006. Evidence for intensification of the global water cycle: Review and synthesis. J. Hydrol. 319, 83–95. doi:10.1016/J.JHYDROL.2005.07.003

Jasechko, S., Sharp, Z.D., Gibson, J.J., Birks, S.J., Yi, Y., Fawcett, P.J., 2013. Terrestrial water fluxes dominated by transpiration. Nature 496, 347–350. doi:10.1038/nature11983

Komatsu, H., 2005. Forest categorization according to dry-canopy evaporation rates in the growing season: comparison of the Priestley-Taylor coefficient values from various observation sites. Hydrol. Process. 19, 3873–3896. doi:10.1002/hyp.5987

Kumar, S., Holmes, T., Mocko, D.M., Wang, S., Peters-Lidard, C., 2018. Attribution of Flux Partitioning Variations between Land Surface Models over the Continental U.S. Remote Sens. 10. doi:10.3390/rs10050751

Lautz, L.K., 2008. Estimating groundwater evapotranspiration rates using diurnal water-table fluctuations in a semi-arid riparian zone. Hydrogeol. J. 16, 483–497. doi:10.1007/s10040-007-0239-0

Lawrence, D.M., Thornton, P.E., Oleson, K.W., Bonan, G.B., Lawrence, D.M., Thornton, P.E., Oleson, K.W., Bonan, G.B., 2007. The Partitioning of Evapotranspiration into Transpiration, Soil Evaporation, and Canopy Evaporation in a GCM: Impacts on Land–Atmosphere Interaction. J. Hydrometeorol. 8, 862–880. doi:10.1175/JHM596.1

Levia, D.F., Frost, E.E., 2006. Variability of throughfall volume and solute inputs in wooded ecosystems. Prog. Phys. Geogr. 30, 605–632. doi:10.1177/0309133306071145

Littell, J.S., Peterson, D.L., Riley, K.L., Liu, Y., Luce, C.H., 2016. A review of the relationships between drought and forest fire in the United States. Glob. Chang. Biol. 22, 2353–2369. doi:10.1111/gcb.13275

Mancosu, N., Snyder, R., Kyriakakis, G., Spano, D., 2015. Water Scarcity and Future Challenges for Food Production. Water 7, 975–992. doi:10.3390/w7030975

Marshall, K.N., Cooper, D.J., Hobbs, N.T., 2014. Interactions among herbivory, climate, topography and plant age shape riparian willow dynamics in northern Yellowstone National Park, USA. J. Ecol. 102, 667–677. doi:10.1111/1365-2745.12225

Marshall, M., Thenkabail, P., Biggs, T., Post, K., 2016. Hyperspectral narrowband and multispectral broadband indices for remote sensing of crop evapotranspiration and its components (transpiration and soil evaporation). Agric. For. Meteorol. 218219, 122–134. doi:10.1016/j.agrformet.2015.12.025

Martens, B., Miralles, D., Lievens, H., Fernández-Prieto, D., Verhoest, N.E.C., 2016. Improving terrestrial evaporation estimates over continental Australia through assimilation of SMOS soil moisture. Int. J. Appl. Earth Obs. Geoinf. 48, 146–162. doi:10.1016/J.JAG.2015.09.012

Martens, B., Miralles, D.G., Lievens, H., van der Schalie, R., de Jeu, R.A.M., Fernández-Prieto, D., Beck, H.E., Dorigo, W.A., Verhoest, N.E.C., 2017. GLEAM v3: satellite-based land evaporation and root-zone soil moisture. Geosci. Model Dev. 10, 1903–1925.

doi:10.5194/gmd-10-1903-2017
McCabe, M.F., Aragon, B., Houborg, R., Mascaro, J., 2017. CubeSats in Hydrology: Ultrahigh-Resolution Insights Into Vegetation Dynamics and Terrestrial Evaporation. Water Resour. Res. 53, 10017–10024. doi:10.1002/2017WR022240
Mccabe, M.F., Ershadi, A., Jimenez, C., Miralles, D.G., Michel, D., Wood, E.F., 2016. The GEWEX LandFlux project: evaluation of model evaporation using tower-based and globally gridded forcing data. Geosci. Model Dev 9, 283–305. doi:10.5194/gmd-9-283-2016
Mccabe, M.F., Rodell, M., Alsdorf, D.E., Miralles, D.G., Uijlenhoet, R., Wagner, W., Lucieer, A., Houborg, R., Verhoest, N.E.C., Franz, T.E., Shi, J., Gao, H., Wood, E.F., 2017. The future of Earth observation in hydrology. Earth Syst. Sci 215194, 3879–3914. doi:10.5194/hess-21-3879-2017
McJannet, D., Fitch, P., Disher, M., Wallace, J., 2007. Measurements of transpiration in four tropical rainforest types of north Queensland, Australia. Hydrol. Process. 21, 3549–3564. doi:10.1002/hyp.6576
Meng, X.H., Evans, J.P., McCabe, M.F., Meng, X.H., Evans, J.P., McCabe, M.F., 2014. The Impact of Observed Vegetation Changes on Land–Atmosphere Feedbacks During Drought. J. Hydrometeorol. 15, 759–776. doi:10.1175/JHM-D-13-0130.1
Merlin, O., Stefan, V.G., Amazirh, A., Chanzy, A., Ceschia, E., Er-Raki, S., Gentine, P., Tallec, T., Ezzahar, J., Bircher, S., Beringer, J., Khabba, S., 2016. Modeling soil evaporation efficiency in a range of soil and atmospheric conditions using a meta-analysis approach. Water Resour. Res. doi:10.1002/2015WR018233
Michel, D., Jiménez, C., Miralles, D.G., Jung, M., Hirschi, M., Ershadi, A., Martens, B., Mccabe, M.F., Fisher, J.B., Mu, Q., Seneviratne, S.I., Wood, E.F., Fernández-Prieto, D., 2016. The WACMOS-ET project – Part 1: Tower-scale evaluation of four remote-sensing-based evapotranspiration algorithms. Hydrol. Earth Syst. Sci 20, 803–822. doi:10.5194/hess-20-803-2016
Miralles, D.G., Gash, J.H., Holmes, T.R.H., De Jeu, R.A.M., Dolman, A.J., 2010. Global canopy interception from satellite observations. J. Geophys. Res 115. doi:10.1029/2009JD013530
Miralles, D.G., Holmes, T.R.H., De Jeu, R.A.M., Gash, J.H., Meesters, A.G.C.A., Dolman, A.J., 2011. Global land-surface evaporation estimated from satellite-based observations. Hydrol. Earth Syst. Sci 15, 453–469. doi:10.5194/hess-15-453-2011
Miralles, D.G., Jiménez, C., Jung, M., Michel, D., Ershadi, A., McCabe, M.F., Hirschi, M., Martens, B., Dolman, A.J., Fisher, J.B., Mu, Q., Seneviratne, S.I., Wood, E.F., Fernaìndez-Prieto, D., 2016. The WACMOS-ET project – Part 2: Evaluation of global terrestrial evaporation data sets. Hydrol. Earth Syst. Sci. Discuss. 12, 10651–10700. doi:10.5194/hessd-12-10651-2015
Molden, D., Oweis, T., Steduto, P., Bindraban, P., Hanjra, M.A., Kijne, J., 2010. Improving agricultural water productivity: Between optimism and caution. Agric. Water Manag. 97, 528–535. doi:10.1016/J.AGWAT.2009.03.023
Mu, Q., Zhao, M., Running, S.W., 2011. Improvements to a MODIS global terrestrial evapotranspiration algorithm. Remote Sens. Environ. 115, 1781–1800. doi:10.1016/j.rse.2011.02.019
Mueller, B., Seneviratne, S.I., Jimenez, C., Corti, T., Hirschi, M., Balsamo, G., Ciais, P., Dirmeyer, P., Fisher, J.B., Guo, Z., Jung, M., Maignan, F., McCabe, M.F., Reichle, R.,

Reichstein, M., Rodell, M., Sheffield, J., Teuling, A.J., Wang, K., Wood, E.F., Zhang, Y., 2011. Evaluation of global observations-based evapotranspiration datasets and IPCC AR4 simulations. Geophys. Res. Lett. 38, n/a-n/a. doi:10.1029/2010GL046230

Muzylo, A., Llorens, P., Valente, F., Keizer, J.J., Domingo, F., Gash, J.H.C., 2009. A review of rainfall interception modelling. J. Hydrol. 370, 191–206. doi:10.1016/J.JHYDROL.2009.02.058

Nizinski, J.J., Galat, G., Galat-Luong, A., 2011. Water balance and sustainability of eucalyptus plantations in the Kouilou basin (Congo-Brazzaville). Russ. J. Ecol. 42, 305–314. doi:10.1134/S1067413611040126

Norman Ay, J.M., Kustas, W.P., Humes, K.S., 1995. Source approach for estimating soil and vegetation energy fluxes in observations of directional radiometric surface temperature. Agric. For. Meteorol. 77, 263–293.

Novick, K.A., Ficklin, D.L., Stoy, P.C., Williams, C.A., Bohrer, G., Oishi, A.C., Papuga, S.A., Blanken, P.D., Noormets, A., Sulman, B.N., Scott, R.L., Wang, L., Phillips, R.P., 2016. The increasing importance of atmospheric demand for ecosystem water and carbon fluxes. Nat. Clim. Chang. 6, 1023–1027. doi:10.1038/nclimate3114

Oki, T., Kanae, S., 2006. Global hydrological cycles and world water resources. Science 313, 1068–72. doi:10.1126/science.1128845

Or, D., Lehmann, P., Shahraeeni, E., Shokri, N., 2013. Advances in Soil Evaporation Physics—A Review. Vadose Zo. J. 12, 0. doi:10.2136/vzj2012.0163

Owe, M., de Jeu, R., Walker, J., 2001. A methodology for surface soil moisture and vegetation optical depth retrieval using the microwave polarization difference index. IEEE Trans. Geosci. Remote Sens. 39, 1643–1654. doi:10.1109/36.942542

Pielke, R.A., Sr, ., Avissar, R., Raupach, M., Dolman, A.J., Zeng, X., Denning, A.S., 1998. Interactions between the atmosphere and terrestrial ecosystems: influence on weather and climate. Glob. Chang. Biol. 4, 461–475. doi:10.1046/j.1365-2486.1998.t01-1-00176.x

Pieruschka, R., Huber, G., Berry, J.A., 2010. Control of transpiration by radiation. Proc. Natl. Acad. Sci. U. S. A. 107, 13372–7. doi:10.1073/pnas.0913177107

Porkka, M., Gerten, D., Schaphoff, S., Siebert, S., Kummu, M., 2016. Causes and trends of water scarcity in food production. Environ. Res. Lett. 11, 15001. doi:10.1088/1748-9326/11/1/015001

Poyatos, R., Granda, V., Molowny-Horas, R., Mencuccini, M., Steppe, K., Martínez-Vilalta, J., 2016. SAPFLUXNET: towards a global database of sap flow measurements. Tree Physiol. 36, 1449–1455. doi:10.1093/treephys/tpw110

Priestley, C.H.B., Taylor, R.J., 1972. On the assessment of sruface heat flux and evaporation using large scale parameters. Mon. Weather Rev. 81–92.

Purdy, A.J., Fisher, J.B., Goulden, M.L., Famiglietti, J.S., 2016. Ground heat flux: An analytical review of 6 models evaluated at 88 sites and globally. J. Geophys. Res. Biogeosciences 121, 3045–3059. doi:10.1002/2016JG003591

Pypker, T.G., Bond, B.J., Link, T.E., Marks, D., Unsworth, M.H., 2005. The importance of canopy structure in controlling the interception loss of rainfall: Examples from a young and an old-growth Douglas-fir forest. Agric. For. Meteorol. 130, 113–129. doi:10.1016/J.AGRFORMET.2005.03.003

R. Myneni, Y.K., n.d. MOD15A2H MODIS/Terra Leaf Area Index/FPAR 8-Day L4 Global 500m SIN Grid V006. doi.org. doi:10.5067/modis/mod15a2h.006

Rana, G., Katerji, N., 2000. Measurement and estimation of actual evapotranspiration in the field under Mediterranean climate: a review. Eur. J. Agron. 13, 125–153. doi:10.1016/S1161-0301(00)00070-8

Robert, C.P., 1995. Simulation of truncated normal variables. Stat. Comput. 5, 121–125. doi:10.1007/BF00143942

Schlesinger, W.H., Jasechko, S., 2014. Transpiration in the global water cycle. Agric. For. Meteorol. 189–190, 115–117. doi:10.1016/j.agrformet.2014.01.011

Schmugge, T.J., Kustas, W.P., Ritchie, J.C., Jackson, T.J., Rango, A., 2002. Remote sensing in hydrology. Adv. Water Resour. 25, 1367–1385. doi:10.1016/S0309-1708(02)00065-9

Seneviratne, S.I., Corti, T., Davin, E.L., Hirschi, M., Jaeger, E.B., Lehner, I., Orlowsky, B., Teuling, A.J., 2010. Investigating soil moisture–climate interactions in a changing climate: A review. Earth-Science Rev. 99, 125–161. doi:10.1016/J.EARSCIREV.2010.02.004

Shukla, J., Mintz, Y., 1982. Influence of Land-Surface Evapotranspiration on the Earth's Climate. Science 215, 1498–501. doi:10.1126/science.215.4539.1498

Spinoni, J., Naumann, G., Carrao, H., Barbosa, P., Vogt, J., 2014. World drought frequency, duration, and severity for 1951-2010. Int. J. Climatol. 34, 2792–2804. doi:10.1002/joc.3875

Stackhouse, P., Gupts, S., Cox, S., Mikovits, J., Zhang, T., Chiachiio, M., 2004. 12-year surface radiation budget data set. GEWEX News 14, 10–12.

Stone, P.H., Chow, S., Quirr, W.J., Stone, P.H., Chow, S., Quirr, W.J., 1977. The July Climate and a Comparison of the January and July Climates Simulated by the GISS General Circulation Model. Mon. Weather Rev. 105, 170–194. doi:10.1175/1520-0493(1977)105<0170:TJCAAC>2.0.CO;2

Sun, L., Anderson, M.C., Gao, F., Hain, C., Alfieri, J.G., Sharifi, A., McCarty, G.W., Yang, Y., Yang, Y., Kustas, W.P., McKee, L., 2017. Investigating water use over the Choptank River Watershed using a multisatellite data fusion approach. Water Resour. Res. 53, 5298–5319. doi:10.1002/2017WR020700

Talsma, C., Good, S.P., Jimenez, C., Martens, B., Fisher, J., 2017. Evaluation of Evapotranspiration Partitioning in Remote Sensing Models. Am. Geophys. Union, Fall Meet. 2017, Abstr. #H11M-08.

Talsma, C.J., Good, S.P., Jimenez, C., Martens, B., Fisher, J.B., Miralles, D.G., McCabe, M.F., Purdy, A.J., 2018. Partitioning of evapotranspiration in remote sensing-based models. Agric. For. Meteorol. doi:10.1016/j.agrformet.2018.05.010

Teuling, A.J., Hirschi, M., Ohmura, A., Wild, M., Reichstein, M., Ciais, P., Buchmann, N., Ammann, C., Montagnani, L., Richardson, A.D., Wohlfahrt, G., Seneviratne, S.I., 2009. A regional perspective on trends in continental evaporation. Geophys. Res. Lett. 36, n/a-n/a. doi:10.1029/2008GL036584

Trenberth, K.E., 2011. Changes in precipitation with climate change. Clim. Res. doi:10.2307/24872346

Valente, F., David, J.S., Gash, J.H.C., 1997. Modelling interception loss for two sparse eucalypt and pine forests in central Portugal using reformulated Rutter and Gash analytical models. J. Hydrol. 190, 141–162. doi:10.1016/S0022-1694(96)03066-1

Vinukollu, R.K., Meynadier, R., Sheffield, J., Wood, E.F., 2011. Multi-model, multi-sensor estimates of global evapotranspiration: climatology, uncertainties and trends. Hydrol. Process. 25, 3993–4010. doi:10.1002/hyp.8393

Wallace, J.., 2000. Increasing agricultural water use efficiency to meet future food production. Agric. Ecosyst. Environ. 82, 105–119. doi:10.1016/S0167-8809(00)00220-6

Wang, K., Dickinson, R.E., 2012. A review of global terrestrial evapotranspiration: Observation, modeling, climatology, and climatic variability. Rev. Geophys. 50. doi:10.1029/2011RG000373

Wang, L., Good, S.P., Caylor, K.K., 2014. Global synthesis of vegetation control on evapotranspiration partitioning. Geophys. Res. Lett. 41, 6753–6757. doi:10.1002/2014GL061439

Williams, D.G., Cable, W., Hultine, K., Hoedjes, J.C.B., Yepez, E.A., Simonneaux, V., Er-Raki, S., Boulet, G., de Bruin, H.A.R., Chehbouni, A., Hartogensis, O.K., Timouk, F., 2004. Evapotranspiration components determined by stable isotope, sap flow and eddy covariance techniques. Agric. For. Meteorol. 125, 241–258. doi:10.1016/J.AGRFORMET.2004.04.008

Yepez, E.A., Huxman, T.E., Ignace, D.D., English, N.B., Weltzin, J.F., Castellanos, A.E., Williams, D.G., 2005. Dynamics of transpiration and evaporation following a moisture pulse in semiarid grassland: A chamber-based isotope method for partitioning flux components. Agric. For. Meteorol. 132, 359–376. doi:10.1016/j.agrformet.2005.09.006

Zaitchik, B.F., Santanello, J.A., Kumar, S. V., Peters-Lidard, C.D., Zaitchik, B.F., Santanello, J.A., Kumar, S. V., Peters-Lidard, C.D., 2013. Representation of Soil Moisture Feedbacks during Drought in NASA Unified WRF (NU-WRF). J. Hydrometeorol. 14, 360–367. doi:10.1175/JHM-D-12-069.1

Zhang, K., Kimball, J.S., Running, S.W., 2016. A review of remote sensing based actual evapotranspiration estimation. Wiley Interdiscip. Rev. Water 3, 834–853. doi:10.1002/wat2.1168

Zhang, Y., Chiew, F.H.S., Peña-Arancibia, J., Sun, F., Li, H., Leuning, R., 2017. Global variation of transpiration and soil evaporation and the role of their major climate drivers. J. Geophys. Res. Atmos. 122, 6868–6881. doi:10.1002/2017JD027025

Zhang, Y., Peña-Arancibia, J.L., McVicar, T.R., Chiew, F.H.S., Vaze, J., Liu, C., Lu, X., Zheng, H., Wang, Y., Liu, Y.Y., Miralles, D.G., Pan, M., 2016. Multi-decadal trends in global terrestrial evapotranspiration and its components. Sci. Rep. 6, 19124. doi:10.1038/srep19124